Contents

1 Introduction

Bound states of two particles have been intensively studied since they were found a long time ago. They play a main role for the explanation of the fundamental interactions. While the weak and the electromagnetic interaction can be treated quite precisely, it was not possible for a long time to explain the strong interaction in a satisfactory way. Based on a quark model, a classification of hadrons was developed by Gell-Mann [1] in the mid sixties. This allowed the description of hundreds of strong interacting particles with three elementary spin-half quarks: the up, down, and strange. In Gell-Mann's classification by quantum numbers it was possible to calculate masses, decay-rates and magnetic moments of mesons and baryons. The feature that quarks obey Fermi-statistics led to the introduction of a new three-valued degree of freedom called color. Its behavior characterized the color to be a suitable strong interacting charge, on which a theory on forces between quarks can be based. This non-abelian color-gauge theory called QCD (**Q**uantum**C**hromo**D**ynamics) describes quarks as fields interacting by massless gauge-bosons, the gluons. Those gluons carry color-charge as well, and are therefore able to interact with each other. For decreasing distances this leads to an increasing effective color-charge and therefore to a decreasing effective coupling. This *asymptotic freedom*, a behavior being contrary to that of QED, is a reason for the fact that perturbation theory is just reasonable at small distances compared to the extension of a hadron being around 10^{-15} m = 1 fm. For larger distances confinement-effects dominate the dynamics. Here the production of quark-pairs is becoming important, because hadrons are able to decay into lighter hadrons or can mix with each other since they have the right quantum numbers. With the discovery of the J/Ψ particle in 1974 [2, 3, 4] there was evidence for the existence of the charm quark, predicted already in earlier theories [5]. In 1977 the Υ-meson family gave a hint for the existence of a fifth particle, named b-quark. The last remaining particle, predicted by the standard model, the top-quark, was found in 1994 [6] at the Fermilab Tevatron Collider in Chicago. The measurements on mesons including a top quark are still ongoing, so that no experimental masses for those mesons are currently available. Even for charm- and bottom-including mesons not all mass-values are determined.

For the discovery of particles like J/Ψ or Υ, the progress in accelerator physics was essential. Without the highly energetic particles produced in, e.g., the Tevatron,

the top could not have been found.

Although great progress has already been made on the development of QCD [7], the search for mesons is still ongoing, accompanied by great advancements in accelerator physics. One of the great outstanding theoretical problems in QCD is the calculation of meson masses. A first step in this direction is done in this thesis.

Therefore an effective Hamiltonian in momentum space is simplified so far that the divergent integral kernel is the main object. The existence of such divergence is known since ten years, but has never been isolated or analyzed. Here its influence is worked out in an extreme model. The divergence gives rise to the discussion of its regulation. To get rid of the regularization parameter μ a simplified renormalization procedure is performed. The fixing of an appropriate pair $(\mu_0, \alpha(\mu_0))$ and of the up- and down-quark mass lays the foundation to calculate the eigenvalues and eigenfunctions of the scalar mesons. Mesons with orbital-angular momentum $L = 0$ are characterized by

$$J^{\mathrm{PC}} = 0^{-+} \quad , \qquad 1^{--} \quad . \tag{1}$$

They are named *pseudo-scalar mesons* and *vectormesons*, respectively. *Pseudo* is a synonym for the 'unnatural' (negative) parity of the scalar particle, because spinless particles normally do not change their prefactor under parity transformation. *Vector* represents a spin content of $S = 1$. Table 1 presents all mesons in their usual nomenclature. This thesis focuses on scalar flavor off-diagonal mesons, which are listed in Tab.1 in the lower rows under the diagonal. The flavor diagonal terms are not discussed, since isospin-effects are not included.

The main issues are the analyzation of the divergence, the performance of the corresponding renormalization program for QCD and the verification of the experimentally measured meson masses. The discussion focuses on the description of the pion. The pion root mean-square radius is evaluated and related to the experimentally measured mean-square radius.

This thesis is a first step to a complex theory, intended to describe all meson masses correctly, and later to serve the experimentalists in checking their results. Therefore, such a simple model is sufficient to settle the techniques and to give evidence for some basic effects according to mesons.

Moreover, the determination of the spectra and the wave functions of these particles with a covariant gauge-theory is one of the most important features in hadronic physics. The method of *Light-Cone Quantization* supports this aim. It uses the

	$\overline{d}$	$\overline{u}$	$\overline{s}$	$\overline{c}$	$\overline{b}$	$\overline{t}$
d	(ρ^0,ω)	ρ^-	$K^{\star 0}$	$D^{\star -}$	$B^{\star 0}$	$T^{\star -}$
	(π^0,η)	π^-	K^0	D^-	B^0	T^-
u	ρ^+	(ρ^0,ω)	$K^{\star +}$	$\overline{D}^{\star 0}$	$B^{\star +}$	$\overline{T}^{\star 0}$
	π^+	(π^0,η)	K^+	$\overline{D}^0$	B^+	$\overline{T}^0$
s	$\overline{K}^{\star 0}$	$K^{\star -}$	Φ	$D_s^{\star -}$	$B_s^{\star 0}$	$T_s^{\star -}$
	$\overline{K}^0$	K^-	η'	D_s^-	B_s^0	T_s^-
c	$D^{\star +}$	$D^{\star 0}$	$D_s^{\star +}$	J/Ψ	$B_c^{\star +}$	$\overline{T}_c^{\star 0}$
	D^+	D^0	D_s^+	η_c	B_c^+	$\overline{T}_c^0$
b	$\overline{B}^{\star 0}$	$B^{\star -}$	$\overline{B}_s^{\star 0}$	$B_c^{\star -}$	Υ	$T_b^{\star -}$
	$\overline{B}^0$	B^-	$\overline{B}_s^0$	B_c^-	η_b	T_b^-
t	$T^{\star +}$	$T^{\star 0}$	$T_s^{\star +}$	$T_c^{\star 0}$	$T_b^{\star +}$	Θ
	T^+	T^0	T_s^+	T_c^0	T_b^+	η_t

Table 1: *Table of mesons with $L = 0$ - the upper line indicates the vector mesons, the lower one the pseudoscalar mesons. The brackets identify states, which come along in different combinations.*

well-known Hamiltonian dynamics as an interface to field theories, quantizes at equal light-cone time and has other remarkable characteristics, which make it suitable for such an application. To reach all goals, the front-form Hamiltonian for QCD has to be truncated to an effective Hamiltonian [8]. By definition, this acts only in the Fock space of one quark (q) and one anti-quark ($\bar{q}$). Such a construction suggests to evaluate all mesons simultaneously. The restriction to spherically symmetric singlet S-states gives also the chance to easily build up the pion form factor from the wave functions and calculate the root mean-square radius, as well as to determine the up- and down mass which are the two last free parameters after renormalization.

Section 2 settles the basics and gives a short review over the evaluation of the effective Hamiltonian in momentum space , while Sect. 3.1 describes the derivation of the model equation. The numerical techniques, such as the counter-term method and Gaussian quadrature, are used in order to handle the singularities are introduced in Sect. 4.2. In Sect. 4.3 the combined model potential, Coulomb plus a regulated delta function, is discussed with respect to the renormalization formalism and the

calculated quark mass values. Sect. 4.4 presents the same for the 'completely regulated' potential, i.e., the Delta and the Coulomb potential are both regulated. In Sects. 5.1 and 5.2 the model corresponding results are collected and their impact on the theory is discussed, especially the pion wave function. The obtained meson masses are compared to the experimental values and the pion root mean-square radius is calculated from the eigenfunctions. Some further aspects concerning the assumptions of the model are theoretically discussed in Sect. 6. In Section 7 the main features are discussed and compared to other theories. The Appendices A to D complete this thesis.

2 Basics

The long way from the Lagrangian in gauge theory to the effective Hamiltonian is briefly reviewed keeping an eye on the advantages of this evolution. This section starts with a short summary of light-cone quantization in order to specify the Hamiltonian dynamics and then leads to the evaluation of the effective Hamiltonian.

2.1 Front Form Dynamics

In 1949 Dirac [9] showed that in a so called 'front form' of Hamiltonian dynamics a maximum number of Poincaré generators become independent of the interaction, including certain Lorentz boosts. In fact, unlike the traditional equal-time Hamiltonian formalism, quantization on a plane tangential to the light-cone can be formulated frame-independently. An operator can be constructed whose eigenvalues are the invariant masses of the composite physical particles. The eigenvectors describe bound-states of arbitrary four-momentum and invariant mass.

Based on the definition of a Hamiltonian H as an operator acting on a state $|\Psi(t)\rangle$, which is equal to the partial derivative of this state with respect to the time t, i.e.

$$H|\Psi(t)\rangle = i\frac{\partial}{\partial t}|\Psi(t)\rangle \quad , \tag{2}$$

each expectation value can be described as a *constant of motion* or *energy*. In a covariant theory, time is one component of four-dimensional space-time. By generalization the space can be redefined as a hypersphere in four-space and the time as its forth component. Dirac showed that there are not more than three parameterizations of space-time with no mapping between them by Lorentz transformations. The only difference is the position of the initial hypersphere which causes different time and Hamiltonian representations. As shown in Fig. 1 the instant form has its hypersphere at $t = 0$, for the front form it lies tangential to the light-cone and in the point form it is a hyperboloid with the time analogous to the eigentime of a physical system.

Consider the front form parameterization in Fig.1: it is convenient to introduce generalized coordinates $\tilde{x}^\nu$. Then $\tilde{x}^3 = x^0 - x^3$ can be interpreted as a space coordinate denoted by $x^- = ct - z$, and therefore $\tilde{x}^0 = x^0 + x^3$ necessarily is the time coordinate with $x^+ = ct + z$, or the *light-cone time* $\tau = t + z/c$.

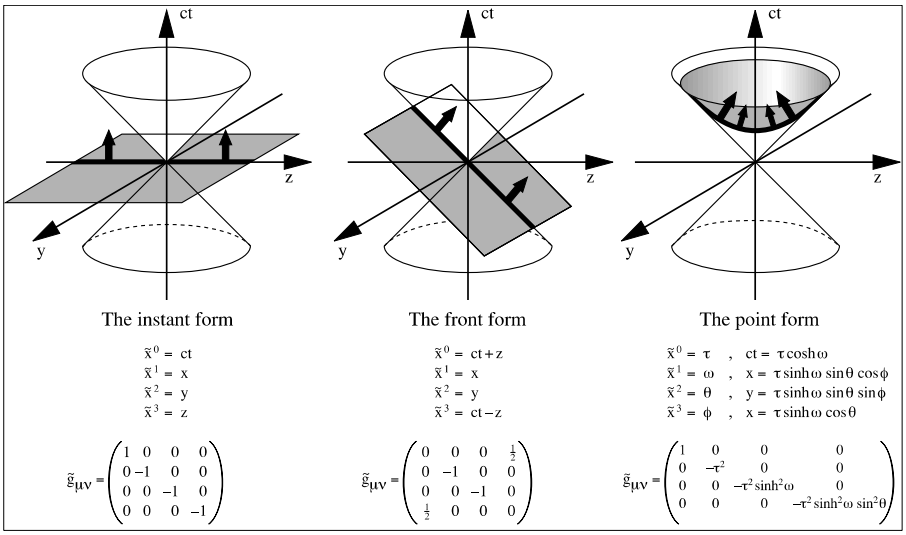

Figure 1: *Dirac's three forms of Hamiltonian dynamics; taken from [10]*

The prescription $x_\mu = g_{\mu\nu}x^\nu$ makes it obvious that $x_+ = \frac{1}{2}x^-$ are space and $x_- = \frac{1}{2}x^+$ are time coordinates. The corresponding spatial derivative is $\partial_- = \frac{1}{2}\partial^+$, while $\partial_+ = \frac{1}{2}\partial^-$ is the time-analogue. This convention is known as the Lepage-Brodsky convention [10], compared to the Kogut-Soper convention, which comes along with a factor of $\sqrt{2}$: $\partial_i = \partial^j$ with $i = -, +\ \ j = +, -$.

The occuring Lorentz indices $+$, $-$ have different physical meanings whether they are sub- or superscribed. There is no relation to co- or contravariant vectors.

In this approach the Hamiltonian is build up by one component of $P^\mu = (\vec{P}_\perp, P^+, P_-)$, usually the interaction depending time-like one, a complicated non-diagonal operator. The partial derivative of the state $|\Psi(x^+)\rangle$

$$P_+|\Psi(x^+)\rangle = i\frac{\partial}{\partial x^+}|\Psi(x^+)\rangle \tag{3}$$

defines – respecting the time- and space-like derivatives – the $P_+ = \frac{1}{2}P^-$ or $P^- = 2P_+$ as the Hamiltonian in transformed coordinates and $P_- = \frac{1}{2}P^+$ as the longitudinal momentum. The other three spatial components $\vec{P}_\perp = (P^1, P^2)$ and P^+ do not depend on the interaction.

The choice of the front-form formalism depends on the lack of experience in the point-form and the amount of disadvantages of the instant form, although this is the conventional one. Even the choice of the name for the front-form approach is not clear, because during a long period of time this approach has been re-invented

several times. One of them is the 'light-cone quantization', which is misleading, since the initial set of data is set on the plane tangential to the light-cone, not directly on it.

In fact, the front form or light-cone quantization is an elegant approach to quantum field theory providing a Hamiltonian gauge-fixed formulation that avoids many of the great problems in conventional equal-time formulation.

2.2 Evaluation of the effective Hamiltonian

In gauge field theory the Lagrangian $\mathcal{L}$ indicates the starting point. Its variation results in the *Euler equations*. Such a canonical formalism is connected with the study of symmetries in a field theory. It is known, that every continuous symmetry of $\mathcal{L}$ is associated with a vanishing four-divergence of a current and a conserved charge. $\mathcal{L}$ is not explicitly coordinate-dependent, therefore every field theory in 3+1 dimensions has ten conserved four-currents. However the four-divergences of the energy-momentum tensor $T^{\mu\nu}$ and of the boost-angular-momentum stress tensor $J^{\lambda,\mu\nu}$ vanish, consequently the Lorentz-group has ten conserved charges: the four components of the total momentum $P^{\mu\nu}$ and the six components of the boost-angular momentum $M^{\mu\nu}$. These constants of motion are observables with real eigenvalues. They are combined to fulfill the commutator-algebra of the Poincaré group. The two group invariants are the operator for the invariant mass squared $M^2 = P^\mu P_\mu$ and the operator for the intrinsic spin squared $S^2 = V^\mu V_\mu$ with V^μ being the Pauli-Lubansky vector $V^\kappa \equiv \epsilon^{\kappa\lambda\mu\nu} P_\lambda M_{\mu\nu}$. They are Lorentz scalars, and commute with all generators P^μ and $M_{\mu\nu}$ [10, 11].

The energy-momentum vector is manifestly gauge-invariant, even in the front form, but it contains time-derivatives and other constraint field components. Therefore P^μ is expressed in terms of free fields and the dependence on the coupling constant is isolated by the application of the color Maxwell- and Dirac-equations. Those four color Maxwell-equations determine the four functions A_a^μ. One of them is identically fulfilled by the chosen light-cone gauge $A_a^+ = 0$. The others give a constraint for the time- and space-derivatives. For the free case A_a^μ is reduced to a free field $\tilde{A}_a^\mu$, which consequently is purely transverse. The color Dirac-equations form by definition of free spinors an expression, which is independent of the interaction. Rewriting the time-like component P_+ it is given by a sum of the kinetic

energy T, the vertex interaction V and three further interactions, especially the four-point gluon interaction, the instantaneous gluon interaction and the instantaneous fermion interaction. It is remarkable that the relativistic Hamiltonian is additive in the kinetic and potential energy, comparable to the non-relativistic Hamiltonian $H = T + U$.

Because of the free solutions of the Maxwell- and Dirac equations the single particle states are specified by the quantum numbers $q = (p^+, p_{\perp x}, p_{\perp y}, \lambda, c, f)$, with λ being the helicity, c the color and f the flavor. Their creation and annihilation operators are contained in the commutating and anti-commutating relations which carry the structure of the theory. Therefore all interactions can be expressed in terms of these ladder operators. The sum of the associated single particle momenta is essentially described by the difference between the sum of the particle momenta and the sum of all momenta. As a consequence, a contribution vanishes if a term has only creation *or* annihilation operators since the longitudinal momenta p^+ are always positive and therefore can not add to zero. For that reason, all energy diagrams which generate vacuum fluctuations in the usual formulation of QFT (**Q**uantum **F**ield **T**heory) are absent in the front form.

The above substitution by ladder operators leads to a Hamiltonian that acts like a Fock-space operator. The *kinetic energy* T becomes a sum of three diagonal operators. The interaction terms are distinguished according to the number of particles changed. The *vertex interaction* V is a sum of four operators: $V = \sum_{i=1}^{4} V_i$. Those contributions V_i represent different Fock states, their particle numbers differing by one. The V_i themselves contain *matrix elements*, which can be displayed as energy graphs. The four-point interactions are separated into *fork* F and *seagull* S interactions, depending on whether they have an odd or even number of creation operators. The *fork interaction* F is a sum of six operators $F = \sum_{i=1}^{6} F_i$, which changes the particle number by two. And the *seagull interaction* S can be written as a sum of seven operators $S = \sum_{i=1}^{7} S_i$, which acts only between Fock states with the same particle number. The F- and S-interactions are as well connected to a number of matrix elements. The matrix elements and their corresponding energy graphs are discussed in detail in Ref.[10]. The Hamiltonian in Fock-space representation is therefore a sum of the kinetic energy plus vertex-, fork- and seagull-interaction contributions.

Now it has to be translated into a relativistic Hamiltonian eigenvalue problem.

In the front form such an eigenvalue problem is in principle given by

$$H|\Psi\rangle = \frac{M^2 + \vec{P}_\perp^2}{P^+}|\Psi\rangle \quad , \quad \text{with} \quad H = P^- \quad . \tag{4}$$

This has several advantages: with P^+ always being positive, there are only positive eigenvalues. It contains no square-root operator, which would restrict the eigensolutions to be determined in the rest frame. The boost-operators are kinematic and the formulation can be done frame-independently. The eigenstates are defined by

$$|\Psi\rangle = \sum_n \int d[\mu_n] |\mu_n\rangle \Psi_{n/h}(\mu) \quad , \tag{5}$$

with $|\mu_n\rangle$ a complete set of basis Fock-states, $\Psi_{n/h}(\mu) \equiv \langle \mu_n | \Psi \rangle$ the wave functions, and h indicating the hadronic particle. The basis of Fock-states is constructed by the application of products of free field creation operators to the vacuum state $|0\rangle$. Those operators create bare particles, i.e. leptons, anti-leptons, vector bosons, which are all 'on-shell': $(k_\mu k^\mu)_i = m_i^2$.

Each Fock state $|\mu_n\rangle = |n : k_i^+, \vec{k}_{\perp i}, \lambda_i\rangle$ is an eigenstate of P^+, $\vec{P}_\perp$, and the free part of the energy P_0^-, with eigenvalues

$$P^+ = \sum_{i \in n} k_i^+ \quad , \quad \vec{P}_\perp = \sum_{i \in n} \vec{k}_{\perp i} \quad , \quad P_0^- = \sum_{i \in n} \frac{m_i^2 + k_{\perp i}^2}{k_i^+} \quad . \tag{6}$$

Since k_i^+ and P^+ are positive, boost-invariant momentum fractions can be defined

$$x_i = \frac{k_i^+}{P^+} \quad , \qquad \text{with} \quad 0 < x_i < 1 \quad ,$$

as well as boost-invariant intrinsic transverse momenta $\vec{k}_{\perp i}$. Corresponding to the intrinsic frame $\vec{P}_\perp = \vec{0}$ their values are fixed at

$$\sum_{i \in n} x_i = 1 \quad \text{and} \quad \sum_{i \in n} \vec{k}_{\perp i} = \vec{0} \quad .$$

All particles in a Fock state $|\mu_n\rangle$ have a boosted four-momentum

$$p_i^\mu \equiv (p^+, \vec{p}_\perp, p^-)_i = \left(x_i P^+, \vec{k}_{\perp i} + x_i \vec{P}_\perp, \frac{m_i^2 + (\vec{k}_{\perp i} + x_i \vec{P}_\perp)^2}{x_i P^+} \right) \quad .$$

Therefore the free invariant mass square of a Fock state is developed as follows

$$\begin{aligned} M_0^2 &= (p_1 + p_2 + \ldots + p_{n_i})^2 \\ &= P^+ P_0^- - \vec{P}_\perp^2 \\ &= P^+ \left(\sum_{i \in n} \frac{m_i^2 + k_{\perp i}^2}{k_i^+} \right) - \vec{P}_\perp^2 \\ &= \sum_{i \in n} \left(\frac{m_i^2 + (\vec{k}_{\perp i} + x_i \vec{P}_\perp)^2}{x_i} \right) - \vec{P}_\perp^2 \\ &= \sum_{i \in n} \left(\frac{m^2 + \vec{k}_\perp^2}{x} \right)_i \quad . \end{aligned} \tag{7}$$

The evaluation includes the fact that the Fock and the physical vacuum have eigenvalues zero, as well as the restriction to $k^+ > 0$. On the light-cone, each particle forming a zero-momentum state must have a small k^+. The free or Fock space vacuum $|0\rangle$ is then an exact eigenstate of the full front-form Hamiltonian. The vacuum in QCD is undoubtedly more complicated due to the possibility of color-singlet states with $P^+ = 0$ built on zero-mode massless gluon quanta, but the physical vacuum in the front form is still far simpler than in the usual instant form.

The last expression of the free invariant mass square in Eq.(7) is a direct consequence of the transverse boost properties. Conventionally, the phase space integration is given by

$$\int d[\mu_n] \ldots = \sum_{\lambda_i \in n} [dx_i d^2 k_{\perp i}] \ldots \quad ,$$

λ being the helicity, which brings Eq.(4) into the form of an infinite set of coupled integral equations. Since P^+ and $\vec{P}_\perp$ are diagonal operators it is possible to define a *light-cone Hamiltonian* H_{LC} as the operator

$$H_{LC} = P^+ P^- - \vec{P}_\perp^2 = P^\mu P_\mu \ , \tag{8}$$

so that its eigenvalues correspond to the invariant mass spectrum M_i^2:

$$H_{LC} |\Psi_i\rangle = M_i^2 |\Psi_i\rangle \ . \tag{9}$$

H_{LC} itself is a Lorentz scalar and the wave functions are boost-invariant, features that reflect the kinematical structure of the boost operators. With respect to the following calculations on mesons we consider a pion in QCD with momentum $P = (P^+, \vec{P}_\perp)$, described by

$$|\pi : P\rangle = \sum_{n=1}^{\infty} \int d[\mu_n] \left| n : x_i P^+, \vec{k}_{\perp i} + x_i \vec{P}_\perp, \lambda_i \right\rangle \Psi_{n/\pi}(x_i, \vec{k}_{\perp i}, \lambda_i) \quad ,$$

with the sum over all Fock space sectors. The ability to specify the wave function frame-independently is a special feature of light-cone quantization. The wave functions $\Psi_{n/\pi}$ do not depend on the total momentum, since x_i is the longitudinal momentum fraction carried by the i^{th} parton and $\vec{k}_{\perp i}$ is its momentum "transverse" to the direction of the meson; both of them are frame-independent quantities. Those wave functions are the probability amplitudes to find a Fock state of bare particles in a physical pion. The attempt to solve Eq.(9) is seriously complicated by *ultraviolet singularities* occuring at very large values of the transverse momenta, and *endpoint singularities* caused by longitudinal momenta close to $x \sim 0$ or $x \sim 1$. Those difficulties demand the introduction of a cut-off, Λ, to regulate the theory, which in turn has to be removed by regularization group analysis. Apart from the fact that such an analysis is not available at the moment, one is confronted with an infinite number of coupled integral equations. Their nature is hidden in the structure of the kernel

$$\langle n|H_{LC}|n'\rangle \equiv \langle n : x_i, \vec{k}_{\perp i}, \lambda_i|H_{LC}|n' : x_i', \vec{k}_{\perp i}', \lambda_i'\rangle \quad .$$

Fig. 2 displays the structure of this many-body problem. Its analysis shows that more than the half of the matrix elements are zero. This is due to the fact that the Hamiltonian is zero for all sectors whose particle number difference is larger than two. All other matrix elements are represented blockwise by the same energy diagram. The infinite coupled integral equations behind that scenery are not easy to handle. However, with periodic boundary conditions they are transformed into a set of coupled matrix equations, which makes field theory more transparent. This procedure is named *Discretized Light-Cone Quantization* (DLCQ). In 3+1 dimensions it has the ambitious goal to calculate spectra and wave functions of physical hadrons from a covariant gauge theory. This approach depends on a fixed cut-off Λ. But the dimensionality of the Hamiltonian matrix increases exponentially with this cut-off.

This problem of dimensional excess is similar to that in conventional many-body physics, where the diagonalization of finite matrices with exponentially large dimensions (typically $> 10^6$) is required. In QFT it is more difficult since the particle number is unlimited. Therefore an *effective theory* is needed which acts in smaller matrix spaces and which has a well defined relation to the full interaction. This is also helpful for the physical understanding. The main goal is to determine an exact effective interaction between a quark and an anti-quark in a meson. To achieve

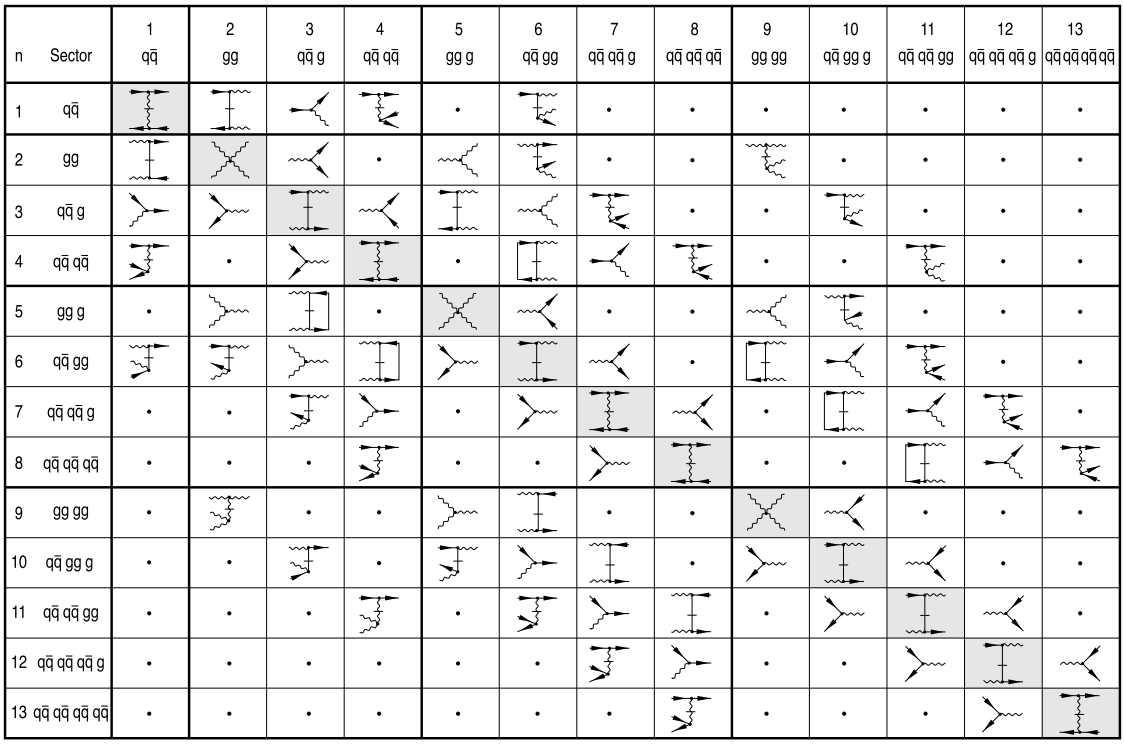

Figure 2: *The Hamiltonian matrix for a meson. The matrix elements are represented by energy diagrams. Within each block they are all of the same type: either vertex, fork or seagull diagrams. Zero matrices are denoted by a dot (·). The single gluon is absent since it cannot be color neutral [10].*

this, the Hamiltonian DLCQ-matrix is discussed in terms of block matrices. Fock space sectors appear quite naturally in a gauge theory and each sector has a finite number of Fock states. Therefore Eq.(9) is rewritten as a block matrix equation with $E_i \equiv M_i^2$,

$$\sum_{j=1}^{N} \langle i|H_{LC}|j\rangle\langle j|\Psi\rangle = E\langle i|\Psi\rangle \qquad \forall \;\; i = 1, 2 \ldots N \;\; . \tag{10}$$

This matrix can now be mapped identically on a matrix equation which only acts in sector $|n = 1\rangle$. Such an effectiveness is based on the approach of Tamm [12] and Dancoff [13]. Their approach can be interpreted as a reduction of the matrix dimension from $N \to N - 1$. It has been extended to the method of *iterated resolvents*, which truncates the matrix step by step until sector $|1\rangle$ is reached. The whole procedure is summarized in a recursion relation, which describes all intermediate steps. Because of this recursive character any higher sector wave function can

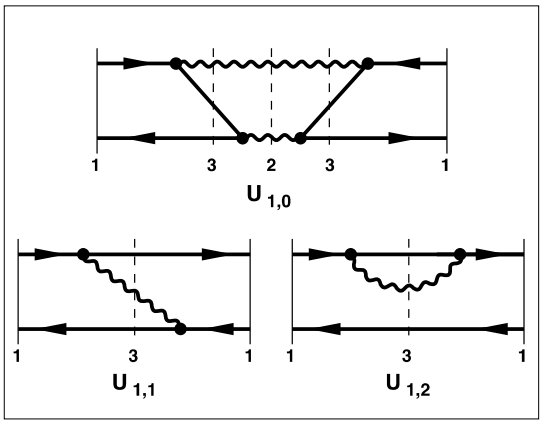

Figure 3: *The three graphs of the effective interaction in the $q\bar{q}$-space.*

be retrieved by matrix multiplications from the eigenfunction in the lowest sector from $\langle 1|\Psi\rangle$. No additional matrix diagonalizations or inversions are required. The method of iterated resolvents is applicable to any many-body theory.

In the continuum limit, the resolvents are replaced by propagators and the eigenvalue problem

$$H_{\rm eff}|\Psi\rangle = M_i^2|\Psi\rangle$$

becomes again an integral equation, but now rather transparent in only three continuous variables $(x, \vec{k}_\perp)$:

$$M_i^2\langle x,\vec{k}_\perp;\lambda_q,\lambda_{\bar{q}}|\Psi_i\rangle = \left[\frac{\overline{m}_q^2+\vec{k}_\perp^2}{x}+\frac{\overline{m}_{\bar{q}}^2+\vec{k}_\perp^2}{1-x}\right]\langle x,\vec{k}_\perp;\lambda_q,\lambda_{\bar{q}}|\Psi_i\rangle \tag{11}$$

$$+\sum_{\lambda_q',\lambda_{\bar{q}}'}\int dx'd^2\vec{k}_\perp'\; R(x',k_\perp')\,\langle x,\vec{k}_\perp;\lambda_q,\lambda_{\bar{q}}|U_{\rm OGE}|x',\vec{k}_\perp';\lambda_q',\lambda_{\bar{q}}'\rangle\,\langle x',\vec{k}_\perp';\lambda_q',\lambda_{\bar{q}}'|\Psi_i\rangle$$

$$+\sum_{\lambda_q',\lambda_{\bar{q}}'}\int dx'd^2\vec{k}_\perp'\; R(x',k_\perp')\,\langle x,\vec{k}_\perp;\lambda_q,\lambda_{\bar{q}}|U_{\rm TGA}|x',\vec{k}_\perp';\lambda_q',\lambda_{\bar{q}}'\rangle\,\langle x',\vec{k}_\perp';\lambda_q',\lambda_{\bar{q}}'|\Psi_i\rangle,$$

represented by the graphs in Fig. 3. This clarifies that QCD has only two structurally different contributions to the effective interaction in the $q\bar{q}$-space: one flavor-conserving and one flavor-changing part. In a diagram both look like low order perturbative graphs, see Fig. 3. The effective one-gluon exchange $U_{OGE} = (U_{1,1}, U_{1,2})$ conserves the flavor along the quark line and describes all fine- and hyperfine interactions. The vertex interaction V creates a gluon and scatters the system virtually into the $q\bar{q}g$-space. As indicated in the figure by the vertical dashed line with subscript

'3', the three particles propagate there under impact of the full Hamiltonian before the gluon is absorbed. This can be done either by the quark or the anti-quark. If it is absorbed by the quark, it contributes to the effective quark mass, $\overline{m}$. The second term in Eq.(11), the effective two-gluon annihilation interaction U_{TGA} is represented by the graph $U_{1,0}$ in Fig. 3. The virtual annihilation of the $q\bar{q}$-pair into two gluons can generate an interaction between different quark flavors.

By and large, the effective interaction scatters a quark with helicity λ_q and four-momentum $p = (xP^+, x\vec{P}_\perp + \vec{k}_\perp, p^-)$ into a state with λ_q' and momentum $p' = (x'P^+, x'\vec{P}_\perp + \vec{k}_\perp', p'n^-)$ and correspondingly the anti-quark.

The domain of integration is set by the cut-off function

$$R(\Lambda) = \Theta\left((p_1 + p_2)^2 - (m_1 + m_2)^2 - \Lambda^2\right) \quad , \tag{12}$$

which is a condition for vertex regularization. The eigenvalues refer to the invariant mass M_i of a physical state. The wave function $\langle x, \vec{k}_\perp; \lambda_q, \lambda_{\bar{q}} | \Psi_i \rangle$ gives the probability amplitude for finding in the $q\bar{q}$-state a flavored quark with momentum fraction x, intrinsic transverse momentum $\vec{k}_\perp$ and helicity λ_q, and correspondingly an anti-quark with $1-x$, $-\vec{k}_\perp$ and $\lambda_{\bar{q}}$. Both, the mass and the wave functions are boost-invariant. The included mass terms are the effective quark masses $\overline{m}_1$ and $\overline{m}_2$ yielded by the diagram $U_{1,2}$ in Fig. 3, i.e.

$$\overline{m}_f^2 = m_f^2 + m_f^2 \frac{\alpha}{\pi} \frac{n_c^2 - 1}{2n_c} \ln \frac{\Lambda^2}{m_g^2} \quad . \tag{13}$$

A similar diagram for the effective gluon mass gives

$$\overline{m}_g^2 = m_g^2 - \frac{\alpha}{4\pi} \sum_f m_f^2 \ln\left(1 + \frac{\Lambda^2}{4m_f^2}\right) \quad . \tag{14}$$

Both are obtained by light-cone perturbation theory [10] combined with vertex regularization. If the free, but perturbative propagators are now substituted by non-perturbative ones, additional graphs to $q\bar{q}$ and gg vacuum polarization will appear. So, the emission and absorption of a gluon along the same quark line changes the bare mass m_f into the physical quark mass $\overline{m}_f$. On the other hand the emission of a gluon from a quark and its absorption by an anti-quark represents an interaction. Therefore it is possible to replace $2m_f \to 2\overline{m}_f \to \mu_f$. Similar considerations hold for the gluon loop and lead to $2m_g \to 2\overline{m}_g \to \mu_g$. Both μ_f and μ_g are interpreted as physical mass scales. The physical gluon mass $\overline{m}_g$ vanishes due to gauge invariance. From a resummation to all orders of the corresponding diagonal propagator

products the effective coupling constant $\overline{\alpha}$ can be extracted for sufficiently large Λ, i.e.

$$\begin{aligned} \overline{\alpha}(Q;\Lambda) &= \frac{1}{1/\alpha - b_0 \ln\left(\Lambda^2/\kappa^2\right) + b(Q)} \qquad (15) \\ \text{with} \qquad & b(Q) = \frac{11 n_c}{12\pi} \ln\left(\frac{\kappa^2}{\mu_g^2 + Q^2}\right) - \frac{1}{6\pi} \sum_f \ln\left(\frac{\kappa^2}{\mu_f^2 + Q^2}\right) \quad . \end{aligned}$$

The constant b_0 is identified by the number of colors and flavors, i.e. $b_0 = (11 n_c - 2 n_f)/12\pi$. The parameter κ is identical to the so-called QCD-scale Λ_{QCD}. Hence, the effective fine structure constant depends on the momentum transfer Q^2 across the vertex and the cut-off Λ.

Now that the effective Hamiltonian is evaluated, it is discussed in more detail and the hadron bound state problem is faced. In this thesis a divergence has to be analyzed. Therefore the whole equation is restricted to a more appropriate model to work out the main effects before starting the discussion of the complete and more complicated equation. In the next Section, 3.1, the applied approximations are explained, and in Section 3.2 regularization comes in. There, the details of renormalization are also discussed.

3 Derivation of the model equation

In this section the derivation of the model is described. Sect. 3.1 introduces the main approximations that restrict the whole equation to a simple model. In Section 3.2 the divergence of the integral kernel is discussed and regulated.

3.1 Evaluation of a model for scalar mesons

The front-form Hamiltonian for QCD has been reduced in Section 2.2 to an effective Hamiltonian, which by definition acts only in the Fock space of one quark (q) and one anti-quark ($\bar{q}$). By excluding flavor-diagonal mesons, as it is the case in this thesis, the two-gluon annihilation interaction can be disregarded. The resulting integral equation in (light-cone) momentum space is (the subscript h indicates the hadron)

$$M_h^2\langle x,\vec{k}_\perp;\lambda_q,\lambda_{\bar{q}}|\Psi_h\rangle = \left[\frac{\overline{m}_q^2(\Lambda)+\vec{k}_\perp^{\,2}}{x}+\frac{\overline{m}_{\bar{q}}^2(\Lambda)+\vec{k}_\perp^{\,2}}{1-x}\right]\langle x,\vec{k}_\perp;\lambda_q,\lambda_{\bar{q}}|\Psi_h\rangle \qquad (16)$$
$$+\sum_{\lambda_q',\lambda_{\bar{q}}'}\int dx'd^2\vec{k}_\perp'^{\,2}\langle x,\vec{k}_\perp;\lambda_q,\lambda_{\bar{q}}|U_{OGE}|x',\vec{k}_\perp';\lambda_q',\lambda_{\bar{q}}'\rangle\langle x',\vec{k}_\perp';\lambda_q',\lambda_{\bar{q}}'|\Psi_h\rangle \quad .$$

An essential achievement of the last section is that the kernel of this integral equation can be written in the explicit form

$$\langle\lambda_q,\lambda_{\bar{q}}|U_{OGE}|\lambda_q',\lambda_{\bar{q}}'\rangle = -\frac{1}{4\pi^2}\frac{4}{3}\frac{\overline{\alpha}(Q)}{Q^2}\langle\lambda_q,\lambda_{\bar{q}}|S(Q)|\lambda_q',\lambda_{\bar{q}}'\rangle\frac{R(x',k_\perp';\Lambda)}{\sqrt{x(1-x)x'(1-x')}} \quad . \qquad (17)$$

All many-body effects reside in the effective quark mass $\overline{m}_q(\Lambda)$ given in Eq.(13) and in the effective coupling constant $\overline{\alpha}(Q;\Lambda)$ (Eq. 15). The first term on the r.h.s. of Eq.(16) is the free invariant mass-square of the quarks in relative motion. At equilibrium,

$$x\equiv\overline{x}\equiv\frac{\overline{m}_1}{\overline{m}_1+\overline{m}_2} \quad , \quad \vec{k}_\perp=0 \quad , \qquad (18)$$

these quarks are in rest relative to each other, and the invariant mass-square becomes the value $(\overline{m}_1+\overline{m}_2)^2$. To remove this 'frozen mass' from both sides it is convenient to introduce [14]

$$T = \left(\frac{\overline{m}_1^2+\vec{k}_\perp^{\,2}}{x}+\frac{\overline{m}_2^2+\vec{k}_\perp^{\,2}}{1-x}\right)-(\overline{m}_1+\overline{m}_2)^2 \quad , \qquad (19)$$

$$D = M^2-(\overline{m}_1+\overline{m}_2)^2 \quad . \qquad (20)$$

Here, $T/(2m_s)$ behaves like the conventional kinetic energy and $D/(2m_s)$ like the conventional binding energy. In the following the reduced mass and the sum are used,

$$\frac{1}{m_r} = \frac{1}{\overline{m}_1} + \frac{1}{\overline{m}_2} \ , \qquad m_s = (\overline{m}_1 + \overline{m}_2) \ \ , \tag{21}$$

which only makes sense when the constituent quark masses are different from zero. The second term on the r.h.s. of Eq.(16) is the relativistic interaction. Its most important aspect is the Coulomb denominator $1/Q^2$. The four-momentum transfer Q^2 is the mean of the single four-momentum transfers between quark and anti-quark,

$$\begin{aligned} Q^2 &= (\vec{k}_\perp - \vec{k}'_\perp)^2 + \frac{(x-x')^2}{2}\left[\frac{m_1^2}{xx'} + \frac{m_2^2}{(1-x)(1-x')}\right] \\ &+ \frac{(x-x')^2}{2}\left[k_\perp^2\left(\frac{1}{1-x} - \frac{1}{x}\right) - k_\perp'^2\left(\frac{1}{1-x'} - \frac{1}{x'}\right)\right] \ \ , \end{aligned} \tag{22}$$

i.e. $Q^2 = (Q_1^2 + Q_2^2)/2$ with $Q_1^2 = Q_q^2 = -(k_q - k'_q)^2$ and $Q_2^2 = Q_{\bar{q}}^2 = -(k_{\bar{q}} - k'_{\bar{q}})^2$. Close to the Coulomb singularity it is legitimate to write $Q^2 = (\vec{k} - \vec{k}')^2$ since both parts are approximately equal [15]. The spinor factor

$$S \equiv \langle \lambda_q, \lambda_{\bar{q}} | S(Q) | \lambda'_q, \lambda'_{\bar{q}} \rangle = \left[\overline{u}(k_q, \lambda_q)\gamma^\mu u(k'_q, \lambda'_q)\right] \left[\overline{u}(k_{\bar{q}}, \lambda_{\bar{q}})\gamma_\mu u(k'_{\bar{q}}, \lambda'_{\bar{q}})\right] \tag{23}$$

represents the current-current coupling and describes all Coulomb, fine and hyperfine interactions. The subscripts on S are dropped when not required. The Dirac spinors are solutions of the free Dirac equations

$$(\gamma^\mu k_\mu - \overline{m})u(k,\lambda) = 0 \ , \ \text{and} \ \ (\gamma^\mu k_\mu + \overline{m})v(k,\lambda) = 0 \ \ . \tag{24}$$

The cut-off function R sets the domain of integration and is defined in Eq.(12).

The goal of reducing the many-body problem of $M^2 = H_{LC}$ to a single-body problem with an effective interaction is reached now. Similar equations for QED have previously been solved numerically [16, 17]. But the solutions for QED and QCD still depend on the cut-off parameter Λ. Therefore, it has to be removed by renormalization group analysis, which is one of the main issues of gauge theory. This is going to be discussed in Sect. 3.2.

The present section is the foundation for later calculations. Therefore a number of assumptions and approximations are introduced to rewrite the equation in order to achieve a clearer starting-point.

Eq.(16) has two different domains of integration. The longitudinal momentum fraction over the range $0 \leq x \leq 1$ and the transversal momentum in the interval $-\infty \leq k_{\perp,x} \leq \infty$. It is useful [16, 17] to transform the light-cone integration variables $(x, \vec{k}_\perp)$ to a new coordinate system $(k_z, \vec{k}_\perp)$ by

$$x = x(k_z) = \frac{E_1 + k_z}{E_1 + E_2} \qquad \text{with} \quad E_{1,2} = \sqrt{\overline{m}_{1,2}^2 + \vec{k}_\perp^{\,2} + k_z^2} \; . \tag{25}$$

All components of $\vec{k} = (k_z, \vec{k}_\perp)$ then have the same domain. The corresponding Jacobian is

$$\frac{dx}{x(1-x)} = \frac{1}{m_r} \frac{dk_z}{A(x, \vec{k}_\perp)} \; , \tag{26}$$

with A defined by

$$A(x, \vec{k}_\perp) \equiv \frac{1}{m_r} \frac{E_1 E_2}{E_1 + E_2} \; . \tag{27}$$

The factor A is absorbed by a redefinition of the wave function Ψ,

$$\Psi \equiv \langle x, \vec{k}_\perp; \lambda_q, \lambda_{\bar{q}} | \Psi_h \rangle = \sqrt{\frac{A(x, \vec{k}_\perp)}{x(1-x)}} \phi(x, \vec{k}_\perp) \; . \tag{28}$$

Setting the conventional kinetic energy in Eq.(19)

$$T(k) \equiv C(k) \vec{k}^2 \quad \text{with} \quad C(k) = (E_1 + \overline{m}_1 + E_2 + \overline{m}_2) \left(\frac{1}{E_1 + \overline{m}_1} + \frac{1}{E_2 + \overline{m}_2} \right) \; , \tag{29}$$

and replacing the invariant mass-square eigenvalue M_h^2 by the binding energy D, see Eq.(20), the original integral equation (16) finally becomes

$$\left[D - C(k) \vec{k}^2 \right] \phi(\vec{k}) = -\frac{1}{4\pi^2 m_r} \int \frac{d^3 \vec{k}'}{\sqrt{A(\vec{k}) A(\vec{k}')}} \frac{4}{3} \frac{\overline{\alpha}(Q)}{Q^2} SR \, \phi(\vec{k}') \; . \tag{30}$$

Therein the explicit reference to the helicity (λ_1, λ_2) has been dropped.

At this point it is completely irrelevant that the equation actually holds for the front form, since it is still exact. Its origin is simply not recognized. It could be an equation in the instant form, where only the (usual) three momenta $\vec{k}$ play the role of integration variables. Fourier transforming it to configuration space would however not be trivial, since the factor $A(x, \vec{k}_\perp)$ prevents all attempts to do that in a standard way.

Since obtaining a recipe for this non-trivial integral equation to be solved directly in momentum space is a primary goal, the non-relativistic approximation is applied

under the integral for simplicity reasons. Therefore, the function is set to

$$\begin{aligned} A(\vec{k}) \simeq A(\vec{k}') &= 1 \ , \\ Q^2 &= (\vec{k}-\vec{k}')^2 \ , \\ C(k) &= \frac{m_s}{m_r} \ . \end{aligned} \tag{31}$$

In complete analogy to the relativistic case, the non-relativistic equation is given by

$$\left[D - \frac{m_s}{m_r}\vec{k}^2\right]\phi(\vec{k}) = -\frac{1}{4\pi^2 m_r}\int d^3\vec{k}'\frac{4}{3}\frac{\overline{\alpha}(Q)}{Q^2}SR\,\phi(\vec{k}') \ . \tag{32}$$

The effects of the complete relativistic expression are discussed in Sect. 6.1. But on the light cone, a non-relativistic equation is an excellent approximation to a relativistic covariant equation.

Actually, Eq.(32) holds for all possible couplings $\overline{\alpha}(Q)$, the spin content S and cut-offs R. To derive a simple description for a $q\bar{q}$-pair those three terms have to be discussed carefully. The coupling $\overline{\alpha}(Q)$ given in Eq.(15) represents a next-to-lowest order approximation (NLA). In the lowest order approximation (LOA) the effective mass $\overline{m}$ coincides with the bare Lagrangian mass m: $\overline{m} = m$, and the effective coupling constant $\overline{\alpha}(Q)$ is equal to the bare Lagrangian coupling constant $\alpha = g^2/4\pi$: $\overline{\alpha} = \alpha$. To this level of approximation, QED and QCD differ by the color factor $(n_c^2-1)/2n_c = 4/3$ for $n_c = 3$.

This thesis uses $\overline{\alpha} = \alpha$ which is sufficient for a simple model and leaves open the possibility to compare the results with known ones from QED. The approximation of the coupling $\overline{\alpha}$ to a constant is also required for a Fourier transformation of the main equation (Eq. 32) to the configuration space. To keep this transformation as simple as possible, the helicity contribution S should be a constant, too. Therefore, a thorough study by spinor analysis of

$$\begin{aligned} \langle\lambda_q,\lambda_{\bar{q}}|T|\lambda_q',\lambda_{\bar{q}}'\rangle &\equiv \frac{1}{2}\frac{\langle\lambda_q,\lambda_{\bar{q}}|S|\lambda_q',\lambda_{\bar{q}}'\rangle}{\sqrt{xx'}\sqrt{(1-x)(1-x')}} \\ &= \frac{1}{2}\frac{[\overline{u}(k,\lambda)\gamma^\mu u(k',\lambda')]_q}{\sqrt{xx'}}\frac{[\overline{u}(k,\lambda)\gamma_\mu u(k',\lambda')]_{\bar{q}}}{\sqrt{(1-x)(1-x')}} \ , \end{aligned} \tag{33}$$

with

$$\langle \lambda_q, \lambda_{\bar{q}} | T | \lambda'_q, \lambda'_{\bar{q}} \rangle = \begin{array}{c} \\ \uparrow\downarrow \\ \downarrow\uparrow \\ \uparrow\uparrow \\ \downarrow\downarrow \end{array} \begin{array}{c} \begin{array}{cccc} \uparrow\downarrow & \downarrow\uparrow & \uparrow\uparrow & \downarrow\downarrow \end{array} \\ \begin{pmatrix} T_{11} & T_{12} & T_{13} & T_{14} \\ T_{21} & T_{22} & T_{23} & T_{24} \\ T_{31} & T_{32} & T_{33} & T_{34} \\ T_{41} & T_{42} & T_{43} & T_{44} \end{pmatrix} \end{array} , \tag{34}$$

is needed.

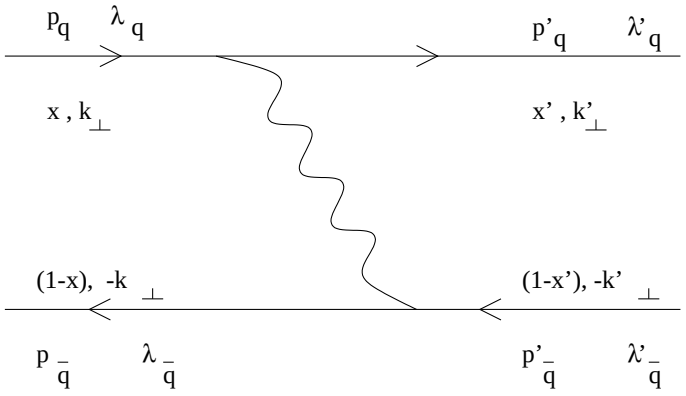

Figure 4: *The relevant vertex interaction graph with corresponding momenta and helicities.*

Fig.4 shows the relevant vertex interaction graph with corresponding momenta and helicities. In the spinor convention of Lepage and Brodsky [18], S has the dimension $[mass^2]$. The matrix elements of T are calculated with respect to the rules given in [10], Table 5. The diagonal and off-diagonal matrix elements are tabulated in App. A. They are given for different quark and anti-quark masses and with a phase φ according to $\vec{k}_\perp$. The upper and lower half of the off-diagonal elements are connected by $T_{ij} = T^*_{ji}(q \leftrightarrow \bar{q})$.

It can be recognized that all off-diagonal matrix-elements vanish for $m_i = 0$, $i = 1, 2$. Therefore, T can be divided into a massive part T_m and a mass-independent one T_0 (with a similar decomposition for S): $T = T_m + T_0$, where T_0 survives the massless limit by definition. It turns out to be diagonal in the helicities, with two contributions to the amplitude, for parallel ($T_{\uparrow\uparrow,\ \downarrow\downarrow}$) and anti-parallel ($T_{\uparrow\downarrow,\ \downarrow\uparrow}$) helicities. Using this knowledge to simplify the matrix-elements, they are given by

$$T_{11} \;=\; T_{22} = \frac{m_1^2}{xx'} + \frac{m_2^2}{(1-x)(1-x')} + T_{\uparrow\downarrow,\ \downarrow\uparrow} \ , \tag{35}$$

$$T_{33} = T_{44} = \frac{m_1^2}{xx'} + \frac{m_2^2}{(1-x)(1-x')} + T_{\uparrow\uparrow,\,\downarrow\downarrow} \ , \tag{36}$$

with

$$T_{\uparrow\downarrow,\,\downarrow\uparrow} = \frac{k_\perp^2}{x(1-x)} + \frac{k_\perp'^2}{x'(1-x')} + k_\perp k_\perp' \left(\frac{e^{-i(\varphi-\varphi')}}{xx'} + \frac{e^{i(\varphi-\varphi')}}{(1-x)(1-x')} \right) \ , \tag{37}$$

$$T_{\uparrow\uparrow,\,\downarrow\downarrow} = \frac{k_\perp k_\perp' e^{-i(\varphi-\varphi')}}{x(1-x)x'(1-x')} \ . \tag{38}$$

Choosing the equilibrium (Eq. 18) and restricting to singlet amplitudes the matrix elements T_{ij} and the momentum transfer Q^2 simplify to

$$T_{11} = T_{22} = 2(m_1+m_2)^2 + \frac{(m_1+m_2)^2}{m_1 m_2} \vec{k'}_\perp^{\,2} \ , \tag{39}$$

$$T_{33} = T_{44} = 2(m_1+m_2)^2 \ , \tag{40}$$

$$T_{12} = 0 \ , \tag{41}$$

$$T_{13} = -k_\perp' e^{i\varphi'} \frac{(m_1+m_2)^2}{m_2} \sim 0 \ , \tag{42}$$

with $Q^2 = \vec{k'}_\perp^{\,2}$

$$T_{\uparrow\uparrow,\,\downarrow\downarrow} = 0 \quad \rightarrow \quad T_{\uparrow\downarrow,\,\downarrow\uparrow} = \frac{(\vec{k'}_\perp)^2}{xy} \quad \rightarrow \quad \frac{S_{\uparrow\downarrow,\,\downarrow\uparrow}}{Q^2} = 2 \tag{43}$$

Therefore, for the mass-independent part the helicity S is a number for all values of $\vec{k'}_\perp$. The evaluation of the massive part at kinematical rest shows as well a diagonal content:

$$\langle \lambda_q, \lambda_{\bar{q}} | S_m | \lambda_q', \lambda_{\bar{q}}' \rangle = 4 m_1 m_2 \ \delta_{\lambda_q,\lambda_q'} \delta_{\lambda_{\bar{q}},\lambda_{\bar{q}}'} \tag{44}$$

Considering only the simple singlet amplitude $(\lambda_q, \lambda_{\bar{q}}) = (\uparrow, \downarrow)$, the helicity contribution becomes $(S = S_0 + S_m)$

$$\frac{\langle \uparrow\downarrow \, |S| \, \uparrow\downarrow \rangle}{Q^2} = \frac{4 m_1 m_2}{Q^2} + 2 \ . \tag{45}$$

This result is essential and thus used in the kernel of the model integral equation. The consequences of the additive constant 2 in the kernel are closely connected with the cut-off function R, used in the model. Because of its special importance this will be discussed in the next section.

3.2 The Divergence

The equation has now the following shape

$$\left[D - \frac{m_s}{m_r}\vec{k}^2\right]\phi(\vec{k}) = -\frac{1}{4\pi^2 m_r}\int d^3\vec{k}'\frac{4}{3}\alpha\left[\frac{4m_1m_2}{Q^2}+2\right]R\,\phi(\vec{k}') \tag{46}$$

The main problem here is that the kernel

$$-\frac{1}{4m_r}\frac{4}{3}\alpha\frac{S}{Q^2}R \qquad \text{with} \quad \frac{S}{Q^2} = \frac{4m_1m_2}{Q^2}+2$$

is divergent. Therefore, the regulator function R has to be fixed. According to the regulator the equation has to be renormalized. With D being $M_h^2 - m_s^2$, all eigenvalues M_h^2 depend on the cut-off Λ, the bare masses m and the bare α. Those are auxiliary parameters and are replaceable by means of the modern interpretation of QFT by $(m_\Lambda, \alpha_\Lambda)$, functions of Λ, such that the eigenvalues are cut-off independent, i.e.

$$\frac{d}{d\Lambda}M_h^2(\Lambda, \alpha_\Lambda, m_\Lambda)) = 0 \qquad \forall n \quad . \tag{47}$$

The effective Hamiltonian $H = H_{LC}^{\text{eff}}$ depends on Λ only through $\overline{m}_f$, $\overline{\alpha}$ and the regulator R. The fundamental equation of the renormalization group (Eq. 47) can then be expressed in operator form

$$d\overline{m}_f\frac{\partial H}{\partial \overline{m}_f}|\Psi_h\rangle + d\overline{\alpha}\frac{\partial H}{\partial \overline{\alpha}}|\Psi_h\rangle + dR\frac{\partial H}{\partial R}|\Psi_h\rangle = 0 \quad . \tag{48}$$

To vary all three terms simultaneously causes severe problems. Therefore, the equation is divided into three independent equations

$$\frac{d}{d\Lambda}\overline{m}_f = 0\ ; \qquad \frac{d}{d\Lambda}\overline{\alpha} = 0\ ; \qquad \frac{dR}{d\Lambda}\frac{\partial H}{\partial R}|\Psi_n\rangle = 0\ . \tag{49}$$

The first two equations are functions of m_Λ, α_Λ. The first one defines the effective flavor masses $\overline{m}_f = \overline{m}_f(\Lambda, \alpha_\Lambda, m_\Lambda)$ as renormalization group invariants. The numerical value of $\overline{m}_f$ must be fixed by experiment. The second equation is then a constraint for α_Λ at fixed values of $\overline{m}_f$. Using the expression for $\overline{\alpha}(Q;\Lambda)$ in Eq.(15) yields then [8]

$$\alpha_\Lambda = \frac{1}{b_0 \ln\left(\frac{\Lambda^2}{\kappa^2}\right)} \qquad \text{, thus} \quad \overline{\alpha}(Q) = \frac{1}{b(Q)} \quad , \tag{50}$$

with b_0 and $b(Q)$ given in Eq.(15). All Λ-dependence cancels exactly in favor of the renormalization group invariant κ. This scale must also be determined by experiment. For a known α_Λ the first equation can be used as a constraint to m_Λ. By

fixing the functions α_Λ and m_Λ all freedom is exhausted [19]. Since the cut-off has been removed by renormalization, Λ can be driven to infinity, thus $R(x', \vec{k'}_\perp; \Lambda) = 1$. Formally, this solves the three equations of renormalization, but the relativistic interaction S/Q^2 in the kernel of the integral equation tends to a constant for large values of $\vec{k'}_\perp$. This causes a problem at large couplings α. The integral kernel after renormalization has then the same shape as in Eq.(46).

Considering the large and small Q^2-limits with $\vec{k'}_\perp \gg \vec{k}_\perp$ shows the connection:

$$\mathcal{K} = \alpha \; S/Q^2 \quad \text{with} \quad S = \begin{cases} 4m_1 m_2 & Q^2 \ll 0 \\ \vec{k'}_\perp^{\,2} & Q^2 \gg 0 \end{cases} \quad . \qquad (51)$$
$$Q^2 = \begin{cases} (\vec{k}_\perp - \vec{k'}_\perp)^2 & Q^2 \ll 0 \\ \vec{k'}_\perp^{\,2} & Q^2 \gg 0 \end{cases}$$

Thus,

$$\frac{S}{Q^2} = \begin{cases} 4m_1 m_2/Q^2 & Q^2 \ll 0 \\ 1 & Q^2 \gg 0 \end{cases} \quad . \qquad (52)$$

Accordingly, at very small momentum transfer $Q^2 \to 0$, where $x \sim x'$ and $\vec{k}_\perp \sim \vec{k'}_\perp$ the effective coupling stays at the finite value $b(0)$, see Eq.(15). The small Q^2-limit of the spinor function S represents the Coulomb-limit of the kernel. Its singularity is square-integrable and can be solved by known numerical techniques [20]. For very large momentum transfer $Q^2 \to \infty$, both S and Q^2 tend to diverge, but their ratio tends to a finite value. Disregarding the very slow logarithmic increase of $b(Q)$, (Eq. 15), the kernel of the integral equation is therefore essentially a dimensionless constant:

$$\mathcal{K} \sim const. \qquad \text{for} \quad Q^2 \to \infty \quad . \qquad (53)$$

This constant has the value 2, because of the proportionality factor between the helicity representation T and S. Therefore the kernel is equal to

$$\mathcal{K} = \frac{1}{b(Q)} \frac{S}{Q^2} = \frac{1}{b(Q)} \left[\frac{4m_1 m_2}{Q^2} + 2 \right] \quad . \qquad (54)$$

There is sufficient evidence [21] that the constant part of the kernel causes all known problems, among which a diverging eigenvalue.

To get rid of the troubleterm a suitable regulator function R has to be fixed. The sharp cut-off as introduced in Eq.(12) is a relic of the Fock-space regularization in DLCQ and not really necessary. This sharp cut-off corresponds to a step-function,

which possibly cuts the tail with most of the information. A possibility to find a suitable regulator function is by multiplying the kernel with a constant factor. Then it can be identically separated into two parts to avoid an infinitive denominator

$$\begin{aligned} \mathcal{K} = \mathcal{K}_1 + \mathcal{K}_2 &= \frac{1}{b(Q)} \frac{S}{Q^2} \frac{\mu^2 + Q^2}{\mu^2 + Q^2} \quad , \\ \mathcal{K}_1 &= \frac{1}{b(Q)} \frac{S}{Q^2} \frac{\mu^2}{(\mu^2 + Q^2)} \quad , \qquad (55) \\ \mathcal{K}_2 &= \frac{1}{b(Q)} S \frac{1}{\mu^2 + Q^2} \quad , \qquad (56) \end{aligned}$$

with an arbitrary mass parameter μ. This method of kernel separation is already known from nuclear physics. Therein it was used to describe the pairing of Cooper-particles in the BCS-theory [22].

The two terms have a quite different behavior. The first one, $\mathcal{K}_1$ (Eq. 55), is well behaved and in the limit of large Q^2 it tends towards a Coulomb singularity. $\mathcal{K}_2$ (Eq. 56) is almost everywhere a constant, as seen before in Eq.(52). Therefore, the addition of a constant to a divergence, here of the kernel, leads again to a divergence. Hence, this is not the best way to fix the regulator, but it gives evidence about the behavior of the kernel.

To get further insight into the approximated integral equation Eq.(46) is discussed more carefully. Start again with Eq.(46):

$$\left[D - \frac{m_s}{m_r} \vec{k}^2 \right] \phi(\vec{k}) = -\frac{4}{3} \frac{\alpha}{\pi^2} \int d^3\vec{k}' \left[\frac{m_s}{Q^2} + \frac{1}{2m_r} \right] R\, \phi(\vec{k}') \quad . \qquad (57)$$

Disregarding the regulator for the moment, $(R = 1)$, the Fourier transformed equation has the shape of a local Schrödinger equation

$$\left[D - \frac{m_s}{m_r} \vec{p}^2 \right] \Psi(\vec{r}) = 2m_s V(r) \Psi(\vec{r}) \quad , \qquad \text{with } \vec{p} \equiv i\vec{\nabla} \; . \qquad (58)$$

The potential $V(r)$ is similar to the familiar non-relativistic hyperfine-interaction in the single channel $V_{hf-s}(r)$

$$\begin{aligned} V(r) &= -\frac{4}{3} \alpha \left(\frac{1}{r} + \frac{2\pi}{m_r m_s} \delta^3(\vec{r}) \right) \quad , \qquad (59) \\ V_{hf-s}(r) &= -\alpha \left(\frac{1}{r} + \frac{\pi}{m_e m_p} \delta^3(\vec{r}) g_p \right) \quad . \qquad (60) \end{aligned}$$

Actually the two expressions are the same with the protons gyromagnetic ratio $g_p = 2$ and if the reduced mass is identified with the electron mass and the summarized

mass with that of the proton.

The way to solve Eq.(58) is well known. First the hyperfine interaction is omitted to receive the Coulomb wave function Ψ_C, then Ψ_C is perturbatively evaluated in first order to derive $\Delta D = 2m_s\frac{4}{3}\langle V_s\rangle$ as an expectation value. Assuming a pion the hyperfine potential is not compatible to the scale given by the pion mass. Therefore the equation has no satisfying solution.

The Delta function is, however, not a suitable function to be regarded as a usual potential. It has to be changed into a distribution without loss of information and worked out in a limiting procedure, realized by regularizing and renormalizing Eq.(46). A possible choice for the regulator function R is with respect to Eq.(55),

$$R = \frac{\mu^2}{\mu^2 + Q^2} \quad , \tag{61}$$

so that

$$\left[D - \frac{m_s}{m_r}\vec{k}^2\right]\phi(\vec{k}) = -\frac{4}{3}\frac{\alpha}{\pi^2}\int d^3\vec{k'}\left[\frac{m_s}{Q^2} + \frac{1}{2m_r}\right]\frac{\mu^2}{\mu^2+Q^2}\phi(\vec{k'}) \quad . \tag{62}$$

Eq.(62) is the main equation of the model. The scale μ does not limit the momentum transfer to any finite value, but it controls the deviation of R from unity. In other words, R is a kind of a 'soft cut-off' and prevents the additive constant to behave like a Dirac Delta-function.

The Fourier transformation of Eq.(62) yields the following potential

$$V(r) = \frac{\alpha}{r}(e^{-\mu r} - 1) - \frac{\alpha}{r}\frac{\mu^2}{2m_r m_s}e^{-\mu r} \quad . \tag{63}$$

Contrary to the 'sharp' Delta-function in Eq.(60) it is here smoothed in the form of a Yukawa potential. The force related to this potential is in dimensionless variables

$$r^2\frac{dV}{dr} = \alpha + \alpha e^{-\mu r}(1+\mu r)\left[\frac{\mu^2}{2m_r m_s} - 1\right] \quad . \tag{64}$$

Close to the origin and for $\mu \to \infty$, it is much stronger than the Coulomb force. But regarding the whole scenery there is asymptotically only the $\frac{1}{r}$-dependence of the Coulomb potential with the coupling $\frac{4}{3}\alpha$ that survives. In fact there is no everlasting confinement.

Since the effects of the constant 2 on the rest of the system are examined, it is at first sufficient to work with the following equation:

$$\left[D - \frac{m_s}{m_r}\vec{k}^2\right]\phi(\vec{k}) = -\frac{4}{3}\frac{\alpha}{\pi^2}\int d^3\vec{k'}\left[\frac{m_s}{Q^2} + \frac{1}{2m_r}\frac{\mu^2}{\mu^2+Q^2}\right]\phi(\vec{k'}) \quad , \tag{65}$$

where only the constant term is regulated and the Coulomb one remains unchanged. This is possible, because the Coulomb potential needs not to be regularized. The Fourier transform corresponding to this model is

$$V(r) = -\frac{4}{3}\frac{\alpha}{r}\left(1 + \frac{\mu^2}{2m_r m_s}e^{-\mu r}\right) \quad , \tag{66}$$

which keeps essentially the same features as regulating the whole potential, see Eq.(63). The main difference comes up for $\mu = 0$. Then Eq.(63) is totally zero, while Eq.(66) is still a Coulomb potential.

In the end the kernel of both main equations (Eqs. 62, 65) is a combined potential of a Coulomb and a smooth Delta-potential. The difference between them is the regulation of the Coulomb potential.

These regulated equations must now be renormalized to become independent of the regularization parameter. Hence, a renormalized coupling constant α_μ must be determined to satisfy the renormalization group equation, Eq.(47). But this is only one part of the renormalization program, which lays the foundation for an extensive calculation of all scalar meson masses with arbitrary flavors. As an example, if the goal is to reproduce the pion masses – especially the π^+ –, the renormalization procedure is started with the choice of the constituent mass for the up- and the down-quark, and of a scale $\mu = \mu_0$. In the next step an $\alpha = \alpha_0$ must be found such that $M_h(\alpha_0, \mu_0) = M_{\pi^+}$. In the following this procedure has to be generalized to all pairs $(\alpha, \mu)_i$ satisfying $M_h(\alpha, \mu)_i = M_{\pi^+}$. Those which are suitable define the renormalized coupling α_μ. With determining α_μ all other quark masses are fixed.

At the moment there is no analytical expression for α_μ, but the numerical value is sufficient for the beginning. It has also to be checked that except for the lowest state (which was used to fix α_μ) even the whole spectrum of excited π^+-states is independent of μ.

In this section the divergence has been analyzed and its consequences have been discussed. Accordingly, the kernel of the integral equation is regulated by a soft cut-off. Afterwards, an outline of the renormalization program executed later in Sect.4.3, 4.4 is given. Generally speaking, all remaining calculations and approximations for the derivation of the model equation (Eq. 62) are performed. For some first examinations of the constant 2, a second model equation (Eq. 65) is introduced.

In the next section the main numerical techniques are presented and the corresponding potentials are discussed in detail.

4 Solving the model equation

In this section all numerical techniques used in this thesis are introduced. By the example of a 'Coulomb minus Yukawa' potential the basic evaluation from the integral equation to a matrix equation is discussed. This relies on an earlier discussed problem [20] and includes a short individual study of the potentials in configuration space and a subsequent Fourier transformation back to momentum space. The model is directly solved in momentum space, since later more complicated functions can not be Fourier transformed anymore. According to a logarithmic divergence of the matrix equation suitable counter terms are needed. This procedure leads to the calculation of eigenvalues and eigenfunctions, where an optimization scale is introduced. Afterwards the reader is guided to the two main equations (Eqs. 62, 65). The renormalization program for the first model equation (Eq. 62) is performed and later extended to the complete problem (Sect. 4.4).

4.1 Behavior in Configuration Space: Coulomb and Yukawa

To study the behavior of the Coulomb and the Yukawa potential individually, the integral equation of reference [20] with equal masses $m_1 = m_2 = m$ is recalled, i.e.

$$\left[E - \frac{\vec{k}^2}{m}\right] \phi(\vec{k}) = -\frac{s^2}{\pi^2} \int d^3\vec{k'}\, \frac{1}{Q^2(Q^2+c^2)}\, \phi(\vec{k'}) \quad \text{with} \qquad Q^2 = (\vec{k}-\vec{k'})^2 \quad , \tag{67}$$

and s^2 a dimensional scale. This looks already like a regularized version of a $1/Q^4$ kernel in the limit $c \to 0$, which is commonly understood as the Fourier transform of a linear potential. Applying the Fourier transformations to configuration space a simple Schrödinger equation is obtained, and the potential is given by

$$V(\vec{x}) = \frac{\beta}{r}\left[e^{-cr} - 1\right] \tag{68}$$

where $\beta = 2s^2/c^2$ is similar to the usual fine-structure constant. The shape of the potential reflects the superposition of a Coulomb and a Yukawa potential, as visualized in Fig. 5. The behavior

$$V(|\vec{x}|) = \begin{cases} -\frac{2s^2}{c} + s^2 r & \text{for } r \to 0 \ , \\ -\frac{2s^2}{c^2}\,\frac{1}{r} & \text{for } r \to \infty \ , \end{cases} \tag{69}$$

can be observed in the figure: For sufficiently small distances the potential is linear (up to an additional constant), and for large r it becomes a Coulomb potential. For

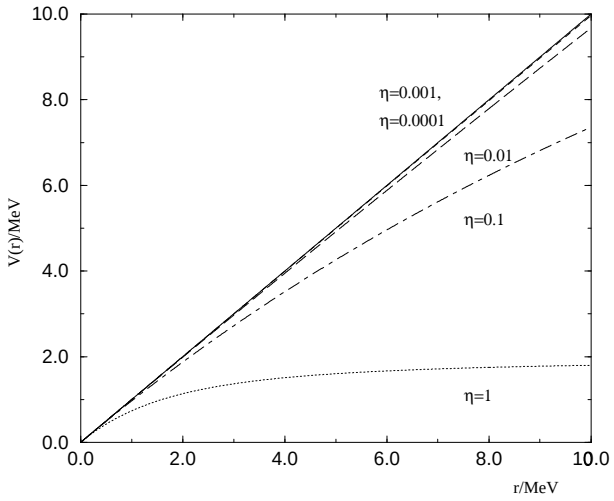

Figure 5: *The potential $V(r)$ is plotted versus r for different values of $\eta = 2c/\beta m$, but with the potential normalized to $V(0) = 0$. – For $r \to 0$ the potential converges to the finite value $-2s^2/c$, with a linear slope.*

either of these extremes the analytic solutions are known. The eigenvalue E used in Eq.(67) depends on the three parameters m, s, and c. It exists a dimensionless combination

$$\eta = \frac{c^3}{ms^2} = \frac{2}{\beta}\frac{c}{m} \ , \tag{70}$$

which appears by introducing dimensionless variables (Bohr units)

$$p = \frac{k}{m_r\beta} \ , \quad q^2 = \frac{Q^2}{m_r^2\beta^2} \ , \quad \varepsilon = \frac{2E}{m_r\beta^2} \ , \tag{71}$$

so that the equation reads

$$\left[\varepsilon - p^2\right]\phi(p) = -\frac{1}{\pi^2}\int d^3p' \left[\frac{1}{q^2} - \frac{1}{q^2+\eta^2}\right]\phi(p') \quad . \tag{72}$$

This equation has two limiting cases:

1. For $\eta \to \infty$ essentially the q^{-2} singularity of the Coulomb problem shows up.

2. For $\eta \to 0$, the q^{-4} singularity corresponding to a linear potential appears, whose eigenfunctions are the Airy functions; This has been the topic of Hersbach's work [23].

The eigenvalues for the Coulomb problem are in the given units

$$\varepsilon_n = -\frac{1}{n^2}\ , \quad \forall\ n \in \mathcal{N}\ . \tag{73}$$

The eigenvalues for the linear potential are

$$\varepsilon_n = -2\eta + \xi_n \eta^{\frac{4}{3}}\ , \quad \forall\ n \in \mathcal{N}\ . \tag{74}$$

where ξ_n are the zeros of the Airy functions $Ai(\xi_n) = 0$ [24]. The knowledge of these two limits is quite useful to test the numerical results.

4.2 Numerical Techniques for Coulomb and Yukawa potential

By restricting to S-waves, i.e rotationally invariant states, the angle-dependence of the three-variable $\vec{p}$ can be integrated out, which leads to an equation in one variable $p = |\vec{p}\,|$, i.e.

$$\left[\varepsilon - p^2\right]\phi(p) = \frac{1}{\pi}\int_0^\infty dp'\,\frac{p'}{p}\left[\ln\frac{(p-p')^2}{(p+p')^2} - \ln\frac{(p-p')^2+\eta^2}{(p+p')^2+\eta^2}\right]\phi(p') \quad . \tag{75}$$

To restore the Hamiltonian symmetry, it is usual [25], to convert this integral equation for the unknown function $\phi(p)$ to a matrix equation for the unknown numbers $u_i \equiv \sqrt{\omega_i}p_i\phi_i$ with $\phi_i \equiv \phi(p_i)$,

$$({p_i}^2 + a_{ii})\,u_i + \sum_{j\neq i} a_{ij}u_j = \epsilon\, u_i\ , \qquad i,j = 1,\ldots N, \tag{76}$$

by approximating the integral with the finite sum according to the Gauss-Legendre algorithm,

$$\int_0^\infty f(p)dp \longrightarrow \sum_{i=1}^{N}\omega_i f(p_i) \quad . \tag{77}$$

Therefore the non-diagonal matrix elements are given by

$$a_{ij} = \frac{1}{\pi}\sqrt{\omega_i\omega_j}\left[\ln\frac{(p_i-p_j)^2}{(p_i+p_j)^2} - \ln\frac{(p_i-p_j)^2+\eta^2}{(p_i+p_j)^2+\eta^2}\right] \quad . \tag{78}$$

It is numerically practical to map the infinite interval of Eq.(75) onto a finite one by transforming variables [26], according to

$$\int_0^\infty f(p)dp = \int_{-1}^{1} f(p(y))\frac{dp}{dy}dy \quad . \tag{79}$$

The mapping function $y(p)$ is arbitrary, but must satisfy the boundaries:

$$y(p=0) = -1 \ , \qquad y(p=\infty) = +1 \ . \tag{80}$$

With respect to the Coulomb contribution it is useful to choose

$$y(p) = 2e^{-\frac{p}{z}} - 1 \quad , \tag{81}$$

with an adjustable 'stretching' parameter z. With $c(y) \equiv dp/dy$, the quadratures then become

$$\sum_i f(p_i)\omega_i = \sum_i f(y_i)c(y_i)\hat{\omega}_i \quad , \tag{82}$$

i.e. the transformation changes the weights ω_i into $\omega_i \equiv c(y_i)\hat{\omega}_i$. Thus

$$p_i = -z \ln \frac{1+y_i}{2} \qquad \text{and} \qquad \omega_i = \hat{\omega}_i \frac{z}{1+y_i} \quad , \tag{83}$$

where the y_i and $\hat{\omega}_i$ are the tabulated abscissas and weights for the interval $[-1,1]$. Finally Eq.(78) can be solved by conventional matrix diagonalization methods.

But, Eq.(76) is not integrable in the usual way: The diagonal matrix elements a_{ii} of the Coulomb potential diverge logarithmically. Such problems can be solved by the Nystrøm method – the technique of counter terms – [26, 27, 28]. They are important to reach a distinct converged result for a comparably small numerical number. In principle a diagonal term $F(p)\phi(p)$ is added and subtracted in Eq.(72). By treating one of them analytically and the other by Gaussian quadratures the singularity in a_{ii} cancels.

The construction of suitable counter terms depends on the potential, therefore the Coulomb and the Yukawa counter terms have to be calculated separately. Practically the Coulomb counter term is given by

$$F_C(\vec{p}) = \frac{1}{\pi} \int d^3\vec{p} \frac{1}{(\vec{p}-\vec{p'})^2} \frac{(1+\vec{p}^2)^2}{(1+\vec{p'}^2)^2} = 1 + \vec{p}^2 \quad , \tag{84}$$

with the function

$$g(\vec{p},\vec{p'}) = \frac{(1+\vec{p}^2)^2}{(1+\vec{p'}^2)^2} \tag{85}$$

basing on the known Coulomb ground wave function. The singularity of the Yukawa potential is of the same kind as that of the Coulomb, therefore the same function $g(\vec{p},\vec{p'})$ can be used. Thus the Yukawa counter term is

$$\begin{aligned} F_Y(\vec{p}) &= \frac{1}{\pi} \int d^3\vec{p} \frac{1}{(\vec{p}-\vec{p'})^2+\eta^2} \frac{(1+\vec{p}^2)^2}{(1+\vec{p'}^2)^2} = \frac{(1+\vec{p}^2)^2 \ [\vec{p}^2+(\eta-1)^2]}{(\vec{p}^2+\eta^2-1)^2+4\vec{p}^2} \\ &= \vec{p}^2 + 1 - \eta(\eta+2) + \frac{[\eta(\eta+2)]^2}{\eta(\eta+2)+\vec{p}^2+1} \quad , \end{aligned} \tag{86}$$

solved by the method of coefficients. Since the Coulomb counter-term in Eq.(84) is included in the Yukawa term in Eq.(86) by setting $\eta = 0$, Eq.(86) can be stated to be a kind of fundamental expression for counter terms to this kind of singularity. Regarding the integral equation, where F_Y should be added to, the expression explains the following: the term $\vec{p}^2$ is cancelled by the kinetic term of the Hamiltonian, the part $(+1 - \eta(\eta+2))$ is indeed related to the eigenvalue and the fraction vanishes for $p \to \infty$. For $\eta = 0$ the expression is exact and gives $F = 1 + \vec{p}^2$, which is the known Coulomb counter-term. Even this term gives a hint for the relation to the eigenvalue, since p^2 is also cancelled in the Coulomb problem. The lowest eigenvalue of the Coulomb potential is in Bohr units $E_1 = -1$, which is directly related to the factor 1. Depending on the form of the coupling α, the integral adds an offset to the eigenvalue. Because of the close connection between Coulomb and Yukawa counter-term, there is generally no need to discuss the Coulomb problem individually, since it is already contained in the Yukawa one.

Combining appropriately the considerations for the Coulomb and the Yukawa problem by including the counter terms $(F_C(p) + F_Y(p))\phi(p)$ yield immediately the extended integral equation

$$\begin{aligned}\left(\varepsilon - p^2 + (1+p^2) - \left(p^2 + 1 - \eta(\eta+2) + \frac{[\eta(\eta+2)]^2}{\eta(\eta+2) + p^2 + 1}\right)\right) = \\ \frac{1}{\pi}\int_0^\infty dp' \frac{p'}{p} \ln\left[\frac{(p-p')^2}{(p+p')^2}\right]\left[\phi(p') - \frac{(1+p^2)^2}{(1+p'^2)^2}\phi(p)\right] \\ - \frac{1}{\pi}\int_0^\infty dp' \frac{p'}{p} \ln\left[\frac{(p-p')^2+\eta^2}{(p+p')^2+\eta^2}\right]\left[\phi(p') - \frac{(1+p^2)^2}{(1+p'^2)^2}\phi(p)\right] \quad .\end{aligned} \tag{87}$$

For $p = p'$ the term in the bracket vanishes, i.e. it is justified to restrict to $j \neq i$ in the summation over j on the r.h.s. of Eq.(76). The improved diagonal elements are now:

$$\begin{aligned} a_{ii} \;=\; & -(1+p_i^2) + (p_i^2 + 1 - \eta(\eta+2) + \frac{[\eta(\eta+2)]^2}{\eta(\eta+2) + p_i^2 + 1}) \\ & - \frac{(1+p_i^2)^2}{\pi p_i} \sum_{j \neq i} \omega_j p_j \ln\left[\frac{(p_i - p_j)^2}{(p_i + p_j)^2}\right] \frac{1}{(1+p_j^2)^2} \\ & + \frac{(1+p_i^2)^2}{\pi p_i} \sum_{j \neq i} \omega_j p_j \ln\left[\frac{(p_j - p_i)^2 + \eta^2}{(p_j + p_i)^2 + \eta^2}\right] \frac{1}{(1+p_j^2)^2} \quad . \end{aligned} \tag{88}$$

The off-diagonal elements a_{ij} are not modified. In the following it should be asked whether the results can be improved by a 'stretching factor' z, as given in Eq.(81).

Therefore the optimization via z has to be so sensitive that no wave function runs out of range. Generally, the wave function of the Bohr spectrum is given by

$$\Psi_B(p) = \frac{\mathcal{N}}{\left[1 + \left(\frac{p}{p_B}\right)^2\right]^2} \quad , \tag{89}$$

with $\mathcal{N}$ an arbitrary normalization. Normalizing the function to Ψ_0,

$$\frac{\Psi_B}{\Psi_0} = \frac{\left[1 + \left(\frac{p_0}{p_B}\right)^2\right]^2}{\left[1 + \left(\frac{p}{p_B}\right)^2\right]^2}$$

defines the observation interval. Choosing $\Psi_B = \Psi_B(N)$, with N the number of Gaussian integration points, the behavior of the ratio Ψ_N/Ψ_0 can be examined with respect to z by plotting it versus $p/\ p_B$. Fig. 6 shows schematically that functions which are more like a Delta-function should be shifted away from the axis, while functions which are out of range with an offset Δ at the interval boundary, should be drawn back. The advantage of this procedure is that a particular choice shifts

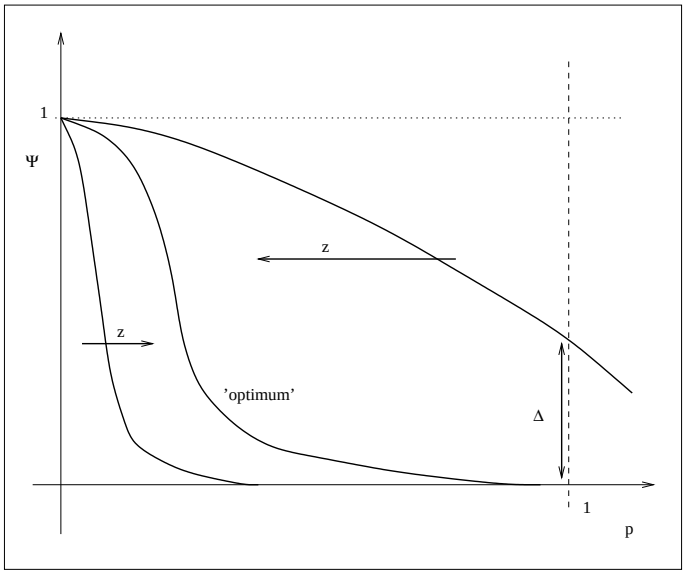

Figure 6: *The effect of the optimization by the 'stretching factor' z is illustrated schematically. Functions out of range with an offset Δ are drawn back; those comparable to a Delta function should be shifted away from the axis. Generally, the corresponding integration points are shifted to a region where the function is significantly different from zero, then their distribution is more equal.*

the bulk of integration points to a region where the wave function is significantly

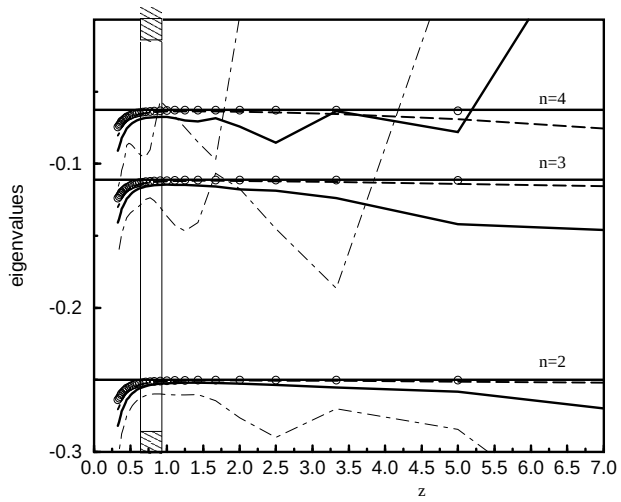

Figure 7: *The Bohr eigenvalues for $n = 2, 3, 4$ are plotted versus the stretching factor z for different matrix dimensions N ($- \cdot -$ N=8, ▬ N=16, ▬ ▬ N=32 and $\circ$ N=64).– The exact eigenvalues $-1/n^2$ are shown as well.– Note the hatched area, in which the numerical results are particularly stable against the number z.*

different from zero. Because of the η-dependence of the example the factor z has to be optimized for each value of η.

Before summarizing the main issues of this combined potential, the results for the single potentials are briefly reviewed. The z-optimization for the Coulomb potential is shown in Fig. 7, where the numerical eigenvalues of Eq.(76) are plotted versus z for different matrix dimensions N. As to be seen in the figure, the functions $\varepsilon_n(z)$ are rapidly varying (almost fluctuating) for low dimensionality and become flatter with increasing N. For a z within the hatched area the numerical results are rather stable as functions of N. All practical requirements are sufficiently satisfied by a value of $N = 32$ (or 16). The lowest eigenvalue ($\varepsilon_1 = -1.0$) is not shown, since the function ($\varepsilon_1(z)$) is completely flat. These observations are somewhat more quantified in Table 2. The final results for the low lying part of the spectrum are accumulated in Fig. 8. The spectrum is – with fixed $z = 0.70$ – remarkably insensitive to the dimensions N. Even the numerical wave function as displayed in Fig. 9 is highly accurate. The same procedure has been applied to the Yukawa potential. It covers the fact that in the limit $\eta \to 0$ the Coulomb problem is restored, which is an explicitly check for the computer programs. For a comparatively small value of

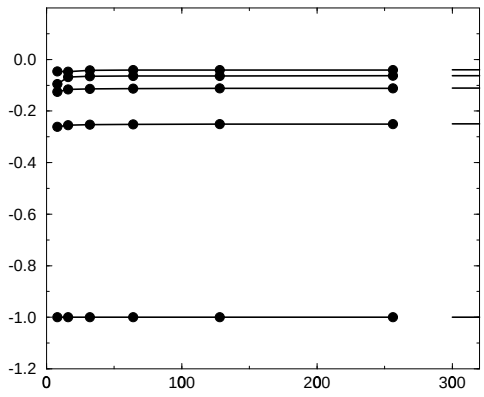

Figure 8: *The numerical eigenvalues for the Coulomb potential are plotted versus the number of integration points N $(8, 16, 32, 64, 128, 256)$ for $z = 0.70$.*

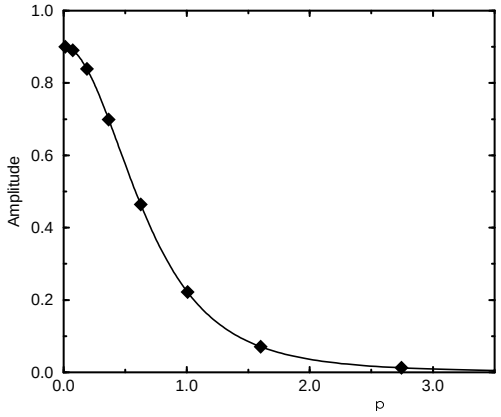

Figure 9: *The exact Coulomb wave function $\phi(p_i)_{1s}$ (—) is plotted versus the momentum p in Bohr units, and compared with the numerical values $u_i/\sqrt{4\pi\omega_i}p_i$ (filled $\diamond$). The Parameters are $z = 0.70$ and $N = 8$.- Note the excellent agreement.*

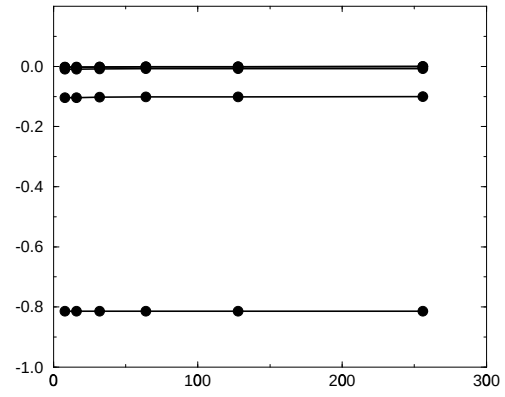

Figure 10: *The numerical eigenvalues of the Yukawa potential for $\eta = 0.1$ are plotted versus the number of integration points N $(8, 16, 32, 64, 128, 256)$ with $z = 0.70$.*

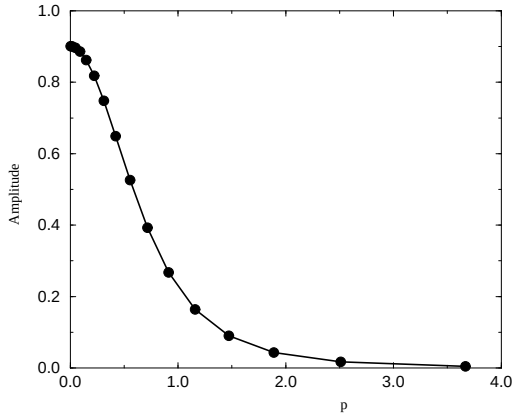

Figure 11: *The Yukawa ground-state wave function for $\eta = 0.1$ is plotted versus the momenta in Bohr units ($N = 16, z = 0.70$). The continuous curve is supposed to guide the eye.*

	Exact	Calculated					
n	$-1/n^2$	N=16	N=32	N=64	N=16	N=32	N=64
		$z = 0.70$			$z = 1.0$		
1	-1.0000	-1.0000	-1.0000	-1.0000	-1.0000	-1.0000	-1.0000
2	-0.2500	-0.2545	-0.2525	-0.2516	-0.2523	-0.2510	-0.2506
3	-0.1111	-0.1160	-0.1135	-0.1126	-0.1145	-0.1122	-0.1117
4	-0.0625	-0.0683	-0.0649	-0.0639	-0.0676	-0.0637	-0.0630
5	-0.0400	-0.0471	-0.0425	-0.0414	-0.0485	-0.0415	-0.0406

Table 2: *The eigenvalues of the Coulomb problem for two values of the stretching factor z and three matrix dimensions N are compared with the exact values.*

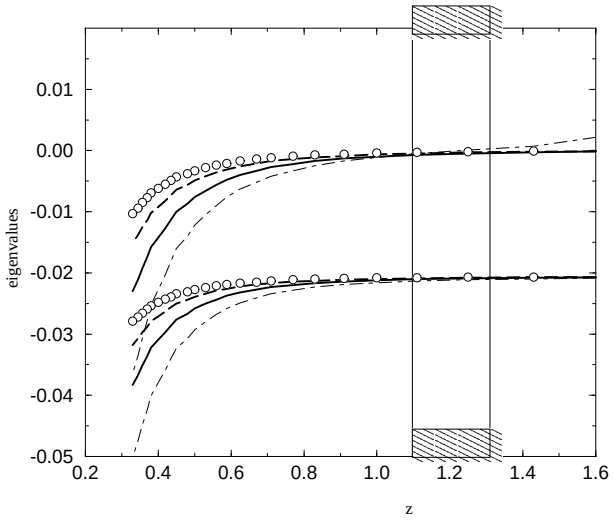

Figure 12: *The two lowest eigenvalues of the Yukawa problem with $\eta = 1.0$ are plotted versus the stretching factor z for different matrix dimensions: ($- \cdot -$ N=8, ▬ N=16, ▬ N=32 and ∘ N=64).*

$\eta = 0.1$, the low lying part of the spectrum and the wave function, as shown in the Figs. 10 and 11, are quite similar to the Coulomb potential in Figs. 8 and 9. In either case, the eigenvalues are practically insensitive to the matrix dimension N, particular for the stretching parameter $z = 0.7$, chosen to be the same as for the Coulomb case. For $\eta = 1.0$ the value of $z = 1.25$ is obtained by the same optimization procedure as shown in Fig. 12. It is notable that the Yukawa problem has only a finite number

of bound states. The best values for $\eta = 0.1$ and $\eta = 1.0$ are listed in Table 3.

nS	1	2	3	4	5
$\eta = 0.1$ ($z = 0.7$)	-0.8141	-0.1022	-0.0084	-0.0019	-0.0019
$\eta = 1.0$ ($z = 1.25$)	-0.0208	-0.0003	–	–	–

Table 3: *The eigenvalues of all bound S-states for the Yukawa problem for two values of η. The matrix dimension is either $N = 32$.*

Combining the results for the Coulomb and for the Yukawa potential not only the spectra and the wave functions depending on η are of interest, even the behavior of the spectrum on η should be discussed carefully. In the limit $\eta \to \infty$ the spectrum of Eq.(75) is expected to be very close to the Coulomb spectrum, $\varepsilon_n = -1/n^2$. In Fig. 13 it is shown that the Coulomb limit is already well achieved for numerical values of $\eta \geq 2.0$. This behavior is contrary to that for the Yukawa case, where the Coulomb limit is reached for $\eta \to 0$. In the limit $\eta \to 0$ the spectrum is expected to approach the spectrum for a linear potential, i.e. $\varepsilon_n = -2\eta + \xi_n \eta^{4/3}$. A typical Airy-solution [24] is only obtained for very small values, i.e. $\eta \leq 0.02$, as to be seen in Fig. 14. For all other values, the spectrum is somehow intermediate between

η	z	$\bar{\varepsilon} = \varepsilon + 2\eta$	Airy regime $\xi_1 \eta^{\frac{4}{3}}$	Coulomb regime $-1 + 2\eta$
0.001	0.0370	0.00021905	0.00023381	
0.01	0.0714	0.00454474	0.00503728	
0.1	0.2174	0.08860885	0.10852499	
1.0	0.3861	1.48676105	2.3381	1
2.0	0.4762	3.31000318		3
4.0	0.8000	7.16112492		7
10.0	0.8333	19.04647165		19

Table 4: *The eigenvalues ε of the combined Coulomb and Yukawa problem derived from integral equation (75) are given for increasing values of the physical parameter η. Column 2 gives the actual stretching parameter z. In the last two columns the corresponding eigenvalue for the Airy or Coulomb regime are quoted for purpose of comparison.*

those two extreme cases, as quantitatively demonstrated in Table 4 (superposition

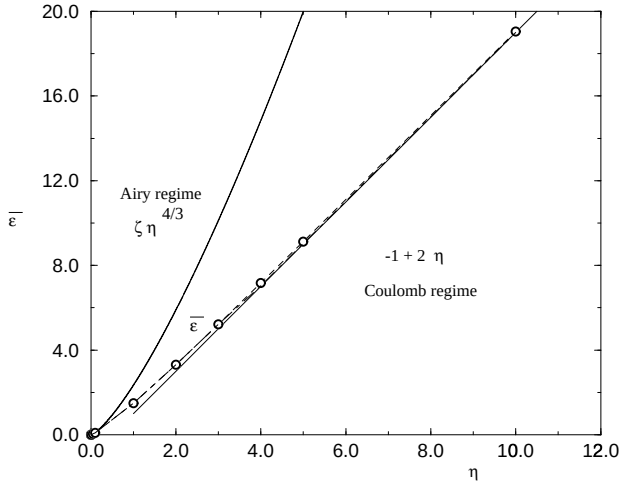

Figure 13: *The lowest eigenvalue* $\bar{\epsilon}(\eta) = \epsilon + 2\eta$ *is plotted versus* η $(\circ)$ *corresponding to the data in Table 4. The upper solid line indicates the Airy-type solution and the lower solid line visualizes the Coulomb-type solution.*

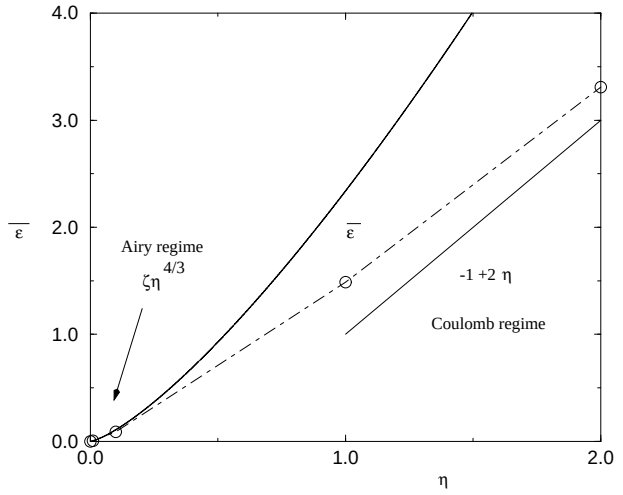

Figure 14: *A zoom of Fig. 13*

of the potentials). It is remarkable how the curve of the calculated eigenvalues $\bar{\varepsilon}(\eta) = 2\eta + \varepsilon_1$ in Fig. 14 interpolates between the two asymptotic curves $\bar{\varepsilon}(1) \sim \eta^{4/3}$ and $\bar{\varepsilon}(1) \sim 2\eta - 1$. Table 5 presents the spectra of the combined potential up to the

n	N=16	N=32	N=64	N=16	N=32	N=64
	$\eta = 0.01$, $z = 0.0714$			$\eta = 0.1$, $z = 0.2174$		
1	0.0045	0.0045	0.0046	0.0884	0.0886	0.0887
2	0.0073	0.0074	0.0075	0.1312	0.1316	0.1317
3	0.0092	0.0094	0.0095	0.1541	0.1548	0.1549
4	0.0106	0.0110	0.0110	0.1674	0.1685	0.1686
	$\eta = 1.0$, $z = 0.3861$			$\eta = 10.0$, $z = 0.833$		
1	1.4860	1.4868	1.4871	19.0456	19.0465	19.0470
2	1.8183	1.8193	1.8196	19.7537	19.7551	19.7555
3	1.9090	1.9102	1.9105	19.8877	19.8898	19.8903
4	1.9447	1.9464	1.9468	19.9339	19.9372	19.9379

Table 5: *The combined spectrum $\varepsilon_n + 2\eta$ for different values of η and N, at the optimized value of z.*

fourth level for various values of η and number of integration points N at optimized z.

By the example of a combined Coulomb and Yukawa potential the techniques have been outlined to solve the interaction kernel in momentum space by discretization via Gaussian quadratures, and diagonalization of the so generated Hamiltonian matrix. Much attention is paid to speed up convergence by counter-term technology already developed for the pure Coulomb case [16, 26]. Special emphasis is put on the free formal parameter, called 'stretching factor' z, which can be adjusted for a considerably increased numerical precision and stability. This optimization supports a restriction – on the average – to matrix diagonalization problems with a dimension $N = 32$. While evaluating the technical tools the single and combined behavior of the Coulomb and the Yukawa potential have been discussed, even their spectra and eigenfunctions have been calculated. The results of this section can now be directly applied to the actual model of this thesis, to be discussed in the next Sect. 4.3.

4.3 Renormalizing the 'Coulomb plus regulated Delta' potential

As derived from the basic equation in Sect. 3.2, the first main equation in this thesis is an effective Hamiltonian with a 'Coulomb plus regulated Delta' potential (see Eq. 65), i.e.

$$\left[D - \frac{m_s}{m_r}\vec{k}^2\right]\phi(\vec{k}) = -\frac{1}{4m_r}\frac{4}{3}\frac{\alpha}{\pi^2}\int d^3\vec{k}'\left[\frac{4m_r m_s}{Q^2} + 2\frac{\mu^2}{\mu^2+Q^2}\right]\phi(\vec{k}') \quad ,$$

with the binding energy D (Eq. 20), the summarized mass $m_s = m_1 + m_2$, the reduced mass $1/m_r = 1/m_1 + 1/m_2$, and the property $m_1 \neq m_2$. This main characteristic of this model is that the 'Delta'-function, the factor 2 from equilibrium considerations, is regulated by a factor $\mu^2/(\mu^2+Q^2)$.

For the reason to calculate all scalar mesons the free parameters α and μ have to be fixed by renormalization. But before the whole program will be worked out, the equation has to be rescaled. The 'Coulomb minus Yukawa'-model has been solved in Bohr units, i.e. in dimensionless quantities. Such an ansatz does not lead to the correct physical numbers, therefore the 'Coulomb plus regulated Delta'-model has to be solved in suitable physical units. The counter terms have to be rewritten as well. Generally, the 'Coulomb plus regulated Delta' integral equation has the following form

$$\begin{aligned} E\phi(k) = \frac{k^2}{2m_r}\phi(k) - \frac{\beta}{2\pi^2}\left(\frac{\mu^2}{4m_r m_s}\right)\int d^3k' \frac{\phi(k')}{\mu^2 + (\vec{k}-\vec{k}')^2} \\ -\frac{\beta}{2\pi^2}\int d^3k' \frac{\phi(k')}{(\vec{k}-\vec{k}')^2} \quad , \end{aligned} \tag{90}$$

where the regulated Delta has apart from a factor $\mu^2 \,/\, 4m_r m_s$ basically the same behavior as the Yukawa potential. The 'β' is an abbreviation for the coupling, it is equal to $4/3\ \alpha$ in QCD or α in QED. To distinguish between both contributions, different couplings t are introduced:

$$\begin{aligned} t_1 &= \frac{\mu^2}{4m_r m_s}\ \beta \qquad \text{regulated Delta / scaled Yukawa} \quad , \\ t_2 &= \beta \qquad \text{Coulomb} \quad . \end{aligned}$$

Hence, the application of the corresponding counter terms leads to the following equation

$$E\phi(k) = C(k)\phi(k) \quad - \quad \frac{t_1}{2\pi^2}\int d^3k' \frac{1}{\mu^2 + (\vec{k}-\vec{k'})^2}\left[\phi(k') - \phi(k)\frac{(k^2+b_1^2)^2}{(k'^2+b_1^2)^2}\right]$$
$$- \quad \frac{t_2}{2\pi^2}\int d^3k' \frac{1}{(\vec{k}-\vec{k'})^2}\left[\phi(k') - \phi(k)\frac{(k^2+b_2^2)^2}{(k'^2+b_2^2)^2}\right] \quad . \tag{91}$$

The scales b_i, $i = 1, 2$, have been invented to guaranty that the equation is correct in its units. The coefficient function $C(k)$ has naturally three contributions, the kinetic term and both analytically solved counter terms from the potentials

$$C(k) = \frac{k^2}{2m_r} \quad - \quad \frac{t_1 b_1}{2}\left(p^2 + \eta^2\frac{(\eta+2)^2}{p^2+(\eta+1)^2} - \eta(\eta+2) + 1\right) \tag{92}$$
$$- \quad \frac{t_2 b_2}{2}\left(p^2+1\right) \quad ,$$

with $\eta = \mu/b_1$ and $p = k/b_1$ for the regulated Delta and $p = k/b_2$ for the Coulomb, p and η dimensionless. Restoring the units leads to

$$C(k) \quad = \quad \frac{k^2}{2m_r}\left(1 - \frac{m_r t_1}{b_1} - \frac{m_r t_2}{b_2}\right) - \frac{t_1 b_1}{2} - \frac{t_2 b_2}{2} \tag{93}$$
$$-\frac{t_1}{2b_1}\left(\mu^2\frac{(\mu+2b_1)^2}{k^2+(\mu+b_1)^2} - \mu(\mu+2b_1)\right) \quad .$$

The scales b_1, b_2 are adjusted by the cancelation of the coefficient of k^2, i.e.

$$\frac{k^2}{2m_r}\left(1 - \frac{m_r t_1}{b_1} - \frac{m_r t_2}{b_2}\right) \stackrel{!}{=} 0 \quad . \tag{94}$$

This makes sense, because in the dimensionless case the kinetic term p^2 cancels automatically. A suitable ansatz is $b_i = m_r t_i/x_i$, $i = 1, 2$, so that $1 - (x_1 + x_2) \stackrel{!}{=} 0$. This is followed by the prescription for a 'combining' scale b with

$$b = b_1 = b_2 = m_r(t_1 + t_2) = \frac{4}{3}\alpha m_r\left(1 + \frac{\mu^2}{4m_r m_s}\right) \quad . \tag{95}$$

This is not the only solution, but the only reasonable one for the limits $t_i \to 0$, $i = 1, 2$, because it then restores the single potentials. The other possibility has no real boundary for $t_i \to 0 \;:\; b_i \to \infty$, $i = 1, 2$. Therefore the coefficient function $C(k)$ can be rewritten by means of the combining scale b,

$$C(k) = -\frac{b}{2}(t_1 + t_2) - \frac{t_1}{2b}\left(\mu^2\frac{(\mu+2b)^2}{k^2+(\mu+b)^2} - \mu(\mu+2b)\right) \quad . \tag{96}$$

The derivation of the function $C(k)$ has been the last piece in the 'history' of preparing the model discretization to a matrix equation and afterwards description of the renormalization procedure to finally calculate the meson masses.

The multiplication of Eq.(91) by $2m_s$ restores the binding energy D, i.e. an approximated relation between the squared mass-eigenvalue and the energy-eigenvalue E is given by

$$M^2 = (m_1 + m_2)^2 + 2(m_1 + m_2)E \quad . \tag{97}$$

With Eq.(20) the connection between both energies is defined by $D = 2m_s E$. Consequently the model equation appears as

$$\begin{aligned} &\left[D + bm_s(t_1 + t_2) + \frac{t_1 m_s}{b}\left(\mu^2 \frac{(\mu+2b)^2}{k^2 + (\mu+b)^2} - \mu(\mu+2b)\right)\right]\phi(k) \\ &= -\frac{t_1 m_s}{\pi^2}\int d^3k' \frac{1}{\mu^2 + (\vec{k} - \vec{k'})^2}\left[\phi(k') - \phi(k)\frac{(k^2+b^2)^2}{(k'^2+b^2)^2}\right] \\ &\quad -\frac{t_2 m_s}{\pi^2}\int d^3k' \frac{1}{(\vec{k} - \vec{k'})^2}\left[\phi(k') - \phi(k)\frac{(k^2+b^2)^2}{(k'^2+b^2)^2}\right] \quad . \end{aligned} \tag{98}$$

As for the example the calculation is restricted to S-waves, therefore the integration over the angles is carried out. Analogue to the procedure in Section 4.2 the integral equation is converted into a matrix equation for the unknown numbers $u_i = \sqrt{\omega_i} k_i \phi(k_i)$ (see Eq. 76). The diagonal elements are now

$$\begin{aligned} a_{ii} &= -b^2\frac{m_s}{m_r} - \frac{t_1}{(t_1+t_2)}\frac{m_s}{m_r}\left(\mu^2\frac{(\mu+2b)^2}{k_i^2 + (\mu+b)^2} - \mu(\mu+2b)\right) \\ &\quad -\frac{t_1 m_s}{\pi}\sum_{j\neq i}\omega_j \frac{k_j}{k_i}\ln\frac{(k_i-k_j)^2+\mu^2}{(k_i+k_j)^2+\mu^2}\frac{(k_i^2+b^2)^2}{(k_j^2+b^2)^2} \\ &\quad -\frac{t_2 m_s}{\pi}\sum_{j\neq i}\omega_j \frac{k_j}{k_i}\ln\frac{(k_i-k_j)^2}{(k_i+k_j)^2}\frac{(k_i^2+b^2)^2}{(k_j^2+b^2)^2} \quad , \end{aligned} \tag{99}$$

and the off-diagonal ones are given by

$$\begin{aligned} a_{ij} &= \frac{t_1 m_s}{\pi}\sqrt{\omega_i\omega_j}\ln\frac{(k_i-k_j)^2+\mu^2}{(k_i+k_j)^2+\mu^2} \\ &+ \frac{t_2 m_s}{\pi}\sqrt{\omega_i\omega_j}\ln\frac{(k_i-k_j)^2}{(k_i+k_j)^2} \quad , \end{aligned} \tag{100}$$

with $t_1,\ t_2$ according to Eq.(91) and b in Eq.(95). These parameters $t_1,\ t_2,\ b$ hide the complexity of this simple model. They are the screws, which have to be turned, to get to another kind of potential. They make this model so sympathetic, because

they enable the chance to test the numerical results. Except for the solution of the Coulomb potential, no values are known. Table 6 summarizes the testing properties. For the Yukawa case $b = 4/3\,\alpha\,m_r$ is independent of μ. But for the smooth Delta

coupling	variation		resulting potential
$t_2 = 4/3\alpha$			Coulomb
$t_1 = 4/3\alpha \cdot A$	$A = \mu^2/(4m_r m_s)$	μ running	regulated Delta
		$\mu = 0$	Null-matrix
	$A = 1$	μ running	Yukawa
		$\mu = 0$	Coulomb

Table 6: *The testing properties for the 'Coulomb plus regulated Delta' potential are shown. In the first row the Coulomb potential is given. In the other rows the different parameter-combinations for the regulated Delta are presented, even the Null-matrix and the Coulomb case are reasonable testing cases.*

potential the scale is a function of the regulator scale μ, even the coupling itself depends on μ.

This is essentially the point where renormalization starts. The procedure has already been described theoretically in Sect. 3.2, here the program is carried out in detail.

The matrix equation of the problem is set up, see Eqs.(99,100). With the goal to reproduce the pion mass – especially the π^+ – the initial constituent masses m_1 and m_2 have to be those of the up- and down-quark mass. But such constituent quark masses are not precisely known, therefore they are chosen to be equal and around 400 MeV. In the progress of the work these two mass values have been adjusted more carefully to the fit parameter, and are therefore fixed to 518.5 MeV. Moreover, the masses m_1 and m_2 occur in the whole integral equation (Eq. 98) in combinations as the reduced or the summarized mass. This gives reason to the assumption that the calculated energies are out of any manageable size. To keep these quantities tractable, it is useful to introduce a suitable scale κ. Hence, the binding energy $D = M^2 - m_s^2$ originally calculated in units of [MeV^2], is now given in units of κ^2, i.e.

$$\varepsilon = D/\kappa^2 \ .$$

Thus, all quantities are expressed in units of κ: $\widetilde{k} = k/\kappa$, $\widetilde{Q}^2 = Q^2/\kappa^2$, $\widetilde{\mu} = \mu/\kappa$, $\widetilde{b} = b/\kappa$ and $\widetilde{m}_i = m_i/\kappa$, $i = r, s$. This changes nothing on the appearance of the integral equation except D being replaced by ε. The 'tilde' over the other variables can be omitted. Because the masses are quite large input-parameters, they deliver a convenient point to fix the scale. It is useful to choose $\kappa = 350$ MeV, so that $\widetilde{m}_{u,d} = m_{u,d}/\kappa = 1.48$. The point of renormalization is to find a coupling α for fixed values of $m_1 = m_u$, $m_2 = m_d$, and μ to satisfy the condition

$$M_h^2(\alpha_i) = M_{\pi^+}^2 \ ,$$

i.e. the calculated eigenvalue depending on α should be equal to the experimental pion mass squared. The commitment of the problem to the π^+ gives an estimate for the eigenvalue

$$\varepsilon = -\frac{(m_1 + m_2)^2}{\kappa^2} + \frac{M_{\pi^+}^2}{\kappa^2} = -8.6208 \ , \tag{101}$$

with $M_{\pi^+} = 139$ MeV, $m_u = m_d = 518.5$ MeV, and $\kappa = 350$ MeV. Table 7 shows the negative of the lowest calculated eigenvalues, i.e. $-\varepsilon = m_s^2 - M^2$, in units of $\kappa = 350$ MeV, given for the mass parameters $m_u = m_d = 1.48$ and different coupling constants α and regulator scales μ. The large values in the last column give evidence for the introduction of a mass scale κ of such size. The values for $\mu = 0$ in the first column represent the Coulomb case. It is even remarkable that for increasing μ and α the first eigenvalue decreases rapidly to $-\infty$.

Table 7 is a pedagogical tool to show the first calculation on the relation between α and μ, which gives a hint where the suitable values for the renormalized coupling α_μ with respect to the pion mass can be found. For the most appropriate values of α for fixed μ the eigenvalues are underlined. For illustration the data of Table 7 is plotted as a plane in a 3 dimensional graph, see Fig. 15. Therein the dots mark the underlined values and represent therefore the function $\alpha(\mu)$. Because the values in Table 7 belong to a first check-up, the dots in Fig. 15 are more qualitatively. It is remarkable how fast the eigenvalue increases for comparably slowly increasing (α, μ).

Fig. 16 shows the negative lowest eigenvalue $-\varepsilon$ versus the coupling constant α for different values of the regulator scale μ. The curves represent the direct connection between the eigenvalue and the value of μ, because with increasing μ the curves increase rapidly unproportional. For each μ and α lower than 0.5 the curves

α	μ =0	μ =2	μ =4	μ =6	μ =8	μ =10
0.00	0.000	0.000	0.000	0.000	0.000	0.000
0.05	0.010	0.010	0.014	0.038	0.100	0.213
0.10	0.039	0.040	0.057	0.168	0.506	1.280
0.15	0.088	0.092	0.132	0.412	1.391	3.908
0.20	0.156	0.168	0.241	0.760	2.731	8.095
0.25	0.244	0.269	0.381	1.145	4.108	12.22
0.30	0.352	0.398	0.551	1.480	4.937	14.11
0.35	0.479	0.559	0.758	1.755	5.217	14.81
0.40	0.625	0.754	1.021	2.101	5.936	19.76
0.45	0.792	0.986	1.369	2.759	8.669	33.41
0.50	0.977	1.260	1.838	4.019	14.66	57.26
0.55	1.183	1.578	2.466	6.149	24.49	91.52
0.60	1.407	1.943	3.289	9.355	38.41	136.1
0.70	1.915	2.823	5.650	19.49	78.86	256.5
0.75	2.199	3.344	7.243	26.58	105.5	332.3
0.80	2.502	3.920	9.139	35.07	136.6	418.7
0.90	3.166	5.246	13.91	56.44	211.9	623.0
1.00	3.909	6.812	20.06	83.79	305.3	870.0
1.10	4.730	8.626	27.65	117.3	416.8	1160.
1.20	5.629	10.69	36.75	156.9	546.6	1493.
1.30	6.606	13.03	47.38	202.9	694.7	1869.
1.40	7.662	15.62	59.58	255.3	861.4	2289.
1.50	8.795	18.48	73.35	313.9	1046.	2752.

Table 7: *The lowest negative eigenvalue of the integral equation, i.e.* $m_s^2 - M^2$, *is given for mass parameters* $m_1 = m_2 = 1.48$ *and different coupling constants* α *and regulator scales* μ. *All masses or energies are given in units of 350 MeV. The underlined values correspond to the most appropriate values of* α *for fixed* μ, *with respect to the first eigenvalue of the pion at* $-\varepsilon = 8.6208$. – *Note the very large values for* $\mu = 10$ *as compared to the Coulomb case* ($\mu = 0$).

seem to lay upon each other, but Table 7 shows that the single contributions can be resolved.

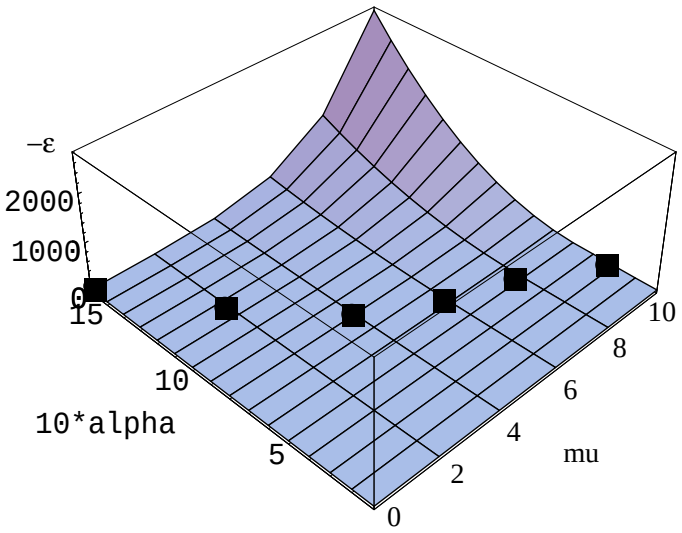

Figure 15: *3D plot of the values shown in Table 7: coupling constant α, regularization scale μ, and eigenvalue $(m_s^2 - M^2)$ in units of $\kappa = 350$ MeV; the dots represent the appropriate values of α for given μ, analogue to the underlined values in the Table. They belong to the renormalized function $\alpha(\mu)$. Note the strong ascent in $(m_s^2 - M^2)$ for increasing μ and α.*

According to Fig. 16 there is a function

$$f(\alpha) = \left[M_\pi^2 - (m_u + m_d)^2 - \varepsilon\right]$$

for each value of μ. Therein an appropriate value $\alpha(\mu)$ has to be found. By the means of the Bisection method, the value $\alpha_{middle} = (\alpha_{low} + \alpha_{up})/2$ is calculated for a chosen initial interval $[\alpha_{low}, \alpha_{up}]$. Whether the functional value is $f(\alpha) > 0$ or $f(\alpha) < 0$, fixes whether the new α_{middle} is calculated left or right from the first. After a given number of runs, usually $X = 20$, one value of α has been localized with $f(\alpha)$ around zero and is put out with a X-dependent uncertainty

$$\alpha_{result} \pm \Delta\alpha = \alpha_{real} \qquad \text{with} \quad \Delta\alpha = (\alpha_{up} - \alpha_{low})2^{-X} \quad . \tag{102}$$

Thus, this method finds one suitable coupling α for each regulator μ, and therefore defines the renormalized coupling $\alpha(\mu)$ more quantitatively. Fig. 17 shows the result of this method, the coupling constant α is plotted versus the regularization scale μ in units of $\kappa = 350$ MeV. The data has been obtained with a slightly modified method by requiring that the mass eigenvalue $\sqrt{m_s^2 + \varepsilon}$ with $m_1 = m_2 = 1.48$ at

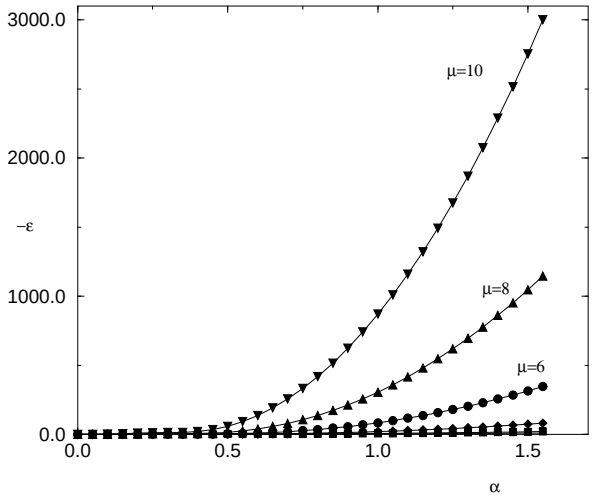

Figure 16: *The lowest eigenvalue* $-\varepsilon = m_s^2 - M^2$ *is plotted versus the coupling constant* α. *The different lines refer to different values of the regularization scale* μ ($\mu = 0, 2, 4, 6, 8, 10$).

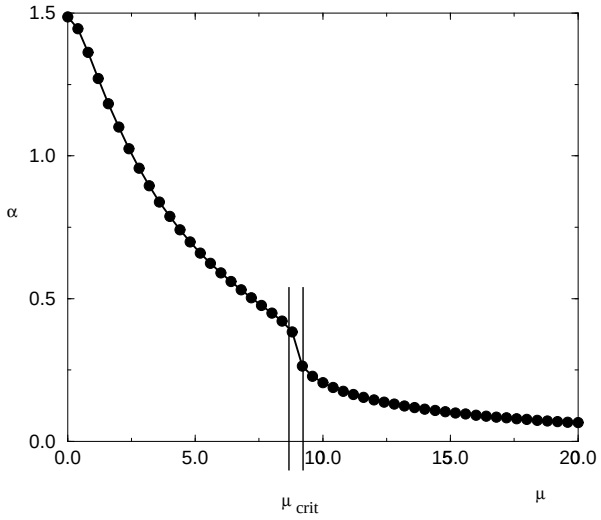

Figure 17: *Renormalized coupling constant* α *versus regularization scale* μ *in units of* $\kappa = 350$ *MeV. The data is obtained by requiring the constraint* $\sqrt{m_s^2 + \varepsilon} = M_{\pi^+}$ *in the Bisection method. – Note the gap at* $\mu \sim 8.5$.

fixed values of μ is equal to the pion mass $M_{\pi^+} = 139.56995(14)$ MeV within 8 significant digits. Hence forward, this is the same constraint as for Table 7, but because of the Bisection method the values are more precisely and quantitatively.

It is remarkable that the behavior of the curve changes at $\mu \sim 8.5$. For lower μ-values the function is exponentially decreasing, while behind the gap the curve is much flatter. Hence the function can be divided into two regions: $\mu \leq \mu_{crit}$ and $\mu \geq \mu_{crit}$ with $\mu_{crit} \sim 8.5$. Where this separation visualized by the gap comes from is not yet really understood. It might be a hint for numerical instability or for an uncertainty in the renormalization procedure, especially 'universality'. It can also be the separation between two different potential regimes, the right corresponding to the Coulomb region the other to something different, but connected to the Yukawa potential.

As already mentioned in Sect. 3.2 the 'universality', i.e. independence of the whole spectrum from μ, has to be checked. At the moment there is no analytical expression for the function $\alpha(\mu)$. Thus, for the beginning the numerical values of the function $\alpha(\mu)$ obtained for the lowest state are considered to hold for the whole spectrum. To become more precise whether the renormalization procedure is successful for higher states, the first and second excited state to the pion are regarded. Thus, two new constraints for the second and third eigenvalue have to be fulfilled. The three demands are therefore

$$\begin{array}{lll} 1 & \sqrt{m_s^2+\varepsilon_1} = M_{0,\pi^+} = 139,6 & S_0 \\ 2 & \sqrt{m_s^2+\varepsilon_2} = M_1 = 980 & S_1 \\ 3 & \sqrt{m_s^2+\varepsilon_3} = M_2 \sim 1010 & S_2 \quad . \end{array} \tag{103}$$

The identification of the second mass value requires a short discussion on quantum numbers and spectral energy levels. The π^+ is a pseudo-scalar meson with $J^P = 0^{-+}$. Its first excited state is therefore characterized by $J^P = 1^{+-}$, being identified with $a_1(980)$. This classification relies on Table 8.

But the ordering of those excited states is all but clear and the literature is full of contradictory statements. On the one hand the 'a' is a scalar meson with quark content $u\bar{d}$ and $J^{PC} = 0^{++}$ [30], on the other hand it is the chiral partner to the π with $(u\bar{u} + d\bar{d})$ [31]. According to Table 8 it is a particle with $(u\bar{u} - d\bar{d})$ and $J^{PC} = 1^{+-}$ [29]. The fact is that several 'a'-particles exist, which are nowhere discussed in detail. The properties to identify the appropriate state are that it has to be a $S = 0$-particle and, for being the first excited state to the π, $L = 1$, so that $J^{PC} = 1^{+-}$ with the parity $P = (-1)^{L+1}$ and the charge conjugation $C = (-1)^{L+S}$. In the model only $(S = 0,\ L = 0)$-states can be calculated. Even the amplitude is

J^{PC}	$(0,2,\ldots)^{-+}$	$(1,3,\ldots)^{+-}$	$(1,2,\ldots)^{--}$	$(1,2,\ldots)^{++}$
$u\bar{u}-d\bar{d}$	π	a	ρ	a'
$u\bar{u}+d\bar{d}$	η	h	ω	f
$s\bar{s}$	η'	h'	ϕ	f'
$c\bar{c}$	η_c	h_c	J/Ψ	χ_c
$b\bar{b}$	η_b	h_b	Υ	χ_b
$t\bar{t}$	η_t	h_t	Θ	χ_t

Table 8: *Meson characteristic for arbitrary L. - For $L \neq 0$ the particles are grouped for $S = 0$ in chains with even or odd J and identical discrete quantum numbers. For $S = 1$-states the total momentum can be build up by $(L-1, L, L+1)$. With the possibility of double occupied places, which can not clearly be fixed from their preserved quantum numbers, two new chains occur: $(0,1,\ldots)^{++}$, $(1,2,\ldots)^{--}$ [29, 30].*

restricted to $\uparrow\downarrow$-states without any mixing. Therefore the received energy levels can be identified as 1^1S_0, 2^1S_0,... Fig. 18 sketches the spectrum of the pion and gives the corresponding quantum numbers [29, 32, 33, 34].

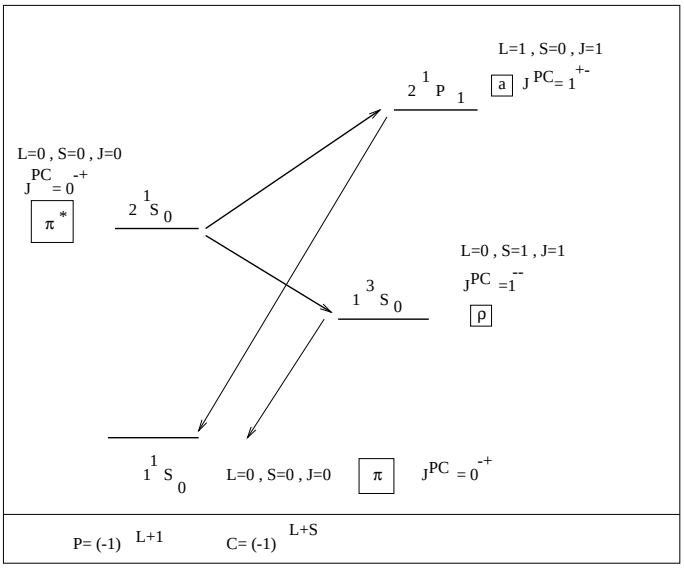

Figure 18: *Scheme of the energetic levels concerning the calculated ground- and first excited state of the pion (π^*) and those for the 'ρ'- and the 'a'-meson. All quantum numbers are given. The arrows $2^1P_1 \to 1^1S_0$, $1^3S_0 \to 1^1S_0$ indicate possible decays, the arrows $2^1S_0 \to 2^1P_1$, $2^1S_0 \to 1^3S_0$ the fit properties.*

The calculated first excited state 2^1S_0 lies energetically lower than the real first excited state 2^1P_1, which corresponds to the 'a' with $J^{PC} = 1^{+-}$. This is clear from the knowledge of any singlet system, because the orbital wave function to $S = 0$ is symmetric and therefore the distance between the particles is smaller than for the anti-symmetric case ($S = 1$), i.e. the Coulomb repulsion reduces its binding energy more than for $S = 1$. Therefore the chosen fit-parameter 'a' is too high, it is supposed to be an upper limit to the really calculated first excited state. The restriction of the amplitude to one combination $\uparrow\downarrow$ even regards only one configuration of the pion. Thus, the ground-state can just be characterized as a quasi-pion, with the correct quantum numbers for a pseudo-scalar particle.

Disregarding the internal parity of the anti-quark, so that the parity is $P = (-1)^J$ and the pion a 'quasi-scalar' particle, it would have $J^{PC} = 0^{++}$. Then its first excited state would be $J^{PC} = 1^{--}$ ($S = 0$, $L = 1$). This state has the same parity as the ρ-meson with ($S = 1$, $L = 0$), which is represented by the 1^3S_1 in Fig. 18. Under this assumption and with the knowledge that states with the same total angular momentum J are quite similar in their energies, the fit to the ρ-meson can be regarded as a lower boundary to the first excited pion state. The corresponding numbers and figures are given in App. C.

As this is the point where the values of the constituent masses $m_1 = m_u$ and $m_2 = m_d$ are adjusted, their choice is too high, because the reference points are upper boundaries. The train of thought has been as follows: the first guess has been $m_u = m_d = 350$ MeV, so that $\widetilde{m}_i = m_i/\kappa = 1$, with $\kappa = 350$ MeV. This brought up the right pion mass, but the higher excited states were much below the real mass values. Therefore the quark masses have been adapted by hand to obey the constraints in (103) for all three s-states. For $m_u = m_d = 518.5$ MeV the result is satisfying the demands. It is also possible to vary the mass scale κ and keep $\widetilde{m}_i$ fixed to 1, the result would be the same. Fig. 19 shows the spectrum of the first three singlet S-states in MeV versus the scale μ in $\kappa = 350$ MeV calculated with the appropriate renormalized α. It is remarkable that the gap at $\mu_{crit} \sim 8.5$ of Fig. 17 has such an effect on the higher states. While the 1S-state is completely flat and insensitive to μ, the 2S- ($\circ$), 3S- ($\Box$), and 4S-state ($\triangle$) are functions of μ. For $\mu \leq \mu_{crit}$ the levels are mainly equidistant and the mass value is in the proclaimed region between $900 - 1000$ MeV. Between $\mu = 3$ and $\mu = 6$ both states form small plateaus. At $\mu_{crit} \sim 8.5$ both functions simultaneously break down to the 1S-level

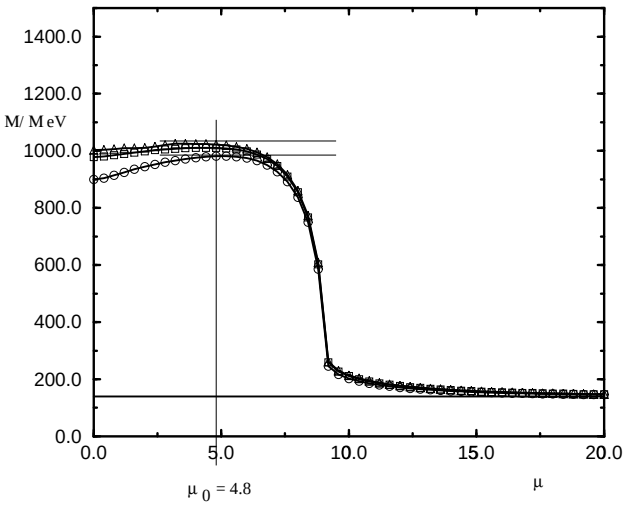

Figure 19: *The spectrum of the first four singlet S-states in [MeV] versus μ in [κ]. The 1S-state is completely flat and insensitive to μ, the 2S- ($\circ$), 3S- ($\Box$), and 4S-state ($\triangle$) are functions of μ. The deep step at $\mu_{crit} \sim 8.5$ corresponds to the gap in Fig. 17. The whole spectrum is insensitive to μ at $\mu \sim 5$, accentuated by the tangents to the plateaus. For $\mu \to \infty$ the spectrum is not resolvable on this mass scale.*

and stay there for $\mu \geq \mu_{crit}$. On the mass scale of Fig. 19 the spectrum can not be resolved for $\mu \to \infty$. For the later calculations on scalar mesons one (α, μ)-pair has to be marked. Therefore the progress of the functions in μ is discussed with respect to the renormalization group equation (see Eq. 47). If $\alpha = \alpha(\mu)$ and the Hamiltonian no longer depends on μ, the main relation $dM_h^2(\alpha, \mu) = 0$ is fulfilled. In Fig. 19 it is obvious that the Hamiltonian is not purely insensitive to μ over the whole range. There are mixings which occur from the Q^2-term in the denominator of the regulator. The most μ-independent parts in this spectrum are the totally independent ground level and both plateaus in 2S, 3S, and 4S. Drawing tangents to the platforms and calculating

$$\frac{dM_h^2}{d\mu} = 0 \quad \text{at} \quad \alpha = \alpha(\mu)$$

restricts the interval of suitable points to a very small region around $\mu \sim 5$. With respect to the mass eigenvalues of the second and third state the appropriate numerical value is $\mu_0 = 4.8 \cdot \kappa$, $\kappa = 350$ MeV with a corresponding renormalized $\alpha(\mu_0) = 0.6977$.

The above method can be described as a kind of poor mans' renormalization, because universality over the whole spectrum is not given. But it is possible to enforce total independence on μ to find one (α, μ)-pair which fulfills the condition. It is remarkable that the found $\alpha(\mu_0)$ is around 0.7, since other theory groups calculate with $\alpha_{strong} \simeq 0.7$ based on experience [35].

Now that μ_0 and $\alpha(\mu_0)$ are fixed, the 'stretching factor' z, invented in Eq.(81) in Sect.4.2, has to be set. The intensity of the wave function is obviously coupled to μ and α. Because of the higher complexity of the problem the 'ordinary' optimization procedure (see Figs. 7, 12) would be too expensive, i.e. for each (α, μ)-pair a suitable z would have to be fixed. Here, the best function for z has been found by trying out several relations in α, μ. Therefore all calculated values are optimized with

$$z = m_r \left(1 + \frac{\mu^2}{4 m_r m_s} \left(\frac{4}{3}\alpha\right)^2\right) \frac{4}{3}\alpha = m_r \left(1 + t_1 t_2\right) t_2 \quad , \tag{104}$$

$t_1 = 4/3\,\alpha\mu^2/\left(4 m_r m_s\right)$ being the coupling of the regulated Delta potential and $t_2 = 4/3\,\alpha$ that of the Coulomb.

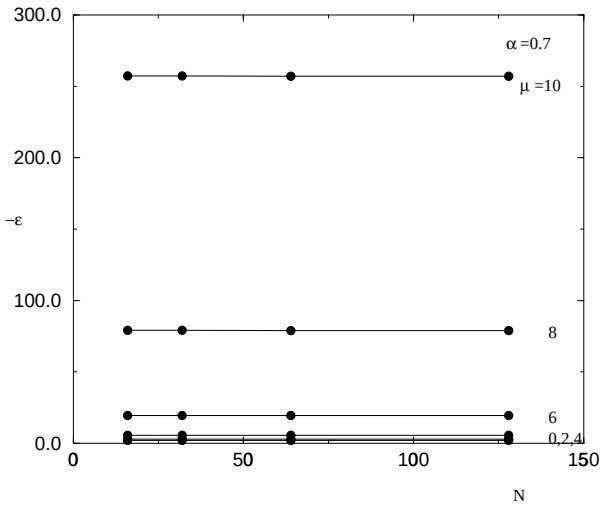

Figure 20: *The first negative eigenvalue $-\varepsilon$ is plotted versus the number of integration points N (16,32,64,128) for $m = 1.48 \cdot \kappa$, $\kappa = 350$ MeV, $\alpha \sim 0.7$, and different values of the scale μ. Note the excellent stability over the whole integration range.*

Fig. 20 shows the first negative eigenvalue $-\varepsilon$ versus the number of integration points N (16,32,64,128) for $m_1 = m_2 = 1.48 \cdot \kappa$, $\kappa = 350$ MeV, $\alpha \sim 0.7$, and different scales μ. It is visible that the function $z(\mu, \alpha)$ supports great stability over the

whole range of integration points N. Therefore it is sufficient to calculate with 16 integration points.

Now the adjusted quark masses $m_1 = m_2 = 518.5$ MeV are used to fix the remaining quark masses. With identifying $m_1 = m_u$ and $m_2 = m_d$, the masses of the strange, charm, and bottom have to be calculated. The top-quark mass can not be derived, since no $t\,\bar{q}$-states are currently known. But with a current mass of $m_t = 174.3 \pm 5.1$ GeV [30], the constituent mass is slightly more, about 175 GeV. This estimate comes from the fact that the constituent mass contains the current or intrinsic mass plus a dynamic term, which belongs to a cloud of gluons and seaquarks, where the quark is wrapped in. That term is somehow related to the scale parameter of strong interactions and a thumb rule fixes it at about $300 - 400$ MeV [29]. Including the found $(\mu_0, \alpha(\mu_0))$-pair the masses are derived by fitting to the appropriate $q\,\bar{u}$-meson, which is again a bisectional iteration. The results are given in Table 9.

fit meson	mass/[MeV]	derived masses/[MeV]
$d\,\bar{u}$	140	$\overline{m}_u = \overline{m}_d$ 518.5 (fixed)
$s\,\bar{u}$	494	$\overline{m}_s$ 597.2
$c\,\bar{u}$	1865	$\overline{m}_c$ 1636.8
$b\,\bar{u}$	5279	$\overline{m}_b$ 5001.2

Table 9: *The fitted remaining quark masses are given in [MeV].– In the first two columns the corresponding fit meson and its mass are mentioned, in the third the derived value is tabulated.*

These four different quark masses (top excluded) together with the renormalized coupling constant α and the regulator scale μ build a complete set of parameters to describe all mesons. The derived eigenfunction for the pion and the meson masses are discussed in Sect. 5.1.

4.4 Renormalizing the 'completely regulated' potential

Before only the Delta function-like constant has been regulated. Now the completely regulated potential, as introduced in Eq.(62), is discussed. With

$$\frac{1}{Q^2}\frac{\mu^2}{\mu^2+Q^2} = \left[\frac{1}{Q^2} - \frac{1}{\mu^2+Q^2}\right] \tag{105}$$

the regulated Coulomb is divided into a Coulomb minus a Yukawa potential. Such combination is known from the first calculations in Sect.4.2. With the regulated Delta being similar to a scaled Yukawa, the potential of the 'completely regulated' equation is again a combination of a Coulomb and a Yukawa, i.e.

$$\left(E - \frac{\vec{k}^2}{2m_r}\right)\phi(k) = -\frac{4}{3}\frac{\alpha}{2\pi^2}\int d^3\vec{k'}\left[\frac{1}{Q^2} + \left(\frac{\mu^2}{4m_r m_s} - 1\right)\frac{1}{\mu^2+Q^2}\right]\phi(k) \quad . \quad (106)$$

This equation can be discussed by means of the factor $\mu^2/(4m_r m_s)$. If $\mu^2/(4m_r m_s)$ is equal to 1, the pure Coulomb potential is restored. For $\mu^2/(4m_r m_s) < 1$ Coulomb and Yukawa are subtracted, and behave as in Sect.4.2. For $\mu^2/(4m_r m_s) > 1$ both potentials are added as in Sect. 4.3. Hence, the solutions of Eq.(106) can be estimated. The potential strongly depends on the quark masses, so that the higher the quark masses are, the smaller the scale $\eta = \mu/b$ gets. Thus, one point exists where the sign between Coulomb and Yukawa turns to the opposite. Generally speaking the 'completely regulated' potential is a refinement of the first model equation. It can be calculated 'ad hoc', because the counter terms are the same as before. The remaining matrix equation is again described by its diagonal

$$\begin{aligned} a_{ii} \;=\; & -b^2\frac{m_s}{m_r} + \frac{t_1}{(t_1+t_2)}\frac{m_s}{m_r}\left(-\mu^2\frac{(\mu+2b)^2}{k^2+(\mu+b)^2} + \mu(\mu+2b)\right) \\ & -\frac{t_1 m_s}{\pi}\sum_{j\neq i}\omega_j\frac{k_j}{k_i}\ln\frac{(k_i-k_j)^2+\mu^2}{(k_i+k_j)^2+\mu^2}\frac{(k_i^2+b^2)^2}{(k_j^2+b^2)^2} \\ & -\frac{t_2 m_s}{\pi}\sum_{j\neq i}\omega_j\frac{k_j}{k_i}\ln\frac{(k_i-k_j)^2}{(k_i+k_j)^2}\frac{(k_i^2+b^2)^2}{(k_j^2+b^2)^2} \quad , \end{aligned} \quad (107)$$

and off-diagonal elements

$$\begin{aligned} a_{ij} \;=\; & \frac{t_1 m_s}{\pi}\sqrt{\omega_i\omega_j}\ln\frac{(k_i-k_j)^2+\mu^2}{(k_i+k_j)^2+\mu^2} \\ + \; & \frac{t_2 m_s}{\pi}\sqrt{\omega_i\omega_j}\ln\frac{(k_i-k_j)^2}{(k_i+k_j)^2} \quad , \end{aligned} \quad (108)$$

with

$$\begin{aligned} t_1 = \; & \left(\frac{\mu^2}{4m_r m_s} - 1\right)\;\frac{4}{3}\alpha \qquad \text{for the scaled Yukawa ,} \\ t_2 = \; & \qquad\qquad\;\frac{4}{3}\alpha \qquad \text{for the Coulomb ,} \end{aligned}$$

and $b = m_r(t_1+t_2) = (\mu^2/4m_s)\,4/3\,\alpha$ as the combining scale. The only difference to the first equation is given by t_1, which contains the contribution of a pure Yukawa.

This term cancels in b against the Coulomb one, and therefore the combining scale has a new appearance. Now the complete renormalization machinery has to be started again as discussed in Sect. 4.3.

The value for the up- and down mass occurs to be $\widetilde{m}_{u,d} = m_{u,d}/\kappa = 1.514$ with $\kappa = 350$ MeV. Thus, to satisfy $M_h^2(\alpha_i) = M_{\pi^+}^2$ the lowest eigenvalue is

$$\varepsilon = -\frac{(m_1 + m_2)^2}{\kappa^2} + \frac{M_{\pi^+}^2}{\kappa^2} = -9.01106 \quad , \tag{109}$$

with $M_{\pi^+} = 139$ MeV.

In a first calculation it is verified that for $\mu = 0$ and $\alpha = 0$ all eigenvalues are zero. Comparing the values to those in Table 7, the numbers for the 'completely regulated' potential are not lying as deep, i.e. the first eigenvalue is not as rapidly decreasing, see Fig. 21.

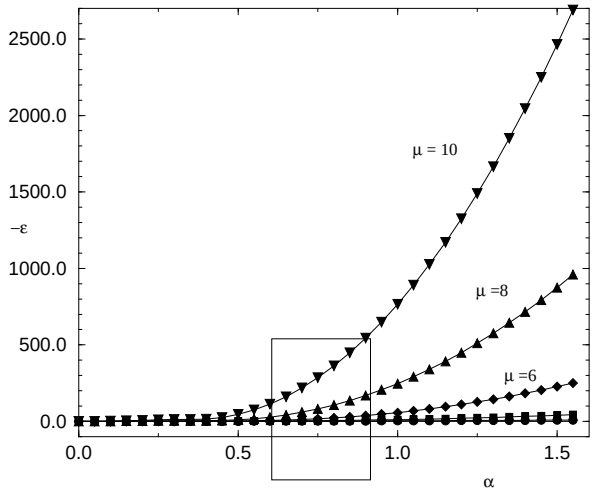

Figure 21: *The lowest eigenvalue $-\varepsilon = m_s^2 - M^2$ is plotted versus the coupling constant α. The different lines refer to different values of the regularization scale μ ($\mu = 0, 2, 4, 6, 8, 10$). The box marks the region around $\alpha \sim 0.7$.*

The figure shows the negative lowest eigenvalue $-\varepsilon$ versus the coupling constant α for different scales μ. The behavior of the curves is analogous to that of the 'Coulomb plus regulated Delta'. To pick up one $(\mu_0, \alpha(\mu_0))$-pair the same constraints on the pion ground state and the first excited one are used (see Eq. 103). The box in Fig. 21 marks the region around $\alpha \sim 0.7$. Choosing an α of about 0.65 and $\mu \sim 6$, the first excited state is not reached. Adjusting the values, the best fitting

numbers are $\alpha = 0.93617$ and $\mu = 4.0$. The appropriate up- and down-quark mass is therefore

$$m_1 = m_2 = 1.514 \cdot \kappa = 529.9 \text{ MeV} \quad , \tag{110}$$

which is 2.2% higher than before. With the found numbers for α, μ, m_1 and m_2 the complete spectrum and the wave functions of the excited π^+ can be described. According to this problem the remaining quark masses are calculated. They are given in Table 10 together with their corresponding fit meson.

fit meson	mass/[MeV]	derived masses/[MeV]
$d\,\bar{u}$	140	$\overline{m}_u = \overline{m}_d$ 529.9 (fixed)
$s\,\bar{u}$	494	$\overline{m}_s$ 616.2
$c\,\bar{u}$	1865	$\overline{m}_c$ 1688.
$b\,\bar{u}$	5279	$\overline{m}_b$ 5056.

Table 10: *The fitted quark masses in [MeV].– In the first two columns the fit meson and its mass are given, in the third the received value is listed.*

In this section the numerical tools have been introduced and the renormalization procedure for the two main equations (62) and (65) has been performed. A guess of the first quark mass pair, the up- and down-mass starts the procedure. All appropriate pairs $(\mu, \alpha(\mu))$ are found via the Bisection method. According to renormalization theory, the spectrum has to be independent of the renormalization scale. This 'universality' holds not over the whole μ-region, it exists a point μ_{crit} which divides the spectrum in two parts. For $\mu \leq \mu_{\text{crit}}$ independence is obeyed, for $\mu \geq \mu_{\text{crit}}$ the spectrum depends strongly on μ. Thus, the question of 'universality' fixes one suitable $(\mu_0, \alpha(\mu_0))$-pair in the $(\mu \leq \mu_{\text{crit}})$-regime. Moreover, the up- and down-mass are adjusted to fit to the first excited state of the pion. The restriction of the model to S-waves causes the problem that the first excited state is not clearly identified. In fact, the real first excited state, the a-meson, is used as a upper boundary to the 2S-state. Under the assumption of having a scalar pion, the ρ-meson provides a lower boundary to the 2S-state. For comparison the fit to the ρ-meson is done as well, see App. C.

Consequently three sets of parameters have been obtained, tabulated in Table 11. The quark masses and μ-values are all in the same region, while the renormalized

parameter	Coulomb plus regulated Delta		complete
	'a'-fit	'ρ'-fit	'a'-fit
α	0.6977	0.6904	0.9362
μ	4.8	3.8	4.0
up	1.48	1.16	1.51
down	1.48	1.16	1.51
strange	1.71	1.45	1.76
charm	4.68	4.76	4.82
bottom	14.29	14.44	14.45
top	498.0	498.0	498.0

Table 11: *Sets of parameters received from two different potentials and two different fits. The quark masses and μ are given in units of the scale $\kappa = 350$ MeV. Up- and down quark mass are supposed to be equal. The top-quark mass is not obtained from a fit.*

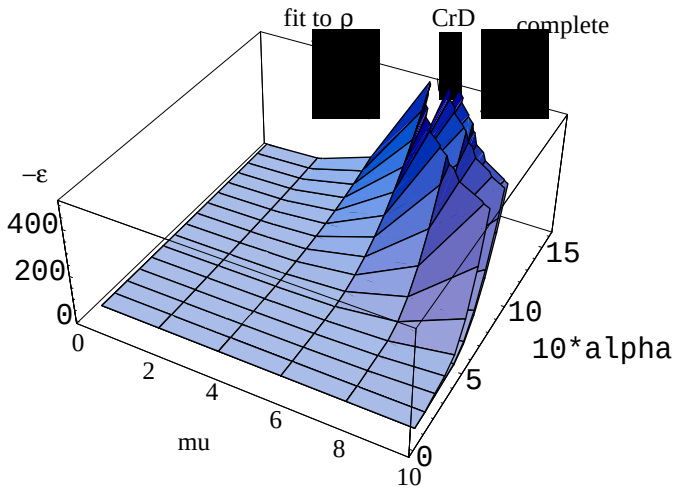

Figure 22: *3D plot of all eigenvalues: coupling constant α, regularization scale μ, and eigenvalue $(m_s^2 - M^2)$ in units of $\kappa = 350$ MeV; This plot shows the values up to an arbitrary limit to show the relation between the three calculated cases. The scalar pion has the strongest ascent, followed by the 'Coulomb plus regulated Delta' (CrD) and the 'completely regulated' potential.*

coupling constant for the 'completely regulated' potential is over 20% higher than the others. Fig. 22 shows how the eigenvalues according to α and μ behave in three

dimensions for all three problems. It is clear that two planes are closer to each other than the third. These two belong to the 'Coulomb plus regulated Delta' (*CrD*) and the 'completely regulated' potential (*complete*) fitted to the a-meson, while the assumed scalar pion is separated. Taking only the scalar pion fitted to the ρ-meson and the complete problem into account, Fig. 22 shows that both can be regarded as an upper and lower boundary. Therefore, the real 2S-state would lie somewhere between both planes.

After this adjustment of quark masses the singlet nS-states for the pion and all other flavor off-diagonal scalar mesons are calculated. The results are discussed in Sects. 5.1 and 5.2, respectively.

5 Pion wave function and meson masses

Corresponding to the parameter sets according to the 'Coulomb plus regulated Delta' and the 'completely regulated' problem the spectrum and the wave functions of the pion and the flavor off-diagonal meson masses are calculated. Those values corresponding to the ρ-fit can be found in App. C.

The results are discussed by physical means. Additionally, for the 'Coulomb plus regulated Delta' potential the pion form factor is approximately calculated and related to the mean square radius.

5.1 'Coulomb plus regulated Delta' potential

This discussion starts with the completely fixed spectrum and the wave functions of the excited π^+.

Table 12 shows the data for $\mu_0 = 4.8 \cdot \kappa$, $\alpha(\mu_0) = 0.6904$ and $m_1 = m_2 = 1.48 \cdot \kappa$ with $\kappa = 350$ MeV. The maximum momentum is at $k_{16} = 15.52 \cdot \kappa$. In the first row the mass eigenvalues M_h^2 (in MeV) for the first six singlet nS-states are given, their energy eigenvalues $\varepsilon = M_h^2 - m_s^2$ (in κ^2) are shown beneath them. The highest eigenvalue is already in the continuum. Fig. 23 shows approximately the

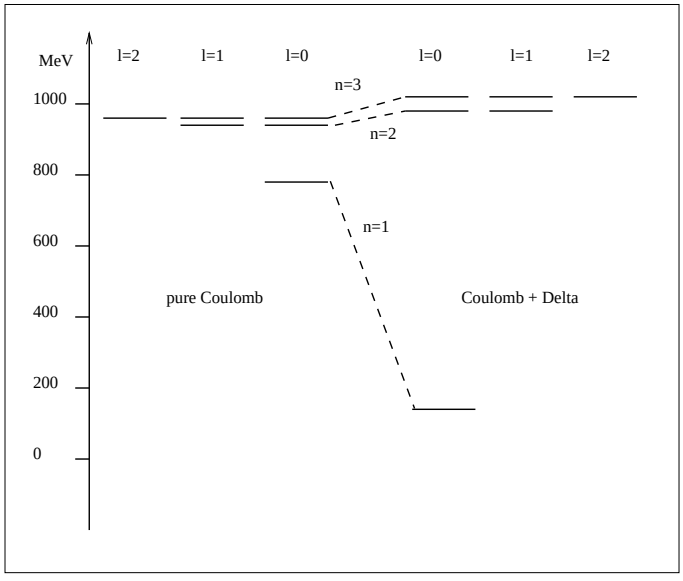

Figure 23: *On the right the spectrum of the pion is plotted as calculated for the parameters $m_1 = m_2 = 518.5$ MeV, $\alpha = 0.6977$, and $\mu = 1680$ MeV.- On the left the pure Coulomb spectrum according to the same α and the same quark masses is shown.*

M_n:	140	980	1009	1021	1034	1130
$k_j \downarrow$	-8.620	-0.934	-0.460	-0.272	-0.058	1.644
0.01	10.000	10.000	10.000	10.000	-0.441	-0.008
0.05	9.928	8.702	5.949	-0.234	1.543	-0.027
0.13	9.560	4.273	-1.058	0.010	-9.717	-0.157
0.25	8.582	0.705	-0.210	0.003	10.000	-1.469
0.40	6.888	-0.079	0.009	-0.000	-0.099	10.000
0.60	4.853	-0.100	0.017	-0.000	-0.464	-1.700
0.85	3.054	-0.055	0.009	-0.000	-0.249	-0.879
1.15	1.783	-0.027	0.005	-0.000	-0.122	-0.404
1.51	0.999	-0.014	0.002	-0.000	-0.060	-0.193
1.95	0.546	-0.007	0.001	-0.000	-0.030	-0.096
2.49	0.292	-0.004	0.001	-0.000	-0.016	-0.049
3.16	0.151	-0.002	0.000	-0.000	-0.008	-0.024
4.01	0.074	-0.001	0.000	-0.000	-0.004	-0.012
5.15	0.033	-0.000	0.000	-0.000	-0.002	-0.005
6.84	0.013	-0.000	0.000	-0.000	-0.001	-0.002
10.00	0.003	-0.000	0.000	-0.000	-0.000	-0.001

Table 12: *The spectrum and the wave functions for the excited π^+. – Parameter values are: α=0.6904, μ= 4.8, $m_1 = m_2$= 1.48 (μ and masses in units of κ = 350 MeV). Calculations are done with 16 Gaussian integration points, with a maximum momentum $k_{16} = 15.52\,\kappa$. – The first row gives the first 6 mass eigenvalues (in MeV), corresponding to the first singlet-nS states. The second row shows the eigenvalues $M_h^2 - m_s^2$ (in units of κ^2). Below each eigenvalue are the 16 eigenfunctions, labeled with the integration points $10k_i/k_{16}$ shown in the first column. They are normalized such that the largest value has the numerical value '10'. As expected the number of nodes increases , and the highest eigenvalue is actually in the continuum.*

spectrum of the first three eigenvalues of the pion for a 'Coulomb plus regulated Delta' on the right, compared to the pure Coulomb spectrum on the left. The parameters corresponding to both spectra are $m_1 = m_2 = 518.5$ MeV, $\alpha = 0.6977$, and $\mu = 1680$ MeV. The spectra are quite different, i.e. the level shift of $n = 1$

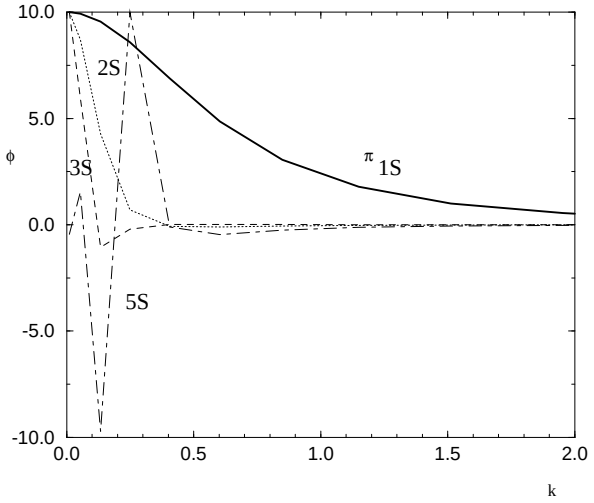

Figure 24: *The first three and the fifth eigenfunction of the excited pion versus normalized momenta* $10\,k_i\,/k_{16}$. *For a better resolution of the single eigenfunctions the* k_j*-interval is stretched to* $k_j = 2$, *the tails of some functions are therefore cut. As expected the number of nodes increases with the excitement. For a higher resolution of the excited eigenfunctions more than 16 integration points are needed.*

is tremendous, while the shift for $n = 2, 3$ is much smaller. The levels for $l = 1, 2$ have not been calculated, they are interpolated by means of quantum mechanic aspects to symbolize higher states. In Table 12, corresponding to each eigenvalue the six eigenfunctions are presented below, each element labeled with its integration point $10\,k_i\,/k_{16}$, tabulated in the first column, and therefore normalized to have the largest value at '10'. Fig. 24 shows a combined plot of the first three and the fifth eigenfunction. As expected the number of nodes increases, also to be seen in the table. The excited eigenfunctions, especially the fifth, are given for imagination. Their awkward appearance implies that more integration points are needed to receive a higher resolution.

Taking only the first eigenfunction for π^+ ($\bullet$), a comparison to the Coulomb wave function ($\Box$) under the same conditions, i.e. same α and quark masses, is shown in Fig. 25. Therein the arbitrarily normalized wave functions are plotted versus the momentum, with the last value at $|\vec{k}|_{max} = 10$. It is astonishing that the pion wave function decreases much slower with the momenta than the Coulomb function. Regarding the potential of a 'Coulomb plus regulated Delta' in the main equation

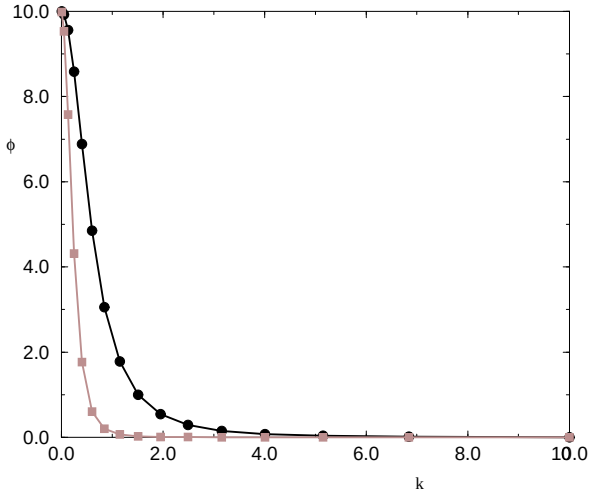

Figure 25: *The arbitrarily normalized pion wave function (•) is plotted versus the momentum, which is normalized to* $|\vec{k}|_{max} = 10$. *It is compared to the Coulomb wave function (□) at the same coupling and quark masses in the same units.- The pion wave decreases much slower with the momentum than the Coulomb wave.*

(98), the difference must be an effect of the smoothed Delta potential. It is known from Sect.4.3 that the regulated Delta is comparable to a scaled Yukawa. Therefore this problem is similar to the first calculations on a combined Coulomb and Yukawa in Sect.4.2, they differ in the relation between Coulomb and Yukawa. With the relations $\mu = \eta\, b$ and $b = m_r(4/3)\alpha\,(1 + \mu^2/\,(4m_r m_s))$ it is possible to calculate the corresponding dimensionless scale η, which for $\mu = 4.8 \cdot \kappa$, $\alpha = 0.6977$ and $m_u = m_d = 1.48 \cdot \kappa$ is $\eta = 1.9211$. Now the behavior of the pion wave function can be compared to that of the pure 'Coulomb minus Yukawa', especially with Figs. 13 and 14. The value of $\eta = 1.9211$ assigns that the new model is situated close to the Coulomb limit. For the 'Coulomb minus Yukawa', the Coulomb-limit was already well achieved for numerical values $\eta \geq 2.0$; therein the width of the eigenfunction was decreasing with increasing η. Now that the Coulomb and Yukawa are added, the width of their wave function increases with increasing η. The shape of the pion wave in Fig. 25 gives evidence for the near of the Coulomb-limit, the width depends on the scaling $\mu^2/\,(4m_r m_s) = 2.6297$, and therefore on the adjustment of the masses and of μ. The appearance of the pion wave function in the near of the Coulomb limit is quite reasonable. Since for the pion the mass and its mean square radius are

known, the general form of the ground state wave function can be estimated. For the pure Coulomb potential the size of the pion is related to the Bohr momentum $p_B = 4/3 m_r \alpha = 0.688 = 1.42$ fm, $m_r = 1.48/2$ and $\alpha = 0.6977$. With $p_B^{-1} \sim \langle r_\pi^2 \rangle^{1/2}$ and $\langle r_\pi^2 \rangle^{1/2} = 0.67$ fm [36, 37] it is obvious that the pure Coulomb radius is much too large and can not describe the pion correctly. However, the Coulomb potential is still the leading term, thus the pion wave function has a Coulomb-type shape. Combining the Coulomb with a Yukawa potential will decrease the radius. Thus, the smaller the root mean-square radius is the more the pion wave function is shifted to higher momenta. The scaling of the Yukawa can also adjust the shift. Whether a 'Coulomb plus regulated Delta' potential can verify the experimental root mean-square radius, will be shown at the end of this section.

Now the scalar flavor off-diagonal mesons as given in the lower rows under the diagonal in Table 1 are calculated.

To have an overview how large the experimental masses of the mesons are, they are listed in Table 13.

	$\bar{u}$	$\bar{d}$	$\bar{s}$	$\bar{c}$	$\bar{b}$
u		768	892	2007	5325
d	140		896	2010	5325
s	494	498		2110	—
c	1865	1869	1969		—
b	5279	5279	5369	∼6400	

Table 13: *Experimental masses of the 'flavor off-diagonal' mesons in MeV. Vectormesons are in the upper triangle, scalars in the lower.*

	$\bar{u}$	$\bar{d}$	$\bar{s}$	$\bar{c}$	$\bar{b}$
u		980	1060	2100	5464
d	140		1060	2100	5464
s	494	494		2174	5535
c	1865	1865	1916		6495
b	5279	5279	5324	6006	—

Table 14: *The calculated mass eigenstates of QCD in MeV. Singlet 1S-states are given in the lower triangle, singlet 2S-states in the upper.*

The vectormesons are given for completeness. The calculation procedure is very simple. The corresponding quark- and anti-quark mass are put into Eqs.(99, 100) and the resulting eigenvalues $D = \varepsilon \cdot \kappa^2$ are directly coupled to the square of the mass eigenvalue,

$$D = \varepsilon \cdot \kappa^2 = M^2 - (m_q + m_{\bar{q}})^2 \quad . \tag{111}$$

The calculated 'flavor off-diagonal' mass-eigenstates are given in Table 14. Because of the restriction to scalar particles it is not possible to compile vectormesons.

Instead of their real value those for the singlet 2S-state are given in the upper triangle. Comparing the calculated singlet 1S-states to the experimental masses, it has to be regarded that the up- and down-mass were fixed from the beginning and that the $q\,\bar{u}$-states have been the fit-values for the remaining quark-masses. With $m_u = m_d$ there can be no difference between the columns $q\,\bar{u}$ and $q\,\bar{d}$. Therefore the values for $c\,\bar{s} = D_s^+$, $b\,\bar{s} = \bar{B}_s^0$, and $b\,\bar{c} = B_c^-$ are really calculated masses. They deviate from experiment between 0.8% ($\bar{B}_s^0$) and 6.2% (B_c^-) (2.7 % D_s^+). This is a really good result, since the model is extremely simple. It has also to be noticed that the experimental value for B_c^- has recently been taken up into the list of the 'particle data group', its mass is therein given as $6.4 \pm 0.39 \pm 0.13$ GeV [30]. It is astonishing how well the singlet 2S-states fit to the vectormeson masses. The ρ^+ has to be disregarded, since the 'a' has been the fitting parameter for the up- and down mass, but even the other values differ just by $\pm$(2.5 to 15.8)%, the mean value is at 4.4% . The experimental masses show some interesting relations between $q\,\bar{u}$ and $u\,\bar{q}$:

(1)		(2)		(2)/(1)
$d\,\bar{u}$	140	$u\,\bar{d}$	768	5.5
$s\,\bar{u}$	494	$u\,\bar{s}$	892	1.8
$c\,\bar{u}$	1865	$u\,\bar{c}$	2007	1.08
$b\,\bar{u}$	5278	$u\,\bar{b}$	5325	1.008

The heavier one of the constituents is, the smaller the difference between scalar ($q\,\bar{u}$) and vector ($u\,\bar{q}$) masses. Examining this effect for d-quark combinations brings along the same proportionalities as for the u-quark:

(1)		(2)		(2)/(1)
$s\,\bar{d}$	498	$d\,\bar{s}$	896	1.7899
$c\,\bar{d}$	1869	$d\,\bar{c}$	2010	1.08
$b\,\bar{d}$	5279	$d\,\bar{b}$	5325	1.008

Testing the last experimentally known couple

(1)		(2)		(2)/(1)
$s\,\bar{c}$	2110	$c\,\bar{s}$	1969	1.072

,leads to a kind of periodicity. The relation factor mirrors which quark is heavier, e.g., a (u,s) or (d,s)-system is dominated by the strange-mass, but a (c,s)-system obeys the charm-mass. With this proportionality factors it is possible to predict the missing masses for $s\,\bar{b}$ and $c\,\bar{b}$. Their order is given by the following

$$\begin{aligned} b\,\bar{s} = 5375 \text{ MeV} \quad &\rightarrow \quad s\,\bar{b} = 1.008 \cdot 5375 \text{ MeV} \;=\; 5418 \text{ MeV} \\ b\,\bar{c} \simeq 6400 \text{ MeV} \quad &\rightarrow \quad c\,\bar{b} \simeq 1.008 \cdot 6400 \text{ MeV} \;\simeq\; 6451.2 \text{ MeV} \quad . \end{aligned}$$

Using the new knowledge and comparing the singlet 1S-states with the singlet 2S-states, shows that the proportionality factors are similar for light-light mesons and higher for heavy-light or heavy-heavy compounds,

quark-combination	experimental 2S / 1S	factor
(d,u)	980 / 140	7
(s,d)=(s,u)	1060 / 494	2.15
(s,c)	2174 / 1916	1.135
(c,d)=(c,u)	2100 / 1865	1.26
(b,c)	6495 / 6006	1.081
(b,s)	5535 / 5324	1.039
(b,d)=(b,u)	5464 / 5279	1.035

,i.e. with one mass increasing and the other decreasing (last three rows for (b,q)) the factor decreases. The first two rows are given for completeness. The difference for the charm quark is not so drastically, because it is the 'lightest' of the heavy quarks, the factor for charmed-mesons is about 1.2. For the b-mesons the value is between 1.04 and 1.08. The difference between singlet 2S-states and calculated 'vectormesons' – with respect to (1S-mass · factor) from the experimental values – is therefore about 5%. This means that the energy levels of the singlet 2S-states for the scalar mesons and the ground state for vectormesons are approximately at the same energy. The only term which can be responsible for such an effect is the modified current-current interaction $S = 4m_1m_2+2Q^2$, especially the Delta-function corresponding factor 2. A tool to calculate the mass splitting between scalar and vectormesons is the non-relativistic hyperfine interaction

$$V_{\text{hyp}} = \frac{2\vec{S}_q \cdot \vec{S}_{\bar{q}}}{3\,m_q\,m_{\bar{q}}}\nabla^2 V_{\text{Coul}} \;=\; \frac{32\pi\alpha\vec{S}_q \cdot \vec{S}_{\bar{q}}}{9\,m_q\,m_{\bar{q}}}\delta^3(\vec{r}) \quad , \tag{112}$$

with $\langle \vec{S}_q \cdot \vec{S}_{\bar{q}} \rangle = 1/4$ for vector , $-3/4$ for pseudo-scalar. For scalar mesons its value is $V_{\rm hyp} = -(8/3)\pi\alpha/(m_1 m_2)\delta^3(\vec{r})$, which is identical to Eq.(60). Therefore the effect occurs from the hyperfine interaction, which is responsible for the splitting of the meson ground state. Even in atomic physics the splitting is decreasing with increasing mass.

A big advantage of this Hamiltonian method applied in the calculations of the spectrum is the fact that spectrum and wave functions are obtained simultaneously. Thus for each meson the appropriate eigenfunction is available. Fig. 26 shows the ground wave functions of the mesons without pion. The data for $(s,u) = (s,d)$, $(c,u) = (c,d)$, (c,s), $(b,u) = (b,d)$, (b,s), (b,c), and all top-combinations are plotted versus the momentum, with the largest value at '10'. It is visible that the wave functions are getting broader the heavier the included quarks are. For top-compounds all waves are lying upon each other, i.e., the top-mass overrules all other possible effects. The other functions are also grouped with respect to the heavier quark mass, but not as strong as for the top. The corresponding values are given in the first three tables of App. B.

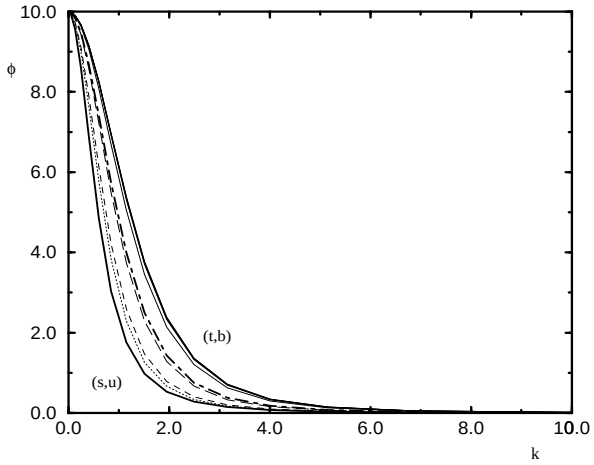

Figure 26: *The 1S eigenfunctions for the calculated mesons are plotted versus the momentum, with the largest value at '10'. The waves appear in their natural order (from left to right):* (s,u), (c,u), (c,s), (b,u), (b,s), (b,c), (t,u) *and* (t,b), *while* $(q,u) = (q,d)$. *The top-wave functions, apart* (t,u), *lie upon each other, represented by* (t,b).

With having all meson eigenfunctions it is possible to touch another interesting topic, the form factor. The knowledge of the form factor would give the advantage

to calculate the mean square-radius and therefore the last two 'free' quark masses, up and down. This goal requires of course the form factor of a meson that contains only up- and down quark, which makes the pion the best candidate. The pionic wave function has already be given in Table 12 and Fig. 24. But first of all the pion form factor has to be adapted to light-cone dynamics. Generally, the form factor describes the difference of the scattering of an object to that of a point-charge at a fixed value for the momentum transfer,

$$\left(\frac{d\sigma}{d\Omega}\right)_{\text{object}} = \left(\frac{d\sigma}{d\Omega}\right)_{\text{point,Mott}} \cdot F^2(\vec{q}) \quad , \tag{113}$$

a typical scattering process is shown in Fig. 27.

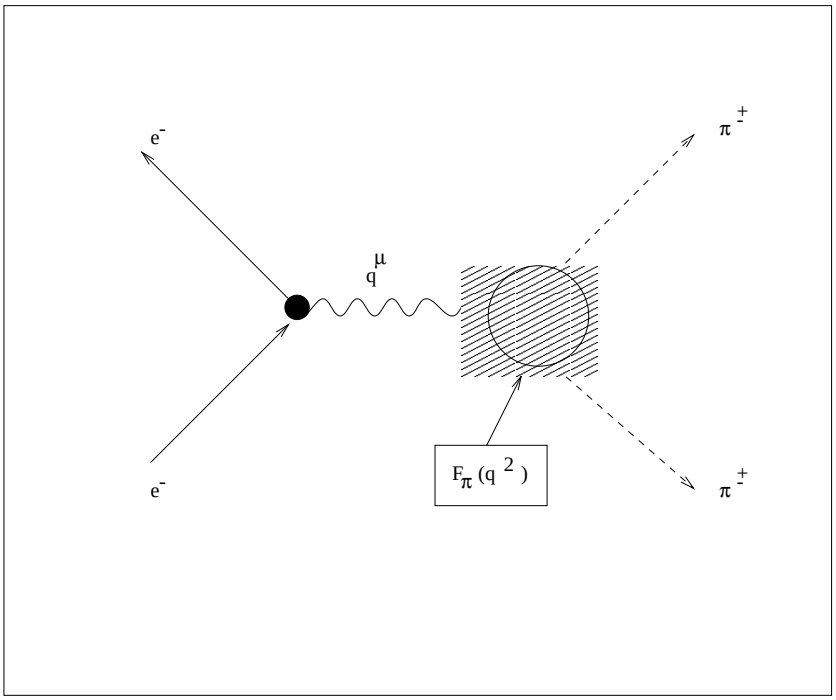

Figure 27: *Illustration of the $\pi e \to \pi e$-process with one-gluon exchange.*

Experimentally the form factor is obtained by dividing the observed cross-section by the calculated point cross-section, i.e. Mott cross-section. For point-like objects the form factor is $F_{\text{point}} = 1$. The above explanation requires that the object is a spherical-symmetric system, so that the momentum transfer has no distinct orientation. Since pions are spin-0-particles, they only have a so-called charge form-factor. Its behavior can be described by a monopole or Dirac form factor,

$$F_\pi(Q^2) = \left(1 + \frac{Q^2}{a^2}\right)^{-1} \qquad \text{with} \quad a^2 = \frac{6}{\langle r^2 \rangle} \quad . \tag{114}$$

If the mean square-charge radius is defined as

$$\langle r^2 \rangle = 4\pi \int_0^\infty r^2 f(r) r^2 dr \quad , \tag{115}$$

with $f(r)$ a charge distribution, the form factor for $Q^2 \to 0$ reads

$$F_\pi(Q^2) = 1 - \frac{1}{6} Q^2 \langle r^2 \rangle + \ldots \quad . \tag{116}$$

From the ascent in the near of the origin the mean square radius can be determined 'by hand' for one value of Q^2 (Eq. 116), or if $F_\pi(Q^2)$ is known up to very small values of Q^2 it can be calculated, i.e

$$\langle r^2 \rangle = -6 \frac{dF(Q^2)}{dQ^2}|_{Q^2=0} \quad . \tag{117}$$

The experimentally measured values for the pion mean-square radius are

$$\langle r^2 \rangle = 0.44 \pm 0.02 \ \ \mathrm{fm}^2 \quad ,$$

$$\sqrt{\langle r^2 \rangle} = 0.657 \pm 0.02 \ \ \mathrm{fm} \ \ [36,\ 37].$$

Compared to the proton with $\sqrt{\langle r^2 \rangle} = 0.862$ fm pions are spatially less expanded. This can be explained by their internal structure; they are $q\bar{q}$-states, while protons are baryons. Kaons are as well meson states, but because of their larger masses, their expansion is smaller than that of pions.

From the literature [8, 10] it is known that physical quantities calculated from the light-cone bound-state wave function such as the form factor and the bound-state spectrum are expected to be rotationally invariant. Thus, the form factor for the lowest Fock-state contribution is given by [18]

$$F(\vec{q}_\perp^{\,2}) = \int dx d^2 \vec{k}_\perp \Psi^\dagger(x, \vec{k}_\perp) \Psi(x, \vec{k}_\perp + (1-x)\vec{q}_\perp) \quad , \tag{118}$$

which is a convolution of two wave functions before and after the scattering by a virtual photon with momentum $q^\mu = (q^+ = 0, q^- = \vec{q}_\perp^{\,2}, \vec{q}_\perp)$ and a momentum transfer $Q^2 = \vec{q}_\perp^{\,2}$. In Eq.(118) $\Psi(x, \vec{k}_\perp)$ is the wave function in $(x, \vec{k}_\perp)$, while the calculated ones are given by $\phi(k_z, \vec{k}_\perp)$. However, the evaluation of Eq.(118) is quite complicated. For such general calculation the following steps are needed: the known function $\phi(\vec{k})$ has to be transformed into the general probability function $\Psi(x, \vec{k}_\perp)$, which then has to be normalized. Afterwards the convolution integral has to be

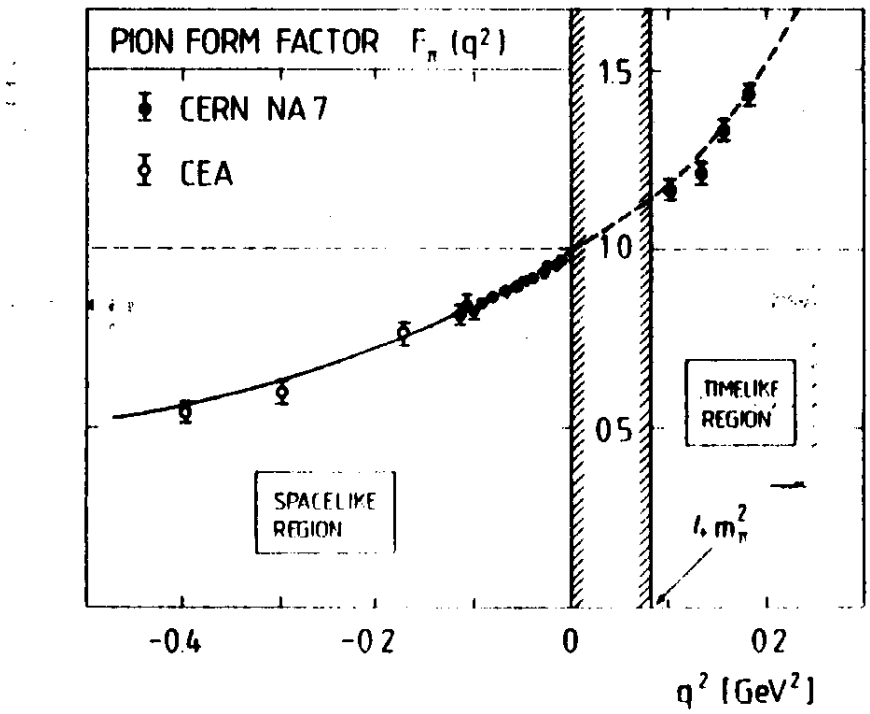

Figure 28: *Pion form factor in the space like-region with $q^2 < 0$ from Amedolia et al. [37]. Its extrapolation to the time-like region is shown to the right. The curve is obtained with an improved ρ meson dominance fit (Brown et al 1986).*

performed to receive $F(Q^2)$ for all Q^2. To imagine how the form factor in Q^2 would look like the data of Amedolia *et al.* is shown in Fig. 28 [37].

To calculate the mean square radius the derivative of the form factors has to be taken in the limit $Q^2 \to 0$. The derivative of the general form factor equation $dF(Q^2)/dQ^2$ together with the experimentally known mean square radius provides the possibility to fix the up- and down-quark mass, which are the last free parameters of the system. A precise adjustment of the up-, down-quark mass has to be done in the near future with the general expressions.

From the shape of the pion wave function the proximity of the Coulomb wave function is known. Thus, it is much easier to approximate the pion wave function by the theoretical Coulomb one, i.e.

$$\phi_j(\vec{k}) \simeq \frac{10}{\left(1 + \frac{k_j^2 - k_0^2}{k_B^2}\right)^2} \quad , \tag{119}$$

with the '10' from the scaling of the calculated wave function, $\phi(p_0) = 10$, k_j the

obtained momenta (see Table 12), ϕ_j the eigenfunction and k_B the Bohr momentum [38]. Fourier transforming the above expression to $\Psi(\vec{x}) \sim e^{-k_B r}$, leads directly to the mean square radius. The Bohr momentum is determined by a fit to the seventh couple of the numerical data in Table 12, $(p, \phi)_7 = (0.85, 3.054)$, its value is $k_B = 1.2595$. This is much larger than the pure Coulomb Bohr momentum $p_B = 4/3\, m_1/2\, \alpha = 0.5339$, with $m_1 = 1.16$ in $[\kappa]$, $\kappa = 350$ MeV, and $\alpha = 0.6904$.

The mean-square radius can thus be defined as the normalized integral of the wave function squared, i.e.

$$\langle r^2 \rangle = \frac{\int d^3r \Psi^*(r) r^2 \Psi(r)}{\int d^3r |\Psi(r)|^2} \quad . \tag{120}$$

Evaluating Eq.(120) the root mean-square radius of the pion becomes,

$$\langle r^2 \rangle^{\frac{1}{2}} = \frac{\sqrt{3}}{k_B} \frac{\hbar c}{\kappa} = 0.665 \text{ fm} \quad . \tag{121}$$

Comparing this result to the experimentally measured value of $\langle r_\pi^2 \rangle^{\frac{1}{2}} = 0.657$ fm, the difference is just 1.2%. Therefore, the root mean-square radius is excellently described by the approximated expression in Eq.(119).

In this section the pion wave function is discussed with respect to the pure Coulomb case. The scalar off-diagonal meson masses are obtained from the 'Coulomb plus regulated Delta model. Some relations between light and heavy mesons are discussed and the hyperfine structure is analyzed. The last point of this section is the relation between the calculated eigenfunctions and the pion root mean-square radius.

5.2 'Completely regulated' potential

Now the pion spectrum and its wave functions for the 'completely regulated' model are discussed. Table 15 shows the data for $\mu_0 = 4\kappa$, $\alpha(\mu_0) = 0.9362$ and $m_1 = m_2 = 1.51\kappa$ with $\kappa = 350$ MeV. In the first row the mass eigenvalues M_n (in MeV) for the first six singlet nS-states are given, beneath them their energy eigenvalues $\varepsilon = M_h^2 - m_s^2$ (in κ^2) are shown. The fifth and sixth eigenvalue are already in the continuum. Corresponding to each eigenvalue the appropriate eigenfunctions are tabulated, each element labeled with its integration point $10k_i/k_{16}$ and normalized to have the largest value at '10'.

Fig. 29 shows a combined plot of the first four eigenfunctions. As for the 'Coulomb plus regulated Delta', the excited eigenfunctions need more than 16 integration points for a higher resolution. A comparison between the ground wave

M_n:	140	980	1023	1039	1119	1380
$k_j \downarrow$	-9.010	-1.321	-0.635	-0.364	1.043	6.388
0.01	10.000	10.000	10.000	10.000	-0.322	1.151
0.05	9.810	7.901	4.627	-0.256	-0.418	1.161
0.13	8.891	2.252	-1.590	0.021	-2.979	1.212
0.25	6.829	-0.068	-0.012	0.000	10.000	1.334
0.40	4.249	-0.160	0.061	-0.001	-1.998	10.000
0.60	2.233	-0.073	0.028	-0.000	-0.874	-4.595
0.85	1.076	-0.031	0.011	-0.000	-0.340	-1.428
1.15	0.504	-0.013	0.005	-0.000	-0.140	-0.533
1.51	0.234	-0.006	0.002	-0.000	-0.061	-0.221
1.95	0.109	-0.003	0.001	-0.000	-0.027	-0.096
2.49	0.050	-0.001	0.000	-0.000	-0.012	-0.043
3.16	0.022	-0.001	0.000	-0.000	-0.005	-0.019
4.01	0.010	-0.000	0.000	-0.000	-0.002	-0.008
5.15	0.004	-0.000	0.000	-0.000	-0.001	-0.003
6.84	0.001	-0.000	0.000	-0.000	-0.000	-0.001
10.00	0.000	-0.000	0.000	-0.000	-0.000	-0.000

Table 15: *The spectrum and the wave functions for the excited π^+. – Parameter values are: α=0.9362, μ= 4.000, $m_1 = m_2$= 1.51 (masses in units of $\kappa = 350$ MeV). Calculations are done with 16 Gaussian integration points, with a maximum momentum $k_{16} = 15.52\,\kappa$. – The first row gives the first 6 mass eigenvalues (in MeV), corresponding to the first singlet-nS states. The second row shows the eigenvalues $M_h^2 - m_s^2$ (in units of κ^2). Below each eigenvalue are the 16 eigenfunctions, labeled with the integration points $10k_i/k_{16}$ shown in the first column. They are normalized such that the largest value has the numerical value '10'. As expected the number of nodes increases , and the two highest eigenvalues are already in the continuum.*

function for π^+ ($\bullet$) and the Coulomb wave function ($\Box$) with the same α and quark masses is shown in Fig. 30, where the wave functions are plotted versus the momentum with $|\vec{k}\,|_{\max} = 10$. Comparing this plot with Fig. 25, it is remarkable that the pion wave function is now closer to the Coulomb wave one. This behavior makes

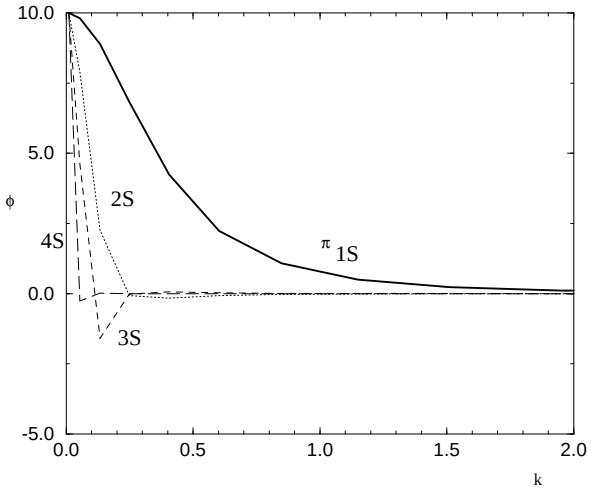

Figure 29: *The first four eigenfunctions of the excited pion versus normalized momenta* $10\,k_i\,/k_{16}$. *For a better resolution of the single eigenfunctions the* k_j*-interval is stretched to* $k_j = 2$, *the tails of some functions are therefore cut. As expected the number of nodes increases with the excitement. All nS wave functions with* $n > 1$ *need more than 16 integration points for a higher resolution.*

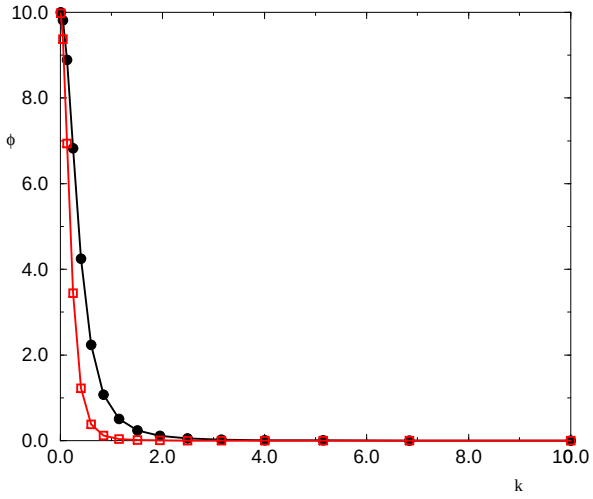

Figure 30: *The arbitrarily normalized pion wave function (•) is plotted versus the momentum, which is normalized to* $|\vec{k}|_{max} = 10$. *It is compared to the Coulomb wave function (□) at the same coupling and quark masses in the same units.– The pion wave function decreases nearly as fast with the momentum as the Coulomb one.*

sense, when the scaling in front of the Yukawa potential is taken into account. The scaling is

$$\left(\frac{\mu^2}{4m_r m_s} - 1\right) = 1.7543 - 1 = 0.75 \quad , \tag{122}$$

this value corresponds to a 71.5% weaker mixing between Coulomb and Yukawa, in Sect. 4.3 the factor has been 2.6296. The appropriate dimensionless scale is $\eta = 2.41935$, which verifies that the pion wave function is dominated by the Coulomb contribution. Thus the radius of the pion is larger than in Sect. 5.1. The obtained value is $\langle r_\pi^2 \rangle^{\frac{1}{2}} = 1.058$ fm, which differs by 38% from the experimental value. The pure Coulomb radius is $\langle r^2 \rangle^{\frac{1}{2}} = 1.033$ fm, so that the 'completely regulated' case pushes the pion wave function too far into the Coulomb-regime.

In Table 16 the meson mass eigenstates for the full problem are tabulated. Again the singlet 1S-states are shown in the lower triangle, and the 2S-states in the upper.

	$\bar{u}$	$\bar{d}$	$\bar{s}$	$\bar{c}$	$\bar{b}$
u		980	1066	2135	5501
d	140		1066	2135	5501
s	494	494		2214	5577
c	1865	1865	1930		6562
b	5279	5279	5337	6218	—

Table 16: *The calculated mass eigenstates of QCD in MeV. Singlet 1S-states are given in the lower triangle, singlet 2S-states in the upper.*

Comparing the calculated singlet meson masses to the experimental masses in Table 13 shows that the values for $c\,\bar{s} = D_s^+$ differ by 1.98%, those for $b\,\bar{s} = \bar{B}_s^0$ by 0.596% and for $b\,\bar{c} = B_c^-$ by 2.84%. This result is much better than that for the 'Coulomb plus regulated Delta'. Even the difference between the singlet 2S-states and the experimental vectormesons is $\pm 4\%$, except $u\bar{d}$, $u\bar{s}$ and $d\bar{s}$. Regarding again the proportionality factors, mentioned in Sect.5.1, the factors are now

quark-combination	experimental 2s / 1s	factor
(d,u)	980 / 140	7
(s,d)=(s,u)	1066 / 494	2.16
(s,c)	2214 / 1930	1.15
(c,d)=(c,u)	2135 / 1865	1.15
(b,c)	6532 / 6218	1.06
(b,s)	5577 / 5337	1.045
(b,d)=(b,u)	5501 / 5279	1.042

The factors are higher than between the experimental values, but they obey the same regularity, as do those in Sect.5.1. The factors for charmed mesons are lower, but clearly grouped. The same holds for bottomed mesons. For the 'Coulomb plus regulated Delta' the factors corresponding to one quark are broader distributed, while now the factors form distinct groups.

Together with the mass eigenstates all suitable eigenfunctions are derived. Fig. 31 shows the ground wave functions of the mesons without pion. The data for $(s,u) = (s,d)$, $(c,u) = (c,d)$, (c,s), $(b,u) = (b,d)$, (b,s), (b,c), and all top-combinations are plotted versus the momentum, with the largest value at '10'. It is visible that the wave functions are getting broader the heavier the included quarks are. For top-compounds all wave functions show a strange behavior contrary to their stable appearance in the 'Coulomb plus regulated Delta' case. A possible explanation is, that for the mesons including the top-quark the interaction has changed into a 'Coulomb minus Yukawa', i.e., the point where the sign flips to the opposite has been crossed. The strength of the coupling is for the (t,u)-pair ($Coulomb$ - 0.99 $Yukawa$), which corresponds more to the 'Airy regime' than to the 'Coulomb regime'. This is contradictory to the behavior of heavy quarks, which since they are non-relativistic particles are situated in or nearby the Bohr regime. Another more likely possibility is that the largeness of the top-quark mass causes numerical instabilities at the boundaries. The other functions are again grouped with respect to the heavier quark mass. The data is shown in the last three tables of App. B.

In this section the numerical results for the 'completely regulated' problem are given and discussed. The received pion wave function is more Coulomb-like than for the 'Coulomb plus regulated Delta' case, thus the mixing of Coulomb and Yukawa is not as strong. The same is verified by the root mean-square radius which is much larger than for the 'Coulomb plus regulated Delta' potential.

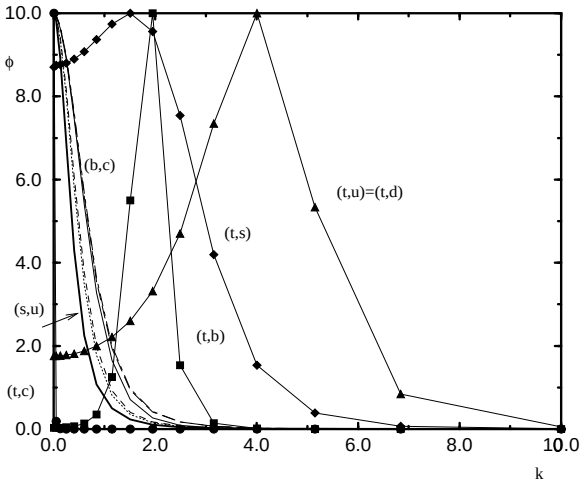

Figure 31: *The 1S eigenfunctions for the calculated mesons are plotted versus the momentum, with the largest value at '10'. The waves appear in their natural order from* (s,u) *to* (t,b)*, while* $(q,u) = (q,d)$*. The top-wave functions show a strange behavior.*

The calculated scalar meson masses differ from the experimental data by not more than 3% (first case 6%), i.e., heavy quark compounds, apart top-including ones, can be described very well non-relativistically, and they are situated in or nearby the Bohr regime. For the top-mesons the interaction changes into a 'Coulomb minus Yukawa', so that they seem to be in the 'Airy or String regime'. However, the higher complexity of the 'completely regulated' problem can cause a higher numerical sensitivity to the effects of large masses, especially those of the top-quark. All programs have been tested with masses around 1 MeV. The top mass is a factor 1000 larger, so that the boundaries can cause instabilities in the routines. The 'Coulomb plus regulated Delta' provides the correct ansatz for the top-compounds. Light quark compounds are not as easy to describe, because they move relativistically. Here, those mesons are used as fit-masses, so that their values are fixed for the whole calculation. However, the pion wave function is correctly described and the spectrum is perfectly described. If all light mesons should be directly calculated like the heavy mesons, the relativistic contributions to the main equation have to be regarded. In the next section the relaxation of the non-relativistic limit and some other suitable aspects of the model are discussed.

6 Further aspects of the model

In this section some aspects concerning the assumptions of the model are discussed to some degree. The first two features are the relaxation of the non-relativistic limit and the isospin effects that will occur from an annihilation contribution. Then the coupling constant is regarded, and the effects of the spin-orbit coupling are also considered as the possibility to include a general spin table.

6.1 Relaxation of the non-relativistic limit

Now that the effects of the 'full' regularization are known the question on the relativistic contributions is obvious. Remembering where the non-relativistic limit comes in (see Eq. 32 in Sect. 3.2) the kinetic and potential energy including the relativistic description of the momentum transfer Q^2 have to be discussed. From Eq.(30) the shape of the relativistic equation is already known

$$\left[D - C(k)\vec{k}^2\right]\phi(\vec{k}) = -\frac{4}{3}\frac{\alpha}{4m_r\pi^2}\int \frac{d^3\vec{k}'}{\sqrt{A(\vec{k})A(\vec{k}')}}\left[\frac{4m_r m_s}{Q^2}+2\right]\frac{\mu^2}{\mu^2+Q^2}\,\phi(\vec{k}') \quad .$$

with $C(k)$, the factor of the kinetic energy, given in Eq.(29) and the A-factor (Eq. 27) corresponding to the Jacobian. Both include the energy $E_i = \sqrt{\overline{m}_i^2 + \vec{k}_\perp^2 + k_z^2}$ and the four-momentum transfer Q^2 (Eq. 22). The momentum itself has surely to be transformed to $(k_z, k_\perp)$ as well, but this expression of Q^2 is so complex, that it is not regarded here. This means that Q^2 remains non-relativistically as $(\vec{k}-\vec{k}')^2$.

Without the expression for Q^2, the first step would be semi-relativistically, only including the terms $C(k)$ and $A(\vec{k})$. Both, the kinetic and the potential term, strongly depend on the chosen mass values m_1, m_2 and they have additional admixtures of momenta. Therefore the equation is given by

$$\begin{aligned}&\left[D - C(k)\vec{k}^2\right]\phi(\vec{k}) = \qquad\qquad (123)\\ &- \frac{t_1 m_s}{\pi^2}\int d^3\vec{k}' B(\vec{k},\vec{k}')\,\frac{\phi(\vec{k}')}{\mu^2+(\vec{k}-\vec{k}')^2} - \frac{t_2 m_s}{\pi^2}\int d^3\vec{k}' B(\vec{k},\vec{k}')\,\frac{\phi(\vec{k}')}{(\vec{k}-\vec{k}')^2} \quad ,\end{aligned}$$

with the abbreviations

$$t_1 = \frac{4}{3}\alpha\left(\frac{\mu^2}{4\,m_r m_s} - 1\right) \quad , \quad t_2 = \frac{4}{3}\alpha \quad \text{and} \quad B(\vec{k},\vec{k}') = \frac{1}{\sqrt{A(\vec{k})A(\vec{k}')}} \quad .$$

The relativistic contribution $B(\vec{k},\vec{k}')$ can also be generalized to a function consisting of the effective running coupling $\overline{\alpha}(Q)$ and the current-current interaction S, apart from the relativistic factor $A(\vec{k})$. This will be considered in due time. The function $C(k)$ is based on the kinetic energy T in Eq.(19) and defined as $T(k) = C(k)\vec{k}^2$ in Eq.(29). The potential energy is varied by the A-factor (Eq. 27). The single energy contributions E_i can be expressed in terms of $E_i = m_i A_i$, which contain the corresponding A-factor for each component. Therefore the overall A-factor itself can be expressed by masses and single A_i-contributions, i.e.

$$A(k) = (m_1 + m_2)\frac{A_1 A_2}{m_1 A_1 + m_2 A_2} \quad . \tag{124}$$

$C(k)$ in Eq.(29) is also given in terms of energies, thus this function can be rewritten in terms of A_i. Including these new relativistic declarations the integral equation of the model is modified

$$\left[D - \frac{\left[m_1(1+A_1(k)) + m_2(1+A_2(k))\right]^2}{m_1 m_2 (1+A_2(k))(1+A_1(k))}\vec{k}^2\right]\phi(\vec{k}) = \tag{125}$$
$$- \frac{t_1 m_s}{\pi^2}\int d^3\vec{k}'\, B(\vec{k},\vec{k}')\,\frac{\phi(\vec{k}')}{\mu^2 + (\vec{k}-\vec{k}')^2} - \frac{t_2 m_s}{\pi^2}\int d^3\vec{k}'\, B(\vec{k},\vec{k}')\,\frac{\phi(\vec{k}')}{(\vec{k}-\vec{k}')^2} \quad ,$$

with

$$B(\vec{k},\vec{k}') = \frac{1}{m_s}\sqrt{\left(\frac{m_1}{A_2(k)} + \frac{m_2}{A_1(k)}\right)\left(\frac{m_1}{A_2(k')} + \frac{m_2}{A_1(k')}\right)}$$

and t_1, t_2 given above.

The non-relativistic limit is restored correctly, which makes the relativistic approach totally compatible to the work done before. The counter terms are already known for the non-relativistic case, they have now to be assimilated to the relativistic case. Replacing $D = 2m_s E$ and including the counter terms, the relativistic equation reads

$$[E - F(k)]\,\phi(k) = \tag{126}$$
$$- \frac{t_1}{2\pi^2}\int d^3\vec{k}'\frac{1}{\mu^2 + (k+k')^2}\left[B(k,k')\,\phi(k') - B(k,k)\,\phi(k)\frac{(k^2+b_1^2)^2}{(k'^2+b_1^2)^2}\right]$$
$$- \frac{t_2}{2\pi^2}\int d^3\vec{k}'\frac{1}{(k+k')^2}\left[B(k,k')\,\phi(k') - B(k,k)\,\phi(k)\frac{(k^2+b_2^2)^2}{(k'^2+b_2^2)^2}\right] \quad ,$$

the new effective kinetic energy has thus the form

$$F(k) = \frac{C(k)}{2m_s}k^2 - B(k,k)\frac{t_1}{2\pi^2}\int d^3\vec{k}'\frac{1}{\mu^2 + (k+k')^2}\frac{(k^2+b_1^2)^2}{(k'^2+b_1^2)^2} \tag{127}$$
$$- B(k,k)\frac{t_2}{2\pi^2}\int d^3\vec{k}'\frac{1}{(k+k')^2}\frac{(k^2+b_2^2)^2}{(k'^2+b_2^2)^2} \quad .$$

This is equivalent to Eq.(93) for the model.

From Sects. 4.3 and 4.4 the introduction of a scale b, to keep the units, is known. In principle b_1 and b_2 can be different numbers, but hence forward it is convenient to find a 'combining scale' $b = b_1 = b_2$. In Sects. 4.3 and 4.4 the appropriate scale b has been independent of the momenta k, but nothing can be said against replacing it by a function $b = b(k)$. The new combining scale $b(k)$ is then given by

$$b(k) = m_r m_s \left(\frac{m_1}{A_2(k)} + \frac{m_2}{A_1(k)} \right) \frac{(1 + A_1(k))(1 + A_2(k))}{(m_1(1 + A_1(k) + m_2(1 + A_2(k))^2} (t_1 + t_2) \quad . \tag{128}$$

Restoring the binding energy D, the relativistic integral equation looks like

$$\begin{aligned} &\left[D + B(k,k) \left(b m_s (t_1 + t_2) - \frac{t_1 m_s}{b} \mu(\mu + 2b) + \frac{t_1 m_s}{b} \mu^2 \frac{(\mu + 2b)^2}{k^2 + (\mu + b)^2} \right) \right] \phi(k) = \\ &- \frac{t_1 m_s}{\pi^2} \int d^3\vec{k}' \frac{1}{\mu^2 + (k + k')^2} \left[B(k,k')\phi(k') - B(k,k)\phi(k) \frac{(k^2 + b^2)^2}{(k'^2 + b^2)^2} \right] \\ &- \frac{t_2 m_s}{\pi^2} \int d^3\vec{k}' \frac{1}{(k + k')^2} \left[B(k,k')\phi(k') - B(k,k)\phi(k) \frac{(k^2 + b^2)^2}{(k'^2 + b^2)^2} \right] \quad . \end{aligned} \tag{129}$$

Restricting to S-waves, and evaluating the matrix equation the non-diagonal elements can be fixed, i.e.

$$a_{ij} = \frac{1}{\pi} \sqrt{\omega_i \omega_j}\, B(k_i, k_j) \left[t_1 m_s \ln \frac{(k_i - k_j)^2 + \mu^2}{(k_i + k_j)^2 + \mu^2} + t_2 m_s \ln \frac{(k_i - k_j)^2}{(k_i + k_j)^2} \right] \quad , \tag{130}$$

as well as the diagonal elements,

$$\begin{aligned} a_{ii} \;=\; & B(k_i, k_i) \left[-b m_s (t_1 + t_2) + \frac{t_1 m_s}{b} \mu(\mu + 2b) - \frac{t_1 m_s}{b} \mu^2 \frac{(\mu + 2b)^2}{k_i^2 + (\mu + b)^2} \right. \\ & - \frac{t_1 m_s}{\pi} \sum_{j \neq i} \omega_j k_j\, B(k_i, k_i)\, \ln \frac{(k_i - k_j)^2 + \mu^2}{(k_i + k_j)^2 + \mu^2} \frac{(k_i^2 + b^2)^2}{(k_j^2 + b^2)^2} \\ & \left. - \frac{t_2 m_s}{\pi} \sum_{j \neq i} \omega_j k_j\, B(k_i, k_i)\, \ln \frac{(k_i - k_j)^2}{(k_i + k_j)^2} \frac{(k_i^2 + b^2)^2}{(k_j^2 + b^2)^2} \right] \quad . \end{aligned} \tag{131}$$

These elements describe the whole relativistic problem with the restriction that Q^2 remains $(\vec{k} - \vec{k}')^2$. All relativistic effects of the considered model are hidden in $B(k, k')$ and the combining scale b. It is obvious that the contribution of the masses and of the momenta is much higher, since $B(k, k')$ and the relativistic completion of b are mainly build up by combinations of m_i and $A_i = \sqrt{1 + (\vec{k}^2 / m_i^2)}$. The effect on the spectrum would be that the levels of the 'relativistic' eigenvalues are lying higher than those for the non-relativistic case.

Since the relativistic system is so sensitive to the mass values, the specification of the constituent masses m_1 and m_2 has a greater effect on the energy levels, i.e. the mass eigenvalue is quite sensitive.

Even the different light and heavy quark masses cause more or less relativistic effects. The influence of the factor A_i decreases with increasing quark mass. If $m_i^2 \gg \vec{k}^2$ $A_i \sim 1$ as in the non-relativistic limit. Thus the relativistic effect increases with decreasing quark mass.

To examine the semi-relativistic effects as well as those of Q^2 more quantitatively is a project for the future.

6.2 Isospin effects

Throughout this thesis only the one-gluon exchange diagrams have been regarded. Here, the third interaction graph, the annihilation diagram, is 'virtually' included, i.e.

$$H_{\text{eff}} = (T + U_{OGE}) + U_{TGA} \quad . \tag{132}$$

As already stated in Sect.2 the effective two-gluon annihilation interaction U_{TGA} destroys a $q\bar{q}$-pair and creates another one with the same or another flavor, which builds up a new Hamiltonian matrix. As already known off-diagonal mesons can be well described, while flavor-diagonal ones are more tricky to handle. The annihilation also mixes the flavors in the charge-neutral flavor-diagonal mesons. These effects on diagonal mesons belong to isospin contributions.

In the thirties Heisenberg introduced the concept of isospin in his studies of the atomic nucleus. Tabl. 17 shows the extension to hadrons. All mesons are grouped into their iso-multiplet.

$I=1$ *ISOTRIPLETS*	$I=\frac{1}{2}$ *ISODOUBLETS*	$I=0$ *ISOSINGLETS*
(π^+, π^0, π^-)	(K^+, K^0)	η , ω, ϕ, Λ
$(\Sigma^+, \Sigma^0, \Sigma^-)$	$(\overline{K}^0, K^-)$	
(ρ^+, ρ^0, ρ^-)	(Ξ^0, Ξ^-)	

Table 17: *Table of Hadron-multiplets*

Isospin has the mathematical properties of an angular momentum, but it is defined in an abstract space [29, 36, 39, 40]. Isospin-physics is based on a Lie-algebra

that is isomorph to the spin algebra, i.e. isospin generators obey $[I_i, I_j] = i\varepsilon_{ijk} I_k$, the application of the third component I_3 determines the place in the multiplet and corresponding ladder operators $I_\pm$ interchange between the elements. According to the famous example of the nucleus as an isospin doublet, isospin symmetry is rather an approximate symmetry than an exact one. If the symmetry would be exact, the isospin generators would commute with the strong Hamiltonian $[I_i\,,\, H_s] = 0$. Then all members of an iso-multiplet would be strictly degenerate in their mass. This is equivalent to the charge independence of nuclear forces. The mass differences in an iso-multiplet are a good measure of symmetry breaking. Zhu and Li [41] have measured the isospin symmetry breaking in terms of the decay constant of the pion $\Delta f_\pi = f_{\pi^\pm} - f_{\pi^0}$. If the symmetry is violated, the degeneracy of the iso-multiplet is cancelled, and the isospin-space is no longer isotropic. According to the Gell-Mann–Nishijima formula $Q = I_3 + Y/2$ with the hypercharge $Y = B + S$, B being the baryon number and S the strangeness, hadrons are arranged in a symmetric $I_3 - Y$-diagram. Its content depends on the fundamental representation and their spectral description J^P. Suppose the three light quarks, up, down, strange. They belong to the SU(3) and have two non equivalent fundamental representations. According to the principles of Young tableaux, the quarks are combined into a singlet and an octet,

$$\square \times \begin{array}{c}\square\\[-4pt]\square\end{array} \;=\; \begin{array}{c}\square\\[-4pt]\square\end{array} + \begin{array}{c}\square\;\square\\[-4pt]\square\end{array} \qquad (133)$$

$$3 \times \overline{3} \;=\; 1 + 8 \;\;.$$

The corresponding $I_3 - Y$-diagram for pseudo-scalar mesons is shown in Fig. 32. The center is doubly occupied, both, the singlet and the triplet, have a 'zero'-component for $Y = 0$. Including the remaining three quarks would need an appropriate higher transformation group.

Under the impact of isospin heavy and light quarks behave differently. Mesons of heavy quarks (charm, bottom, (top)) are relatively simple to describe. The pure quarkonia as charmonium ($c\bar{c}$) and bottomium ($b\bar{b}$) have quite different masses and two strictly separated groups. This grouping is already verified by the model equations, see Figs. 26 and 31. The 'D'- and 'B'-mesons are with respect to flavor and charge clearly put in the right $q\bar{q}$-order. Because of their large masses it is possible

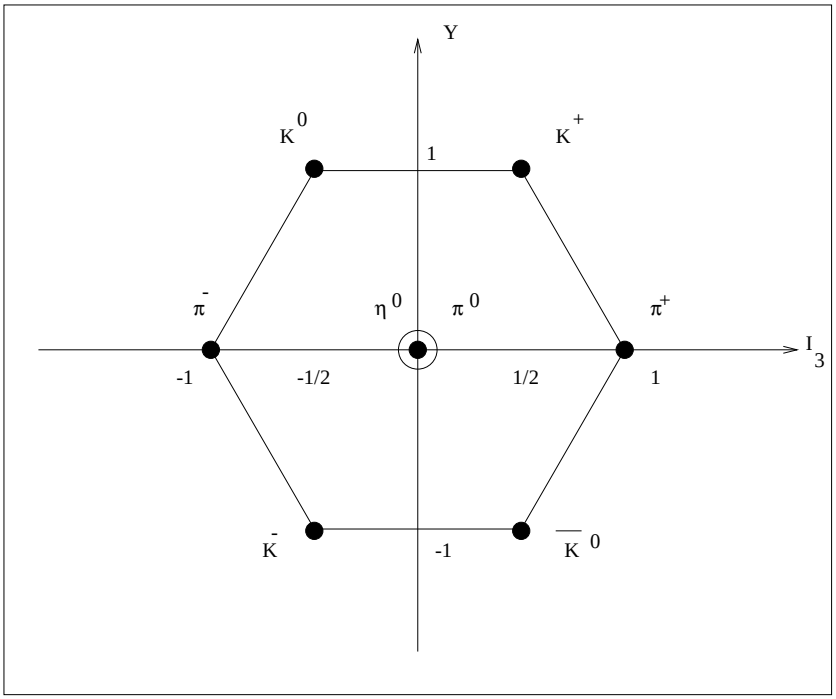

Figure 32: *The meson octet with spin $S = 0$ and $L = 0$.*

to describe them approximately non-relativistic, which has been seen in Sect. 4.4. The mass difference between heavy quark meson-states can be attributed to the spin-spin interaction of the components

$$V_{ss}(q\bar{q}) = \frac{8\pi\hbar^3}{9c}\alpha_s \frac{\vec{\sigma}_q \vec{\sigma}_{\bar{q}}}{m_q m_{\bar{q}}} \delta(\vec{x}) \quad , \tag{134}$$

with

$$\vec{\sigma}_q \vec{\sigma}_{\bar{q}} = 4\vec{s}_q \vec{s}_{\bar{q}}/\hbar^2 = 2[S(S+1) - s_q(s_q+1) - s_{\bar{q}}(s_{\bar{q}}+1)] \quad , \tag{135}$$

and

$$S^2 = (s_q + s_{\bar{q}})^2 = \begin{cases} -3 & S = 0 \\ +1 & S = 1 \end{cases} \quad . \tag{136}$$

Hence, the mass splitting is given by [36]

$$\Delta E_{ss} = \langle \Psi | V_{ss} | \Psi \rangle = 4\frac{8\pi\hbar^3}{9c} \frac{\alpha_s}{m_q m_{\bar{q}}} |\Psi(0)|^2 \quad , \tag{137}$$

which is only valid for S-states, where $\Psi(0) \neq 0$. The description of light quarks (up, down, strange) is more difficult. Their constituent masses are only slightly different. There is no demand for a strictly separated catalogue in quark-flavors, therefore mixing states are possible. The relatively small mass makes a non-relativistic treatment

questionable. But from considerations of meson mass-spectra, it is known that even light quarks analogue to heavy ones can be described semi-quantitatively in a non-relativistic model, see results in Sects. 5.1 and 5.2. This gives a physical meaning to the concept of constituent quarks, up- and down-quark have the same constituent mass. This degeneracy leads to the fact that states with the same quantum number, $u\bar{u}$ and $d\bar{d}$, can mix. A description is given by the isospin-formalism; up and down form an isodoublet with $I = 1/2$, and $I_3 = 1/2$ (up), $I_3 = -1/2$ (down). Analogue to the spin, up and down couple to a singlet and a triplet. The strange quark comes along with the quantum number S ('strangeness'), which can only be changed in weak interactions. Therefore, combinations of $(s, \bar{s}) + (q, \bar{q})$ are eigenstates of the strong interaction. Any s, $\bar{s}$ can mix with u, $\bar{u}$ or d, $\bar{d}$ with the same quantum number J^P. But the strange constituent mass is larger than the up- and down-mass, which suppresses the degree of mixing. This mass difference breaks isospin-invariance, and thus the SU(3)-symmetry is less obvious. In an isotriplet the masses are quite similar, in an iso-octet there are great differences. Including any heavier quark would further decrease the symmetry. For pseudo-scalar mesons with $J^P = 0^-$ three states exist with $S = I_3 = 0$, especially one symmetric flavor singlet-state and two corresponding to the octet. From the octet-states, one has $I = 1$ and therefore a mixing of $u\,\bar{u}$ and $d\,\bar{d}$, which can be identified with the neutral pion, π^0. The remaining octet-state and the singlet-state are able to mix because of flavor SU(3)-symmetry breaking ($m_s \neq m_{u,d}$). For pseudo-scalar mesons this mixing is quite small, η and η' are nearly pure states, i.e.

$$\begin{aligned} |\eta\rangle \sim |\eta_8\rangle &= \frac{1}{\sqrt{6}}\Big[|u\uparrow\bar{u}\downarrow\rangle + |d\uparrow\bar{d}\downarrow\rangle - 2|s\uparrow\bar{s}\downarrow\rangle\Big] \\ |\eta'\rangle \sim |\eta_1\rangle &= \frac{1}{\sqrt{3}}\Big[|u\uparrow\bar{u}\downarrow\rangle + |d\uparrow\bar{d}\downarrow\rangle + |s\uparrow\bar{s}\downarrow\rangle\Big] \quad . \end{aligned} \tag{138}$$

The quark structure of vectormesons is similar, but their singlet- and octet-states are stronger mixed. This belongs to the naturally given mixing angle of about $\arctan 1/\sqrt{2}$, so that the ϕ-meson is a nearly pure $s\,\bar{s}$-state and the 'ω' a state of $u\,\bar{u}$ and $d\,\bar{d}$ with negligible $s\,\bar{s}$-contribution. Analogue to the heavy quarkonia with $S = 0,\ 1$ it is possible to derive the intra-multiplet mass difference from the spin-spin interaction given in Eq.(134). The mass shift is given by

$$\Delta M_{ss} = \begin{cases} -3\frac{8\hbar^3}{9c^3}\frac{\pi\alpha_s}{m_q m_{\bar{q}}}|\Psi(0)|^2 & \text{for pseudo-scalar mesons} \\ +1\frac{8\hbar^3}{9c^3}\frac{\pi\alpha_s}{m_q m_{\bar{q}}}|\Psi(0)|^2 & \text{for vectormesons} \quad . \end{cases} \tag{139}$$

The value of the shift depends on the constituent quark masses. The difference is increasing the lighter the system is, it remains dominant although $|\Psi(0)|^2 \sim 1/r_B^3$ increases for heavy quarks. Thus the mass shift for light quarks is larger than for heavy ones. Phenomenologically the absolute mass value for light quarks can be described by

$$M_{q\bar{q}} = m_q + m_{\bar{q}} + \Delta M_{ss} \quad , \tag{140}$$

with $m_{u,d,s}$ not known, but $m_u = m_d$ fixed and $\alpha_s|\Psi(0)|^2 \sim const.$ Then only a mean mass of each multiplet can be calculated, small mass differences according to electromagnetic interactions are not explainable. Since no isospin is included in the model, the multiplet can not be resolved.

In this sequel the main features of isospin and its effect on mesons with heavy and light quarks are explained. Those give evidence for the fact that the flavor diagonal mesons have not been calculated. The intra-multiplet mass-shifts are described as well as flavor mixing effects with respect to flavor-SU(3).

6.3 Some more aspects

A further assumption has been the lowest order approximation (LOA) of the effective running coupling. The model has been figured out with $\overline{\alpha}(Q^2) = 4/3\,\alpha$ and a kind of a running coupling occurs therein in the form of the renormalized $\alpha(\mu)$. Relaxing this assumption means to introduce from the beginning an effective running coupling, that has a similar form as Eq.(15). However, the expression is too complicate for some first steps in this direction. Therefore the coupling has to be approximated. Emphasis has to be put on the well-behavior in the near of a Coulomb singularity.

Another main approximation has been that of the spin content. As in Eq.(23) the spinor function can be identified with the product of two four-currents, $S = J^2 \equiv j_q^\mu j_{\bar{q}\mu}$. The complete calculation is given in the appendix of [42]. The next important term to be included is the spin-orbit interaction or finestructure, because it provides the possibility to enlarge the model to triplet states, and therefore to vectormesons. It is obvious that the suppression of all other $S = 1$-contributing terms brings along a new simplified spin content, but with more structural input. A possibility might be with respect to the existing coupling

$$S_{\text{new}} = 4m_1m_2 + 2\vec{q}^2 + 4i(\vec{P} \times \vec{q})\vec{S} \quad , \tag{141}$$

with $2\vec{P} = (\vec{k'}+\vec{k})$, $\vec{q} = (\vec{k'}-\vec{k})$, and $\vec{S} = 1/2(\vec{\sigma}+\vec{\tau})$, including quark $(\vec{\sigma})$ -anti-quark $(\vec{\tau})$ spinor relations. The spin-orbit coupling can be expressed as $4i\vec{L}\cdot\vec{S}$, with

$$\vec{L}\cdot\vec{S} = \frac{1}{2}(\vec{P}\times\vec{q})(\vec{\sigma}+\vec{\tau}) \quad ,$$

where $\vec{P}$ can be identified with a kind of a radius and $\vec{q}$ with a momentum.

According to the new finestructure content it might be interesting to discuss whether a $q\bar{q}$-state behaves similar to a multi-electron system in pure quantum mechanics. As for a multi-particle system the single spins of the quarks are added via Russell-Saunders mechanism to a total Spin $\vec{S} = \sum_i s_i$ with quantum numbers $S = 0,\ 1$. The same holds for the orbital-angular momentum $\vec{L} = \sum_i l_i$. The discussed model has been for the quantum numbers $S = 0$ and $L = 0$, i.e. singlet states, so that an implementation of the finestructure should verify that there is no splitting according to S-terms. For quantum numbers $S = 1$, $L = 0$ there should be a finestructure splitting in $(2S+1) = 3$ states, the usual triplet. Even the description of the spin-orbit coupling for $S = 1$ with arbitrary L is interesting, but therefore a completely generalized description of the spin content is needed. A generalization attempt of the spin content is shortly discussed in App. D.

In this section the relaxation of some assumptions and the appropriate effects are theoretically discussed. The individual calculation and the later relaxation of all assumptions in the model is a project for the future.

7 Discussion and Conclusions

In this thesis the full many-body Hamiltonian of QCD has been reduced to a gauge-invariant effective Hamiltonian acting only in $q\bar{q}$ space. The present work is motivated by the question of how the divergent integral kernel effects the results, how to perform the renormalization program in QCD, and whether an extremely reduced model in a light-cone formalism can verify the experimentally measured meson masses. With this thesis the technical basics are introduced for further more complicated calculations.

The analysis of the interaction of the model at equilibrium uncovered the crucial point that it contains a divergence related to the hyperfine interaction in configuration space. It is regulated by a smoothing function, which provided a structure that is equal to a Coulomb plus a scaled Yukawa potential.

Such a structure is already known from calculations carried out in Ref. [20]. This approach reproduces the long and short range asymptotics of the eigenvalues $\epsilon(\eta)$. The numerical values show that for $\eta \geq 2.0$ the data reach the Coulomb limit and for $\eta \to 0$ the values tend to the Airy-solution, as predicted.

Considering this result, the model equations with their specific interactions, 'Coulomb plus regulated Delta' and 'completely regulated' potential, are used to derive the scalar meson masses. Generalized counter terms are set up and the combination of both potentials is obtained by introducing a combining scale parameter b. The 'stretching factor' z is given as a function of the masses and the parameters (α, μ). A stability test shows that convergence is already obtained for small matrix dimensions.

Utilizing the advantage to compute the whole flavor-singlet spectrum at once, all wave functions and eigenvalues of the singlet scalar mesons are calculated. It is possible to reproduce all mesons, i.e. their spectra and wave functions. In comparison with the experimental data the calculated values for the 'Coulomb plus regulated Delta' comply with an average error of 3%, while the numbers for the 'completely regulated' potential differ from the measured ones by approximately 2%. These are excellent results for such a simple model.

A comparison between the 2S-states and the experimental vectormesons shows for both interaction kernels that the values deviate by 4% in average. Proportionality factors are found, which group the mesons according to their contributing quark

masses. The combination of the obtained meson ground state wave functions in one plot has verified that for the 'Coulomb plus regulated Delta' the waves are strictly grouped with respect to their quark content. For the 'completely regulated' potential the grouping is stronger, but the top-mesons cause difficulties. This is possibly related to the fact that the sign in the full potential can flip between 'Coulomb plus scaled Yukawa' and 'Coulomb minus scaled Yukawa', or more likely to numerical instabilities because of the large quark mass.

Comparing the pion ground state wave function with the Coulomb wave function in the same variables illustrates that the pion is close to the Coulomb limit. The pion wave function decreases slower than the pure Coulomb case. According to the type of potential, or the fitting property, the decrease is different, i.e. for the 'Coulomb plus regulated Delta' the wave function decreases slower than for the 'full regulated' potential. This depends on the coupling strength between Coulomb and scaled Yukawa, which is related to the mean square radius of the pion: The stronger the coupling the smaller the radius. But the larger the radius the less the wave function is shifted to higher momenta. The root mean-square radius of the 'Coulomb plus regulated Delta' agrees excellently with the experimental value. This result is the same for 'a'- or 'ρ'-fitted masses. For the 'completely regulated' potential the obtained values comply with an average error of 38%, while the pion root mean-square radius and the pure Coulomb root mean-square radius differ by only 2.4%. Thus, in this case the radius is highly sensitive to the mass-values and the chosen couple $(\mu_0, \alpha(\mu_0))$.

The distance from the Coulomb regime is tested by transforming μ to the scale η in Ref. [20], i.e. for the 'Coulomb plus regulated Delta' the scale is $\eta = 1.9211$ corresponding to the pion and for the 'completely regulated' potential it is $\eta = 2.41935$, which are both situated nearby or in the Coulomb-regime. Also the coupling strength between Coulomb and Delta/Yukawa is tested by the factor $\mu^2/4m_r m_s$. For the 'complete regulated' case with $(\mu^2/4m_r m_s) - 1 = 0.75$ for the pion the potentials are 71.5% more weakly coupled than for 'Coulomb plus regulated Delta', therefore the pion wave function is nearer by the Coulomb wave function. The large root mean-square radius verifies this point. Taking the quark masses of the top and the up, the coupling strength is -0.99, which indicates that the 'Coulomb minus scaled Yukawa' regime has been reached.

The knowledge of the meson wave functions implies that the structure functions

including the contributions from higher Fock states can be calculated from a covariant theory. Those light-cone wave functions encode the properties of hadrons [43]. Given the wave function, any spacelike electromagnetic or electroweak form factor can be constructed exactly from the diagonal overlap of the functions [44].

According to the assumptions and approximations used to derive the model, some of them are discussed on a theoretical level to guide future studies. Relaxing the non-relativistic limit illuminates the fact that heavy quarks are non-relativistic particles, while light ones are not. Thus, to obtain the correct values for light-light mesons the relativistic calculation is important. Another aspect concerns the isospin effects that cause the mass differences between iso-multiplet members. Its inclusion would also give the possibility to describe flavor-diagonal pseudo-scalar mesons and vectormesons.

To compare this model and its techniques with other theories, conventional phenomenological models and lattice gauge calculations have to be mentioned.

Phenomenologically, the quark-structure of mesons and renormalization procedures are of some interest [45, 46, 47, 48, 49]. The variety of theories lies somewhere between a kind of 'tube' model in (1+1)-dimensions, which is semi-analytical solvable [45], and the derivation of the structure of hadrons from the fundamental theory of the strong interaction, QCD [46]. The last approach does not work without a renormalization scheme tailored to it. The author in [46] has a controversy opinion on a Pauli-Villars renormalization since it would drastically increase the size of the Fock space and destroys the hermiticity of the Hamiltonian. Other authors [47] explore how the bound-state energy scales emerge to guide the renormalization procedure. They discuss the similarities that may survive in a non-perturbative QCD calculation, in the context of a precision non-perturbative QED-calculation, in a pedagogical review. They estimate that a renormalization group is needed to produce a regulated effective Hamiltonian, which contains all interactions found in the canonical Hamiltonian, and try to solve it by bound-state perturbation theory. Eq.(43) in [47] is equivalent to the bare Coulomb equation (Eq. 72) in Sect. 4.1. The authors examine this equation by means of an example the known Lamb shift in hydrogen. In fact their work is proclaimed to 'advanced state-of-art for bound-state problems in light-front Hamiltonian gauge theory. Some other renormalization approaches are introduced on one hand by [48] in a method designed to be applied to QCD. But for simplicity they illustrate their model by computing the second- and third-order

matrix elements of the Hamiltonian in massless ϕ^3-theory in six dimensions. On the other hand, in [49] the author defines and illustrates on a few perturbative examples a general method of calculating light-front Hamiltonians which can be used for the relativistic description of interacting particles.

Compared to the work done here, nowhere else has a complete renormalization procedure been worked out to calculate hadronic spectra in light-cone formalism and in the continuum. Mostly authors concentrate on several theoretical aspects concerning the broad variety of QCD-puzzles. All of them have to compute large matrices to get numbers, since loop-effects are taken into account. Recently, Brodsky, Hiller and McCartor have shown [50], that the Pauli-Villars method has advantages for regulating light-cone quantized Hamiltonian theory.

Another method to calculate meson masses is lattice gauge theory. The difficulty with lattice calculations is the time needed to compute the data and the restriction to only one or two states. There also occur uncertainties which belong to finite size effects, discretization, and the lattice spacing a. The lattices used for the compilations are between $12^3 \times 24$ [51] and $16^3 \times 32$ [52]. On the smaller lattice flavor singlet mesons have been calculated by using dynamical quark configurations from UKQCD. They explored the scalar and pseudo-scalar meson channels with $N_f = 2$ [51]. The larger lattice was used for the determination of masses of the light and strange quarks using high-statistics lattice simulation of QCD with dynamical Wilson fermions in $\overline{MS}$ scheme [52]. They calculated the bare up-/ down and strange mass, not their constituent one. The dynamical quarks are identified with the degenerate doublet of isospin symmetric quarks. With a simulation upon sea-quarks and by introducing valence quarks the authors are able to calculate K, K^*, ϕ. They state a high sensitivity to lattice artifacts, which gains control. For their calculations they needed three sets of configurations, each set comprises 200 independent gauge configurations. This consumes a great of computer time.

It has also been possible to perform the masses of low-lying heavy-light mesons in quenched approximation using multi-state smearing technique from a spinless relativistic quark model Hamiltonian [53]. For the calculation a static approximation has been invented and the heavy quark propagator is replaced by timelike Wilson line. This produces an overall scale uncertainty in the quenched approximation, large one-loop renormalization suggests two-loop correction to be sizable.

As well as meson masses the strong coupling α_s has been derived from a lattice-

potential [54]. The potential has been determined from a static quark-anti-quark force at short distances, in quenched QCD. Here, the discretization effects occur, and the authors had difficulties in dealing with logarithmic effects.

This sequel illustrates the main problems lattice-gauge calculations have to deal with. Thus, the presented Hamiltonian method provides a less computationally intensive and complete approach to receive the meson spectra. No problems with discretization or logarithmic effects occur.

An other approach to practical calculations involves combining light-cone quantization with the transverse lattice formulation. Here the transverse dimensions $x_\perp$ are discretized, while the longitudinal plane is left continuous. The light-cone Hamiltonian is written down in terms of longitudinal gauge fields and transverse link fields, and the resulting theory is studied numerically using a combination of LC and Monte-Carlo techniques [55]. This formulation is advantageous for several reasons, e.g. confinement is manifest for finite lattice spacing, there is no need to diagonalize the entire Hamiltonian to study lowest states, but it has technical difficulties in translating the solutions of the non-linear sigma model for application of light-cone techniques.

In other applications, such as the calculation of the axial, magnetic, and quadrupole moments of light nuclei, the QCD relativistic Fock state description provides new insights which go beyond the usual assumptions of traditional hadronic and nuclear physics [56].

Concluding, the main advantages of this approach are summarized. According to the Hamiltonian theory all mesons are derived from one simple model and they verify the experimental values excellently. In this environment the pion is perfectly reproduced. Contrary to lattice gauge theory more than one or two states are computed, even wave functions are produced. Knowing the wave functions, form factors and thus the mean square radius can be calculated exactly. The hyperfine structure is very important. After regularization it provides the correct interaction input to describe the mesons properly. Contrary to the hydrogen atom it is here not treated in first order perturbation theory.

The difference between QCD and QED is given in the factor of strong or weak coupling and the non-abelian nature of QCD resides in the factor 4/3. As seen, renormalization can be carried out exactly. The final equation of the model is of such a simple form, that it can be solved on a desktop computer. Contrary to

lattice gauge theory, calculations have required only seconds. The results show quantitative agreement with the experiment. If the two-gluon exchange diagram would be included, even the isospin structure of the theory could be understood.

With their simplicity, all techniques derived here can be applied to other theories. Even light-front coordinates play a distinguished role in many high energy scattering experiments (e.g. DIS) and light-front quantization represents the most physical approach towards a fundamental theoretical description of such experiments [57]. The knowledge of the hadron wave function also opens a window to a deeper understanding of the physics of QCD at the amplitude level, illuminating exotic effects of the theory such as intrinsic heavy quark effects, color transparency and diffractive processes [43].

For the near future, the four main improvements that have to be kept in mind are:

1. the calculation of the semi-relativistic equation,
2. the relaxation of the Q^2-approximation to derive a full relativistic description;
3. the inclusion of the full spinor structure, and
4. the application of the effective coupling constant to the theory.

A Spinor matrix T

As mentioned in Sect. 3.2 in this Section the matrix elements according to Eq.(33) are tabulated. The diagonal elements are

$$\begin{aligned} T_{11} &= \frac{m_1^2}{xx'} + \frac{m_2^2}{(1-x)(1-x')} + \frac{k_\perp^2}{x(1-x)} + \frac{k_\perp'^2}{x'(1-x')} \\ &\quad + k_\perp k_\perp' \left(\frac{e^{-i(\varphi-\varphi')}}{xx'} + \frac{e^{i(\varphi-\varphi')}}{(1-x)(1-x')} \right), \\ T_{33} &= \frac{m_1^2}{xx'} + \frac{m_2^2}{(1-x)(1-x')} + \frac{k_\perp k_\perp' e^{-i(\varphi-\varphi')}}{x(1-x)x'(1-x')}, \\ T_{22} &= T_{11}, \qquad T_{44} = T_{33}, \end{aligned} \tag{142}$$

with m_1 and m_2 being the masses of quark and anti-quark, respectively, and φ the phase according to $\vec{k}_\perp$. The upper half of the off-diagonal matrix is

$$\begin{aligned} T_{12} &= -\frac{m_1 m_2 (x-x')^2}{xx'(1-x')(1-x)}, \\ T_{13} &= -\frac{m_2}{1-x'}\frac{x}{1-x}\left(\frac{k_\perp}{x} e^{i\varphi} - \frac{k_\perp'}{x'} e^{i\varphi'} \right), \\ T_{14} &= \frac{m_1}{x'}\frac{1-x}{x}\left(\frac{k_\perp}{1-x} e^{-i\varphi} - \frac{k_\perp'}{1-x'} e^{-i\varphi'} \right), \\ T_{23} &= -\frac{m_1}{x'}\frac{1-x}{x}\left(\frac{k_\perp}{1-x} e^{i\varphi} - \frac{k_\perp'}{1-x'} e^{i\varphi'} \right), \\ T_{24} &= \frac{m_2}{1-x'}\frac{x}{1-x}\left(\frac{k_\perp}{x} e^{-i\varphi} - \frac{k_\perp'}{x'} e^{-i\varphi'} \right), \\ T_{34} &= 0, \end{aligned} \tag{143}$$

and the lower half of the off-diagonal matrix is with $T_{ij} = T_{ji}^*(q \leftrightarrow \bar{q})$

$$\begin{aligned} T_{21} &= -\frac{m_1 m_2 (x'-x)^2}{xx'(1-x')(1-x)}, \\ T_{31} &= \frac{m_2}{1-x}\frac{x'}{1-x'}\left(\frac{k_\perp}{x} e^{-i\varphi} - \frac{k_\perp'}{x'} e^{-i\varphi'} \right), \\ T_{41} &= -\frac{m_1}{x}\frac{1-x'}{x'}\left(\frac{k_\perp}{1-x} e^{i\varphi} - \frac{k_\perp'}{1-x'} e^{i\varphi'} \right), \\ T_{32} &= \frac{m_1}{x}\frac{1-x'}{x'}\left(\frac{k_\perp}{1-x} e^{-i\varphi} - \frac{k_\perp'}{1-x'} e^{-i\varphi'} \right), \\ T_{42} &= -\frac{m_2}{1-x}\frac{x'}{1-x'}\left(\frac{k_\perp}{x} e^{i\varphi} - \frac{k_\perp'}{x'} e^{i\varphi'} \right), \\ T_{43} &= 0. \end{aligned} \tag{144}$$

B Eigenfunctions

In this section the eigenvalues and eigenfunctions of the ground states for the 'Coulomb plus regulated Delta' and the 'completely regulated' potential are tabulated. It is possible to compute all excited states to each spectrum with the same program. The following tables include predictions for mesons with top-quarks.

The first three tables belong to the 'Coulomb plus regulated Delta' potential. The first eigenfunctions of the calculated mesons are given in Fig. 26. Parameters are $\alpha = 0.6977$ and $\mu = 4.8 \cdot \kappa$, $\kappa = 350$ MeV. The last three tables show the eigenvalues and ground states wave functions for the 'completely regulated' case. The wave functions of the calculated mesons are plotted in Fig. 31. The parameters are $\alpha = 0.9362$ and $\mu = 4.0 \cdot \kappa$, $\kappa = 350$ MeV. In both cases the dimension of the matrix is 16 and the quark masses are given in units of κ and the meson masses in [MeV].

particle	π	K	D	D
	(u,d)	(s,u)=(s,d)	(c,u)=(c,d)	(c,s)
q	$m_2 = 1.48$	$m_3 = 1.71$	$m_4 = 4.68$	$m_4 = 4.68$
$\bar{q}$	$m_1 = 1.48$	$m_1 = 1.48$	$m_1 = 1.48$	$m_3 = 1.71$
mass	139.570	493.677	1864.600	1915.790
eigenvalue	-8.620	-8.172	-9.538	-10.778
momentum	eigenfunction 10*u[j,i]			
0.010	10.000	10.000	10.000	10.000
0.054	9.928	9.928	9.951	9.957
0.133	9.560	9.561	9.696	9.734
0.249	8.582	8.584	8.986	9.107
0.405	6.888	6.886	7.637	7.888
0.603	4.853	4.840	5.768	6.132
0.849	3.054	3.029	3.835	4.219
1.150	1.783	1.755	2.284	2.596
1.513	0.999	0.975	1.259	1.468
1.954	0.546	0.529	0.662	0.784
2.492	0.292	0.281	0.338	0.404
3.159	0.151	0.145	0.168	0.201
4.010	0.074	0.071	0.080	0.096
5.153	0.033	0.032	0.036	0.042
6.843	0.013	0.012	0.014	0.016
10.000	0.003	0.003	0.003	0.004

particle	B (b,u)=(b,d)	B (b,s)	B (b,c)
q	$m_5 = 14.29$	$m_5 = 14.29$	$m_5 = 14.29$
$\bar{q}$	$m_1 = 1.48$	$m_3 = 1.71$	$m_4 = 4.68$
mass	5278.9	5323.913	6006.391
eigenvalue	-21.231	-24.479	-65.196
momentum	eigenfunction 10*u[j,i]		
0.010	10.000	10.000	10.000
0.054	9.973	9.975	9.983
0.133	9.831	9.845	9.892
0.249	9.423	9.469	9.627
0.405	8.579	8.685	9.059
0.603	7.222	7.406	8.079
0.849	5.495	5.739	6.689
1.150	3.740	3.992	5.053
1.513	2.289	2.498	3.452
1.954	1.282	1.427	2.136
2.492	0.670	0.756	1.207
3.159	0.330	0.377	0.627
4.010	0.153	0.176	0.299
5.153	0.066	0.075	0.128
6.843	0.024	0.028	0.046
10.000	0.006	0.007	0.011

particle	T (t,u)=(t,d)	T (t,s)	T (t,c)	T (t,b)
q	$m_6 = 498$	$m_6 = 498$	$m_6 = 498$	$m_6 = 498$
$\bar{q}$	$m_1 = 1.48$	$m_1 = 1.71$	$m_1 = 4.68$	$m_5 = 14.29$
mass	174593.7	174638.3	175230.8	177179.9
eigenvalue	-641.195	-738.625	-2023.902	-6173.167
momentum	eigenfunction 10*u[j,i]			
0.010	10.000	10.000	10.000	10.000
0.054	9.984	9.985	9.985	9.985
0.133	9.902	9.903	9.904	9.905
0.249	9.662	9.663	9.668	9.669
0.405	9.142	9.145	9.156	9.159
0.603	8.234	8.240	8.262	8.266
0.849	6.919	6.927	6.960	6.967
1.150	5.324	5.335	5.376	5.384
1.513	3.709	3.720	3.761	3.770
1.954	2.334	2.343	2.377	2.384
2.492	1.333	1.339	1.363	1.367
3.159	0.695	0.699	0.713	0.715
4.010	0.331	0.333	0.340	0.341
5.153	0.141	0.142	0.145	0.146
6.843	0.050	0.051	0.052	0.052
10.000	0.012	0.012	0.012	0.012

particle	π (u,d)	K (s,u)=(s,d)	D (c,u)=(c,d)	D (c,s)
q	$m_2 = 1.51$	$m_3 = 1.76$	$m_4 = 4.82$	$m_4 = 4.82$
$\bar{q}$	$m_1 = 1.51$	$m_1 = 1.51$	$m_1 = 1.51$	$m_3 = 1.76$
mass	139.570	493.677	1864.600	1930.041
eigenvalue	-9.010	-8.734	-11.775	-12.934
momentum	eigenfunction 10*u[j,i]			
0.010	10.000	10.000	10.000	10.000
0.054	9.810	9.816	9.895	9.905
0.133	8.891	8.920	9.361	9.422
0.249	6.829	6.888	7.991	8.164
0.405	4.249	4.301	5.795	6.080
0.603	2.233	2.253	3.477	3.771
0.849	1.076	1.074	1.772	1.978
1.150	0.504	0.496	0.812	0.921
1.513	0.234	0.228	0.353	0.402
1.954	0.109	0.105	0.150	0.170
2.492	0.050	0.048	0.063	0.071
3.159	0.022	0.021	0.026	0.029
4.010	0.010	0.009	0.011	0.012
5.153	0.004	0.004	0.004	0.004
6.843	0.001	0.001	0.001	0.001
10.000	0.000	0.000	0.000	0.000

particle	B (b,u)=(b,d)	B (b,s)	B (b,c)
q	$m_5 = 14.45$	$m_5 = 14.45$	$m_5 = 14.45$
$\bar{q}$	$m_1 = 1.51$	$m_3 = 1.76$	$m_4 = 4.82$
mass	5278.9	5336.9	6218.396
eigenvalue	-27.245	-30.148	-55.638
momentum	eigenfunction 10*u[j,i]		
0.010	10.000	10.000	10.000
0.054	9.946	9.947	9.927
0.133	9.675	9.684	9.634
0.249	8.937	8.969	8.907
0.405	7.542	7.612	7.464
0.603	5.587	5.684	5.405
0.849	3.548	3.639	3.276
1.150	1.939	2.000	1.655
1.513	0.936	0.965	0.710
1.954	0.411	0.421	0.268
2.492	0.168	0.170	0.092
3.159	0.065	0.064	0.029
4.010	0.023	0.023	0.009
5.153	0.008	0.007	0.003
6.843	0.002	0.002	0.001
10.000	0.000	0.000	0.000

particle	T (t,u)=(t,d)	T (t,s)	T (t,c)	T (t,b)
q	$m_6 = 498$	$m_6 = 498$	$m_6 = 498$	$m_6 = 498$
$\bar{q}$	$m_1 = 1.51$	$m_3 = 1.76$	$m_4 = 4.82$	$m_5 = 14.45$
mass	171912.3	174024.8	175971.6	123390.5
eigenvalue	-8258.5	-2538.9	-47.1	-138313.6
momentum	eigenfunction 10*u[j,i]			
0.010	1.759	8.704	10.000	0.029
0.054	1.762	8.745	0.188	0.029
0.133	1.766	8.760	0.006	0.032
0.249	1.780	8.802	0.001	0.041
0.405	1.812	8.898	0.000	0.066
0.603	1.876	9.079	0.000	0.133
0.849	1.996	9.369	0.000	0.348
1.150	2.211	9.741	0.000	1.251
1.513	2.598	10.000	0.000	5.499
1.954	3.315	9.564	0.000	10.000
2.492	4.705	7.543	0.000	1.533
3.159	7.344	4.192	0.000	0.142
4.010	10.000	1.536	0.000	0.016
5.153	5.337	0.390	0.000	0.002
6.843	0.838	0.069	0.000	0.000
10.000	0.053	0.006	0.000	0.000

C Scalar pion

As discussed in Sect.5.1 the fit-state to the first excited pion state is all but clear. Assuming a scalar pion leads to a first excited state corresponding to the ρ-meson. For completeness some numbers and main results according to this assumption are given in this appendix.

A first calculation of the lowest eigenvalue shows that the values for $\mu = 0$ in the first column represent the Coulomb case. It is also remarkable that for increasing μ and α the first eigenvalue decreases more rapidly to $-\infty$ than for $m_u = m_d = 1.48$.

Fig. 33 shows the result of this method, the coupling constant α is plotted versus the regularization scale μ in units of $\kappa = 350$ MeV. The behavior of the curve changes at $\mu \sim 7$. Hence the function can be divided into two regions: $\mu \leq \mu_{crit}$ and $\mu \geq \mu_{crit}$ with $\mu_{crit} \sim 7$.

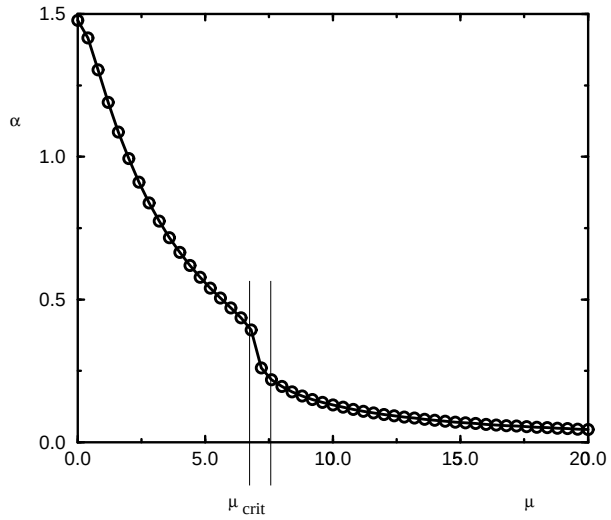

Figure 33: *Renormalized coupling constant α versus regularization scale μ in units of $\kappa = 350$ MeV. The data is obtained by requiring the constraint $\sqrt{m_s^2 + \varepsilon} = M_{\pi^+}$ in the Bisection method. – Note the gap at $\mu \sim 7$.*

The assumption comes in, when 'universality' is checked to hold for the whole spectrum. The constraints for the second eigenvalue is thus modified

$$\sqrt{m_s^2 + \varepsilon_2} = M_1 = 769 \quad . \tag{145}$$

This mass value is now identified as the ρ-meson. The values of the constituent masses $m_1 = m_u$ and $m_2 = m_d$ are adjusted to be $m_u = m_d = 406$ MeV $= 1.16 \cdot \kappa$,

which is more than 100 MeV smaller than for the 'Coulomb plus regulated Delta' or the 'full regulated' problem fitted to the 'a'-meson. Fig. 34 shows spectrum of the

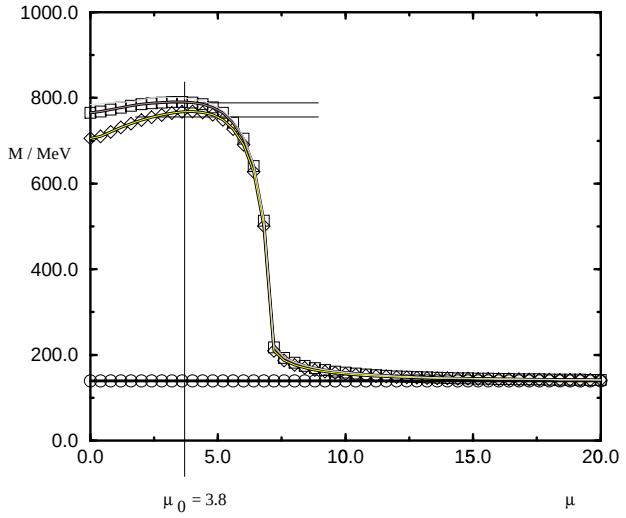

Figure 34: *The spectrum of the first three singlet S-states in MeV versus μ. The 1S-state is completely flat and insensitive to μ, the 2S- ($\diamond$) and 3S-state ($\Box$) are functions of μ. The deep step at $\mu_{crit} \sim 7$ corresponds to the gap in Fig. 33. The whole spectrum is insensitive to μ at $\mu \sim 4$, accentuated by the tangents to the plateaus. For $\mu \to \infty$ the spectrum is not resolvable on this mass scale.*

first three singlet S-states in MeV versus the scale μ calculated with the appropriate renormalized α. The higher states show the same behavior as before, the gap at $\mu_{crit} \sim 7$ causes their 'break-down'. For $\mu \leq \mu_{crit}$ the levels are mainly equidistant and the mass value is in the region of 800 MeV. Between $\mu = 3$ and $\mu = 5$ both states form small plateaus. The appropriate (α, μ)-pair is found at (3.8, 0.6904).

The completely fixed spectrum and the wave functions of the excited π^+ are listed in Table 18.

Taking only the first eigenfunction for π^+ ($\circ$), a comparison to the Coulomb wave function ($\diamond$) under the same conditions, i.e. same α and quark masses, is shown in Fig. 35. Therein the arbitrarily normalized wave functions are plotted versus the momentum, with the last value at $|\vec{k}|_{max} = 10$. The corresponding scale for the pion is found to be $\eta = 0.9326$, which indicates that the pion is situated farer away from the Coulomb regime than the two model equations. Therefore it is not astonishing that the pion wave function is slower decreasing than in the 'Coulomb

M_n^2:	140	768	790	799	809	883
$k_j \downarrow$	-5.223	-0.568	-0.283	-0.169	-0.042	0.980
0.01	10.000	10.000	10.000	10.000	-0.448	-0.017
0.05	9.929	8.705	5.952	-0.234	1.576	-0.037
0.13	9.564	4.285	-1.054	0.010	-9.776	-0.168
0.25	8.592	0.713	-0.211	0.003	10.000	-1.497
0.40	6.908	-0.077	0.009	-0.000	-0.085	10.000
0.60	4.878	-0.099	0.017	-0.000	-0.460	-1.678
0.85	3.077	-0.055	0.009	-0.000	-0.248	-0.873
1.15	1.801	-0.027	0.005	-0.000	-0.121	-0.402
1.51	1.012	-0.014	0.002	-0.000	-0.060	-0.193
1.95	0.554	-0.007	0.001	-0.000	-0.031	-0.096
2.49	0.297	-0.004	0.001	-0.000	-0.016	-0.049
3.16	0.154	-0.002	0.000	-0.000	-0.008	-0.024
4.01	0.076	-0.001	0.000	-0.000	-0.004	-0.012
5.15	0.034	-0.000	0.000	-0.000	-0.002	-0.005
6.84	0.013	-0.000	0.000	-0.000	-0.001	-0.002
10.00	0.003	-0.000	0.000	-0.000	-0.000	-0.001

Table 18: *The spectrum and the wave functions for the excited π^+. – Parameter values are: α=0.6904, μ= 4.800, $m_1 = m_2$= 1.48 (masses in units of $\kappa = 350$ MeV). Calculations are done with 16 Gaussian integration points, with a maximum momentum $k_{16} = 15.52\,\kappa$. – The first row gives the first 6 mass eigenvalues (in MeV), corresponding to the first singlet-nS states. The second row shows the eigenvalues $M_h^2 - m_s^2$ (in units of κ^2). Below each eigenvalue are the 16 eigenfunctions, labeled with the integration points $10k_i/k_{16}$ shown in the first column. They are normalized such that the largest value has the numerical value '10'. Note that the number of nodes increases as expected, and that the highest eigenvalue is actually in the continuum.*

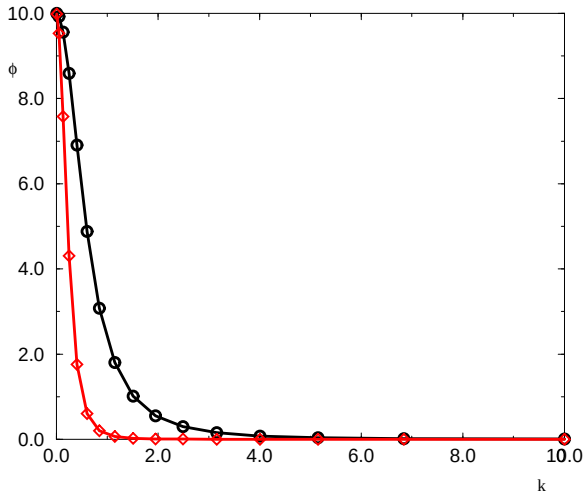

Figure 35: *The arbitrarily normalized pion wave function (∘) is plotted versus the momentum, which is normalized to* $|\vec{k}|_{max} = 10$. *It is compared to the Coulomb wave function (⋄) at the same coupling and quark masses in the same units.– The pion wave function decreases much slower with the momentum than the Coulomb wave function.*

plus regulated Delta' fitted to the 'a'-meson, i.e. the width depends on the scaling $\mu^2/(4m_r m_s) = 2.6828$, and therefore on the strength of the interaction between Coulomb and Yukawa. Here the interaction is 72% stronger the in the 'completely regulated' case, but just 2% stronger than in the 'Coulomb plus regulated' one. Therefore, the root mean-square radius of the pion is $\langle r_\pi^2\rangle^{\frac{1}{2}} = 0.662$ fm, which is 0.4% smaller than in the 'Coulomb plus regulated Delta' case. The pure Coulomb radius has $\langle r_\pi^2\rangle^{\frac{1}{2}} = 1.8249$ fm.

With the received basic parameters (α, μ, m_u, m_d) the remaining quark masses are calculated and tabulated in Table 19.

fit meson	mass/[MeV]	derived masses/[MeV]
$d\,\bar{u}$	140	$\overline{m}_u = \overline{m}_d$ 406 (fixed)
$s\,\bar{u}$	494	$\overline{m}_s$ 508
$c\,\bar{u}$	1865	$\overline{m}_c$ 1666
$b\,\bar{u}$	5279	$\overline{m}_b$ 5054

Table 19: *The fitted quark masses are given in [MeV].- In the first two columns the corresponding fit meson and its mass is mentioned, in the third the derived value is tabulated.*

With this complete set of parameters all mesons are described. The derived 'flavor off-diagonal' mass-eigenstates are given in Table 20. For comparison, the experimental values are shown in Table 13.

	$\bar{u}$	$\bar{d}$	$\bar{s}$	$\bar{c}$	$\bar{b}$
u		768	871	2030	5418
d	140		871	2030	5418
s	494	494		2124	5510
c	1865	1865	1929		6580
b	5279	5279	5338	6114	—

Table 20: *The calculated mass eigenstates of QCD in MeV. Singlet 1S-states are given in the lower triangle, singlet 2S-states in the upper.*

Again the singlet 2S-state are given in the upper triangle, instead of the real vectormesons. Comparing the calculated singlet 1S-states to the experimental masses, and regarding that the up- and down mass were fixed from the beginning, the values for $c\,\bar{s} = D_s^+$, $b\,\bar{s} = \bar{B}_s^0$, and $b\,\bar{c} = B_c^-$ are the really calculated masses. They deviate from experiment by approximately 3%. Even in this case the singlet 2S-states fit to the vectormeson masses. The ρ^+ has been a fitting parameter for the up- and down mass, but the other values differ just by $\pm$(1.1 to 2.9)%. They are therefore closer to the masses of the vectormesons than for the other calculations. The proportionality factors between 1S- and 2S-states are similar for light-light mesons and higher for heavy-light or heavy-heavy compounds,

quark-combination	experimental 2s / 1s	factor
(d,u)	768 / 140	5.5
(s,d)=(s,u)	871 / 494	1.76
(s,c)	2124 / 1929	1.101
(c,d)=(c,u)	2030 / 1865	1.088
(b,c)	6580 / 6114	1.076
(b,s)	5510 / 5338	1.032
(b,d)=(b,u)	5418 / 5279	1.026

Comparing the factors to those for both cases fitted to the 'a', the present numbers

are closest to the experimental proportionalities between scalar- and vectormeson. The periodicity is clearly visible.

Remembering that this calculation has been on the assumption of a scalar pion, the values fit quite well into the puzzle. Obviously, the singlet 2S-state of the pion is in reality closer to the 'ρ'-level than to the 'a'-level. In fact the ρ-fitting seems to be a possibility for a lower boundary to the problem.

D Generalization attempt of the spin content

There are several possibilities to receive a system for arbitrary spins. The first is to convert the helicity table $\langle\lambda_q, \lambda_{\bar{q}}|T|\lambda'_q, \lambda'_{\bar{q}}\rangle$, already calculated in Eqs.(142, 143, 144) (see Sect. 3.1), into a spin matrix depending on the quantum numbers S and S_z. A possibility is to use a Melosh transformation, which ensures that the meson will be an eigenfunction of the spin operator by rotating the quark helicities. Therefore a spin-orbit wave function for Spin (S, S_z) is defined as [58, 59, 60]

$$\begin{aligned}&\mathcal{R}_{S,S_z}(x, \vec{k}_\perp, \lambda_q, \lambda_{\bar{q}}) \qquad (146)\\ &= \sum_{\lambda,\lambda'} \langle\lambda_q|\mathcal{R}^\dagger_M(x, \vec{k}_\perp, m_q)|\lambda\rangle\langle\lambda_{\bar{q}}|\mathcal{R}^\dagger_M(1-x, -\vec{k}_\perp, m_{\bar{q}})|\lambda'\rangle\langle\frac{1}{2}\frac{1}{2}, \lambda\lambda'|SS_z\rangle \quad ,\end{aligned}$$

where the Melosh rotation is given by

$$\mathcal{R}^\dagger_M(x, \vec{k}_\perp, m_q) = \frac{m + xM_0 - i\vec{\sigma}(\hat{n} \times \hat{k})}{\sqrt{(m + xM_0)^2 + \vec{k}^2_\perp}} \quad , \qquad (147)$$

with $\hat{n} = (0, 0, 1)$ being a unit vector in z-direction, and the meson mass square taken as $M_0^2 = (E_1 + E_2)^2$. To receive a spin matrix from the helicity matrix T the following steps are required: first calculate $\langle\lambda_q|\mathcal{R}^\dagger_M(x, \vec{k}_\perp, m_q)|\lambda\rangle$, then the corresponding for the anti-quark with $x \to (1-x)$ and $\vec{k}_\perp \to -\vec{k}_\perp$. Hence both terms are combined in Eq.(146) and $\mathcal{R}_{S,S_z}(\lambda_q, \lambda_{\bar{q}})$ is developed. After taking its inverse the new spin matrix is performed in a 'sandwich procedure', i.e.

$$\sum_{\lambda_q,\lambda_{\bar{q}}} \sum_{\lambda'_q,\lambda'_{\bar{q}}} \mathcal{R}^{-1}_{S,S_z}(\lambda_q, \lambda_{\bar{q}})\langle\lambda_q, \lambda_{\bar{q}}|T|\lambda'_q, \lambda'_{\bar{q}}\rangle\mathcal{R}_{S,S_z}(\lambda'_q, \lambda'_{\bar{q}}) \quad . \qquad (148)$$

With having a spin-half system of a quark and an anti-quark, which couple to a singlet with $S = 0$, $S_z = 0$ and a triplet $S = 1$, $S_z = -1,\ 0,\ 1$, this matrix will obviously be a 4×4 matrix which contains all possible spin combinations. Under the impact of the rotational invariance of the Lagrangian in the x-y plane, which is related to the projection of the total angular momentum J_z, the coordinates can be written as $\vec{k} = (k_\perp \cos\varphi, k_\perp \sin\varphi, k_z)$. Therefore the Melosh rotations are

$$\mathcal{R}_q = \frac{1}{\sqrt{a^2 + k^2_\perp}} \begin{pmatrix} a & -k_\perp e^{-i\varphi} \\ k_\perp e^{i\varphi} & a \end{pmatrix} \quad , \quad a = m_q + xM_0 \quad , \text{ and} \qquad (149)$$

$$\mathcal{R}_{\bar{q}} = \frac{1}{\sqrt{b^2 + k^2_\perp}} \begin{pmatrix} b & k_\perp e^{-i\varphi} \\ -k_\perp e^{i\varphi} & b \end{pmatrix} \quad , \quad b = m_{\bar{q}} + (1-x)M_0 \quad . \qquad (150)$$

For the derivation of Eq.(146) the system corresponding Clebsch-Gordan elements are needed [61]. In the end Eq.(146) has the shape of a rotational matrix

$$\begin{array}{ccccc} \lambda_1,\lambda_2/S,S_z & (1,-1) & (1,0) & (0,0) & (1,1) \\ \uparrow\downarrow & -bk_\perp e^{-i\varphi} & \frac{1}{\sqrt{2}}(ab+k_\perp^2) & \frac{1}{\sqrt{2}}(ab-k_\perp^2) & -ak_\perp e^{i\varphi} \\ \downarrow\uparrow & ak_\perp e^{-i\varphi} & \frac{1}{\sqrt{2}}(ab+k_\perp^2) & \frac{1}{\sqrt{2}}(k_\perp^2-ab) & bk_\perp e^{i\varphi} \\ \uparrow\uparrow & -k_\perp^2 e^{-2i\varphi} & \frac{k_\perp}{\sqrt{2}}e^{-i\varphi}(a-b) & \frac{k_\perp}{\sqrt{2}}e^{-i\varphi}(a+b) & ab \\ \downarrow\downarrow & ab & -\frac{k_\perp}{\sqrt{2}}e^{i\varphi}(a-b) & \frac{k_\perp}{\sqrt{2}}e^{i\varphi}(a+b) & -k_\perp^2 e^{2i\varphi} \end{array} \quad , \qquad (151)$$

with a denominator $D = \sqrt{a^2+k_\perp^2}\sqrt{b^2+k_\perp^2}$ and the mass terms $a = m_q + xM_0$, $b = m_{\bar{q}} + (1-x)M_0$. The determinant of the matrix $\mathcal{R}(S,S_z)$ is unity, $\det\mathcal{R} = 1$, therefore the unitarity condition $\mathcal{R}^\dagger\mathcal{R} = 1$ is satisfied and the inverse of $\mathcal{R}$ is equal to its adjoint. With these matrices the position is reached to compute the transformation of the helicity to the spin table. The mathematical operation $T(S,S_z) = \mathcal{R}^\dagger T(\lambda_1,\lambda_2)\mathcal{R}$ has not yet come to a result. The calculation is quite complex since all terms of the elements T_{ij} are necessary. The matrix multiplication brings up a new matrix $T(S,S_z)$ with complicate elements and no obvious structure. It is known from former tests that the helicity matrix has eigenvalues and can therefore be diagonalized, but including the Melosh transformation everything even gets worse. Though the Melosh transform is a usual way to rotate basis states, it is used for total angular momentum J, while here the single contributions to angular momentum j_i are implemented. This might cause difficulties and therefore this method has to be improved.

Another possibility to think of is the separation of the integral equation into a radial wave function and a spin-orbit part [32], i.e. $\Psi = \Phi(x,\vec{k}_\perp)\chi(\lambda_1,\lambda_2)$. This method is already known from the hydrogen atom, where the solution to the Schrödinger equation has been found by a separation ansatz, i.e. $\Psi(r,\theta,\varphi) = R(r)F(\theta,\varphi)$. The hydrogen problem is exact solvable. For a multi-particle problem everything is more complicate. Ji *et al.* [59, 62, 63] used a separation ansatz, but for a fixed radial wave function and a spin-orbit one corresponding to J^{PC}. Therefore the whole system was settled and no integrals occured. But in a flexible system with the angular momentum operators carrying the interaction, they are problematic to define in front form dynamics. A way to proceed is that of Trittmann [21] who Fourier transformed the spinor matrix T, i.e.,

$$\langle x,\vec{k}_\perp;J_z,\lambda_1,\lambda_2|\widetilde{T}|x',\vec{k'}_\perp;J_z',\lambda_1',\lambda_2'\rangle \qquad (152)$$

$$= \frac{1}{2\pi}\int_0^{2\pi} d\varphi e^{-iL_z\varphi}\int_0^{2\pi} d\varphi' e^{iL_z\varphi'}\langle x,\vec{k}_\perp;\varphi,\lambda_1,\lambda_2|T|x',\vec{k'}_\perp;\varphi',\lambda_1',\lambda_2'\rangle$$

The integration over (φ,φ') gives a helicity table for arbitrary $J_z = n$ with $n \in Z$, which is then implemented in the model equation. This method has the disadvantage that it contains a double integral and is therefore not as comfortable as a separation ansatz. But at the moment it seems to be the best alternative.

References

[1] M. Gell-Mann, Phys. Lett. **8**, 214 (1964).

[2] J. E. Augustin *et al.*, Phys. Rev. Lett. **33**, 1406 (1974).

[3] J. J. Aubert *et al.*, Phys. Rev. Lett. **33**, 1404(1974).

[4] M. K. Gaillard, B. W. Lee, and J. L. Rosner, Rev. Mod. Phys. **47**, 277 (1975).

[5] S. L. Glashow, J. Iliopoulos, and L. Maiani, Phys. Rev. **D 2**, 1285 (1970).

[6] Fermilab Publication 94/097-E (1994).

[7] S. Brodsky, eprint hep-ph/9710288 (1997).

[8] H. C. Pauli, Eur. Phys. J. C **7**: 289 - 303 (1999).

[9] P. A. M. Dirac, Rev. Mod. Phys. **21**, 392 (1949).

[10] S. J. Brodsky, H. C. Pauli, and S. S. Pinsky, Phys. Rep. **301**: 299-482 (1998).

[11] J. P. Vary and F. Wölz, *Light-Front Quantization and Non-Perturbative QCD*, International Institute of Theoretical and Applied Physics, Ames, Iowa (1997).

[12] I. Tamm, J. Phys. (USSR) **9**, 449 (1945).

[13] S. M. Dancoff, Phys. Rev. **78**, 382 (1950).

[14] H.C. Pauli, Max-Planck-Institut f. Kernphysik Report No. MPI-H-V19-1999 (1999).

[15] H. C. Pauli, and J. Merkel, Phys. Rev. D **55**, 4 (1997).

[16] M. Krautgärtner, H. C. Pauli, and F. Wölz, Phys. Rev. D **45**, 3755 (1992).

[17] U. Trittmann, eprints: hep-th/9808077, hep-th/9704215, hep-th/9705021, hep-th/9705072.

[18] S. J. Brodsky, and G. P. Lepage , Phys. Lett. B **87**, 359 (1979).

[19] S. Weinberg, *The Quantum Theory of Fields. Vol. 1: Foundations.*, Cambridge University Press, Cambridge, UK (1995).

[20] S. Bielefeld, J. Ihmels, and H. C. Pauli, Max-Planck-Institut f. Kernphysik Report No. MPIH-V-14-1999, eprint hep-ph/9904241 (1999).

[21] U. Trittmann, and H. C. Pauli, *Quantum electrodynamics at strong couplings*, Max-Planck-Institut f. Kernphysik Report No. MPIH-V4-1997; eprint hep-th/9704215 (1997)

[22] M. Brack *et al.*, Rev. Mod. Phys. **44**, 320 - 405 (1972).

[23] H. Hersbach, Phys. Rev. D **47**, 7 (1993).

[24] Abramowitz, *Pocket Book of Mathematical Functions*, Verlag Harri Deutsch - Thun - Frankfurt/Main, Chap.10, p.172 (1984).

[25] T. Eller, and H. C. Pauli, Z. Phys. C **42**, 59 (1989).

[26] F. Wölz, Diploma Thesis, Heidelberg University, February 1990, unpublished.

[27] Numerical Recipes in C, W. H. Press et al., 797-803, Cambridge University Press (1992), and references therein.

[28] Y. R. Kwon, F. Tabakin, Phys. Rev. C **18**, 932 (1978).

[29] F. W. Bopp, *Kerne, Hadronen, und Elementarteilchen*, Teubner Studienbücher Stuttgart (1989).

[30] Particle Data Group, C. Caso *et al.*, Eur. Phys. J. C **3**, 1 (1998) and (1999) partial update for edition 2000; http://pdg.lbl.gov.

[31] M. Jaminon, B. Van den Bossche, eprint nucl-th/9701038 (1997).

[32] H. Haken, and H. C. Wolf, *Atom- und Quantenphysik*, forth edition, Springer Verlag Berlin-Heidelberg (1990).

[33] H.Rollnik, *Teilchenphysik I*, Bibliographisches Institut Mannheim / Wien / Zürich (1971).

[34] H.Rollnik, *Teilchenphysik II*, Bibliographisches Institut Mannheim / Wien / Zürich (1971).

[35] S. J. Brodsky, C. R. Ji, A. Pang, and D. G. Robertson, hep-ph/9705221, Phys. Rev. D **57**, 245-252 (1998).

[36] B. Povh *et.al.*, *Teilchen und Kerne*, third edition, Springer Verlag Berlin-Heidelberg (1995).

[37] S. R. Amedolia *et al.*, Phys. Lett. B **146**, 116 (1984).

[38] H. C. Pauli, *private communications* (1999).

[39] W. J. Thompson, *Angular Momentum*, John Wiley & Sons, Inc., New York (1994).

[40] U.-G. Meißner, eprint nucl-th/9910019 (1999).

[41] S. Zhu, and Z. Li, eprint hep-ph/9703371 (1997).

[42] J. Merkel, Diploma Thesis, Heidelberg University, December 1994.

[43] S. Brodsky, SLAC Report No. SLAC-PUB-8240, eprint hep-ph/9909234 (1999).

[44] S. Brodsky and S. D. Drell, Phys. Rev. D **22**, 2236 (1980).

[45] M. Burkardt, eprint hep-ph/9705224 v2 (1997).

[46] R. Perry, eprint hep-th/9710175 (1997).

[47] B. D. Jones and R. Perry, eprint hep-th/9612163 (1996).

[48] B. H. Allen, and R. Perry, eprint hep-ph/9804136 (1998).

[49] S. Głazek, eprint hep-th/9712188 (1997).

[50] S. Brodsky, J. R. Hiller and G. McCartor, Phys. Rev. D **58**, 025005 (1998).

[51] UKQCD collaboration: C. Michael *et al.*, eprint hep-lat/9909036 (1999).

[52] SESAM collaboration: N. Eicker *et al.*, eprint hep-lat/9704019 (1997).

[53] A. Duncan *et al.*, eprint hep-lat/9312046 (1993).

[54] K. Schilling and G. Bali, eprint hep-lat/9311054 (1993).

[55] S. Dalley, B. van de Sande, eprint hep-lat/9908035 (1999).

[56] S. J. Brodsky, D. G. Robertson, SLAC Report No. SLAC-PUB-95-7056 (1995).

[57] M. Burkardt, eprint hep-ph/9709421 (1997).

[58] D. Arndt and C.-R. Ji, eprint hep-ph/9905360 (1999).

[59] H. M. Choi, and C.-R. Ji, Nucl. Phys. A **618**, 291 (1997).

[60] F. Schlumpf, eprints: hep-ph/9305293 , hep-ph/9212250.

[61] A. R. Edmonds, *Angular Momentum in Quantum Mechanics*, Princeton University Press (1964).

[62] H. M. Choi, and C.-R. Ji, Phys. Rev. D **59**, 074015 (1999).

[63] H. M. Choi, and C.-R. Ji, eprint hep-ph/9711450 v4 (1998).